DOE/NASA/0176-10
NASA CR-168223

Preparation and Evaluation of Advanced Catalysts for Phosphoric Acid Fuel Cells

Final Technical Report

Paul Stonehart, John Baris,
and John Hockmuth
Stonehart Associates, Inc.

June 1984

Prepared for
NATIONAL AERONAUTICS AND SPACE ADMINISTRATION
Lewis Research Center
Under Contract DEN 3-176

for
U.S. DEPARTMENT OF ENERGY
Morgantown Energy Technology Center

stonehart associates

DOE/NASA-10176-10
CR 168223

PREPARATION AND EVALUATION OF ADVANCED ELECTROCATALYSTS FOR PHOSPHORIC ACID FUEL CELLS

FINAL REPORT

Paul Stonehart, John Baris, John Hochmuth and Peter Pagliaro

May 25, 1983

PREPARED FOR:

NATIONAL AERONAUTICS AND SPACE ADMINISTRATION
Lewis Research Center
Under Contract DEN-3-176
Prepared Under Interagency Agreement DEAI-03-80ET17088

FOR:

U.S. DEPARTMENT OF ENERGY
Energy Technology
Division of Fossil Fuel Utilization

17 Cottage Road, Madison, Connecticut 06443
Telephone Area Code 203 245-7507

ABSTRACT

This research program details the preparation and characterization of platinum electrocatalysts supported on carbon substrates. In the first instance, the platinum electrocatalysts were characterized for their crystallite sizes and the degree of dispersion on the carbon supports. One application of these electrocatalysts was for anodic oxidation of hydrogen in hot phosphoric acid fuel cells, coupled with the influence of low concentrations of carbon monoxide in the fuel gas stream. In a similar way, these platinum on carbon electrocatalysts were evaluated for oxygen reduction in hot phosphoric acid.

An extension of these catalyst preparation techniques involved the preparation of binary noble metal alloys for anodic oxidation of hydrogen and the preparation of noble metal-refractory metal mixtures for oxygen reduction.

An exemplar alloy of platinum and palladium (50/50 atom %) was discovered for anodic oxidation of hydrogen in the presence of carbon monoxide, and patent disclosures were submitted. For the cathode, platinum-vanadium alloys were prepared showing improved performances over pure platinum.

Preliminary experiments on electrocatalyst utilization in electrode structures showed low utilization of the noble metal when the electrocatalyst loading exceeded one weight percent on the carbon. Further gains are to be expected from improving the electrode structures.

TABLE OF CONTENTS

File #1

Objective and Scope of Work

The overall objective of this electrocatalysis program was to define the feasibility of lowering the electrocatalyst cost and increasing the activity in phosphoric acid fuel cells, as a way to increase the commercial viability of fuel cells for producing electric power.

The specific objectives of the present tasks are the preparation of a series of high surface area electrocatalysts for evaluation in phosphoric acid fuel cells. This involves fabrication of efficient gas-diffusion electrode structures and determining their electrochemical parameters for hydrogen oxidation and oxygen reduction. When possible, new experimental techniques and theoretical interpretations will be forwarded towards an understanding of the relevant electrochemical parameters.

Task 1 - Preparation and Characterization of Platinum-Carbon Electrocatalysts

A previous contract performed by Stonehart Associates (DE-AC03-78ET15365) was concerned with the formation of a series of platinum based electrocatalysts on different carbon surfaces. Carbons as supports were selected and processed under a companion EPRI Program (1200-2). These catalysts so far produced were manufactured by an impregnation technique. As a consequence of the impregnation technique, the wetting of the carbon surfaces by the catalyst salt solution is critical. That is to say that the wettability of different carbons is modified by their surface tension. During the drying process, the crystallization of the salt within the carbon pore structure is a pre-cursor to the platinum crystallite that is obtained by reduction of the crystallized platinum salt. The resultant platinum supported catalysts had different crystallite sizes depending on the wetting characteristics and pore volume characteristics of the carbon surfaces. It is also believed that the adhesion characteristics of the platinum crystallite to the carbon supports are modified by the degrees of graphitization of the carbon. Adhesion forces are not known between platinum and carbon. In order to vary the characteristics of the platinum electrocatalysts, colloidal platinum particles were prepared using a peroxide activated sodium dithionite reduction technique described in

U.S. Patent #4,136,059 (1979).

Another process to make colloidal platinum particles is described according to U.S. Patents #3,992,331 and 4,044,193.

Samples of carbon black were impregnated with these preformed colloidal solutions, dried and reduced with hydrogen. Characterizations of these electrocatalysts were carried out by forming them into flooded electrode structures containing small amounts (less than 10%) of PTFE and determining the electrocatalyst surface areas from potentiodynamic stripping of adsorbed hydrogen on the platinum crystallites.

A platinum electrocatalyst on Vulcan XC-72R had been prepared and tested in this program as well as an electrocatalyst comprising platinum on a different carbon support. The latter catalyst was platinum on a steam-activated acetylene black (Consel I). This particular catalyst support has shown high stability against corrosion and was developed under a companion EPRI 1200-2 program.

Although the support projected the required lifetime for phosphoric acid fuel cells (40,000 hrs. at 200°C) and has been efficiently catalyzed with platinum, no information was obtained previously on the reactivity of this catalyst for oxygen reduction and hydrogen molecule oxidation. The surface of the steam-activated acetylene black has a graphitic overlayer that is a consequence of the steam-treatment process. This graphitic overlayer confers stability to the carbon support against corrosion. It also causes difficulty in the formation of optimized electrode structures, since the interaction with Teflon and the wettability of the carbon surface is modified by the graphitic overlayer; nevertheless, catalyzation was achieved with an initial surface area in excess of 130 m^2/g.

Task 2 - Anodic Activity of Platinum-Carbon Electrocatalysts

During the present contract, Teflon-bonded electrocatalyst electrode structures were used to determine the hydrogen oxidation activity and the performance of the electrocatalysts in the presence of hydrogen containing 1%

carbon monoxide and 10% carbon monoxide. The reason for choosing the 1% and the 10% carbon monoxide levels was that in the previous Contract (DEN-AC03-78ET15365) anodic oxidation of impure hydrogen was performed at 2% carbon monoxide levels and 30% carbon monoxide levels. Typical polarization data are shown for pure hydrogen in Figure 1 and the apparent Arrhenius plot shown in Figure 2. It can be seen that the slope for the activation line is the same for the present work as was obtained for the previous work (Contract DE-AC03-78ET15365). The carbon monoxide tolerance is shown in Figure 3 for the 1% carbon monoxide level and Figure 4 for the 10% carbon monoxide level. Again, the changes in the apparent activation energies are plotted in Figure 2. Clearly, at the 1% carbon monoxide level there is minimal poisoning at temperatures above 160°C whereas at 10% carbon monoxide level, the poisoning becomes minimal above 180°C.

One feature needs to be explored further and this concerns the influence of the water concentration. In Figure 1 we have shown the polarization data in 104% acid and then a single curve for the polarization in 100% acid at 180°C. The performance in the latter case increased dramatically and we do not understand why this should be so. It is not clear that this performance increase is solely due to the increased water concentration but may be related to some mysterious improvement in the electrode structure on going to the more dilute acid.

It is probable that the results shown in Figures 1-4 have electrode structures that are operating in a flooded control mode rather than in a kinetically controlled mode, since the performance of platinum on carbon as an electrocatalyst material for hydrogen oxidation should be much better than was shown in Figures 1-4. It has long been thought that, since the reaction rate for hydrogen oxidation is very high on platinum electrocatalysts and that the polarization characteristics are controlled solely by mass transport considerations. To a large extent this may well be so but in the presence of carbon monoxide, it is believed that kinetic effects are seen since the carbon monoxide severely restricts the platinum surface available for hydrogen molecule dissociation.

The performance characteristics for electrodes fabricated from 10% platinum on

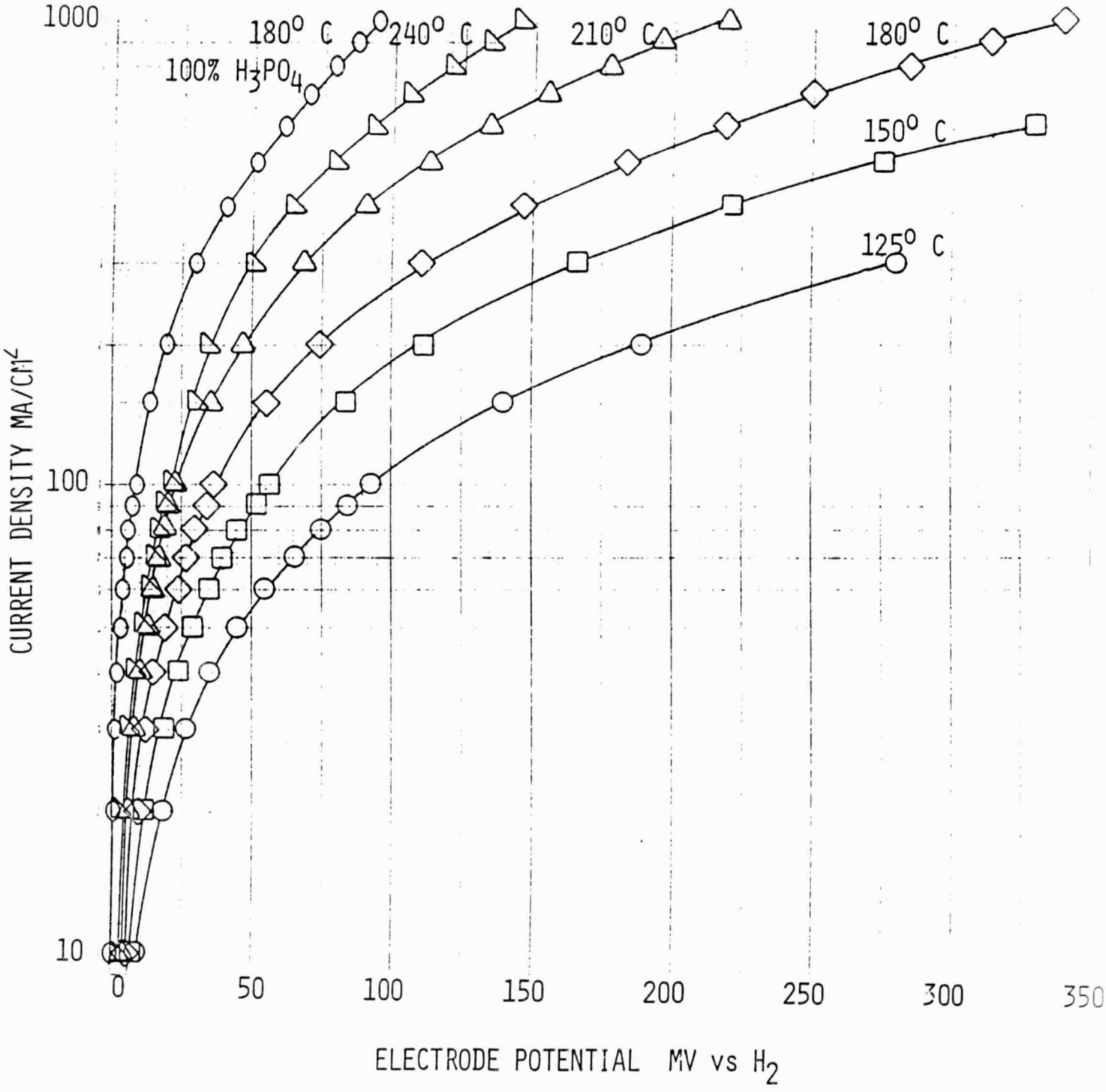

Figure 1. Polarization curves for hydrogen oxidation at various temperatures in 104% H_3PO_4. Catalyst is 10% Platinum on Vulcan. Electrode is 50% catalyst - 50% PTFE, 0.25 mg Pt/cm^2.

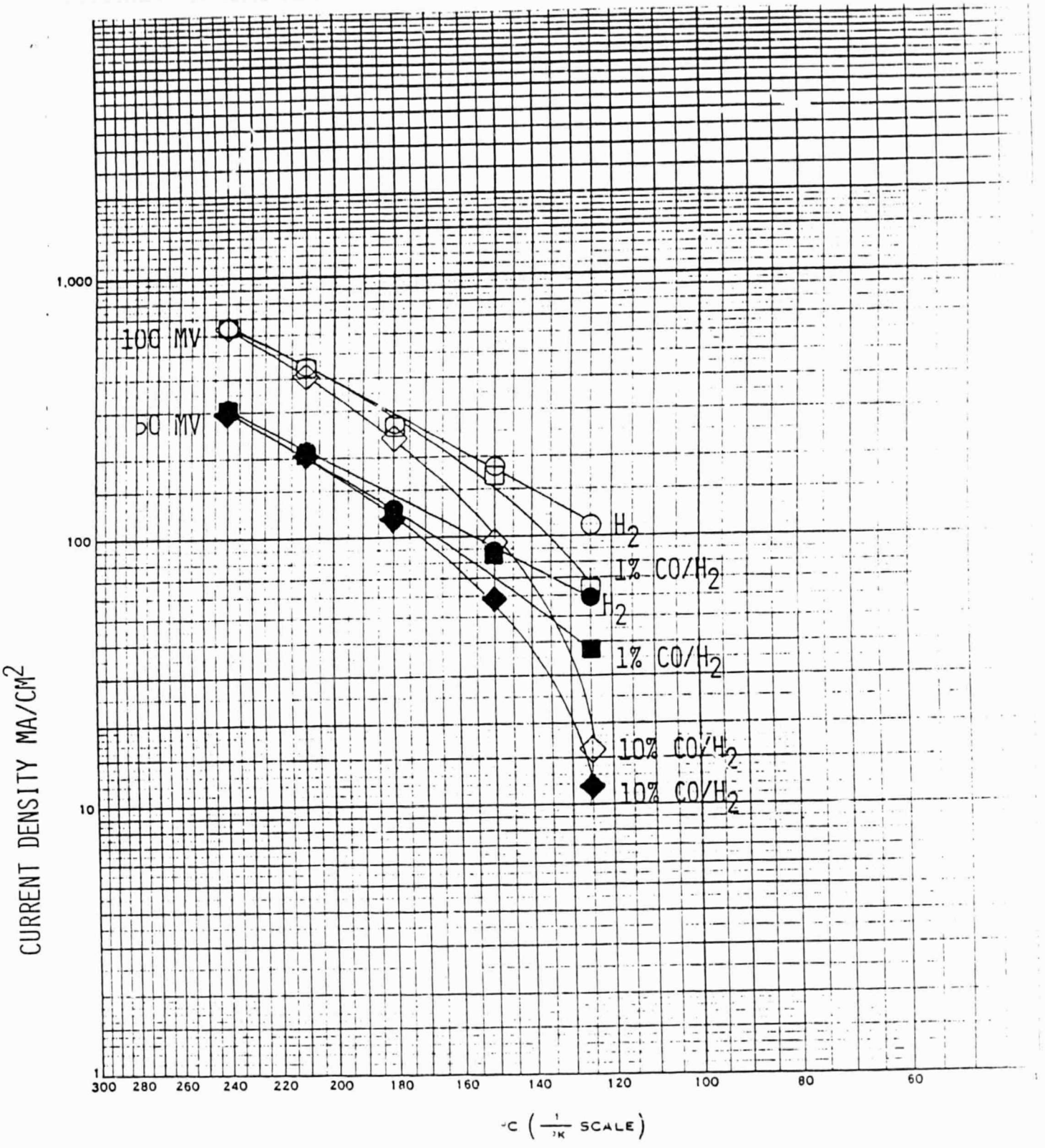

Figure 2. Current density as a function of 1/T for hydrogen oxidation on 100% H_2, 1% CO/H_2, at 50 and 100 mV polarization, in 104% H_3PO_4. 0.25 mg Pt/cm^2, 10% Pt/Vulcan, 50% PTFE.

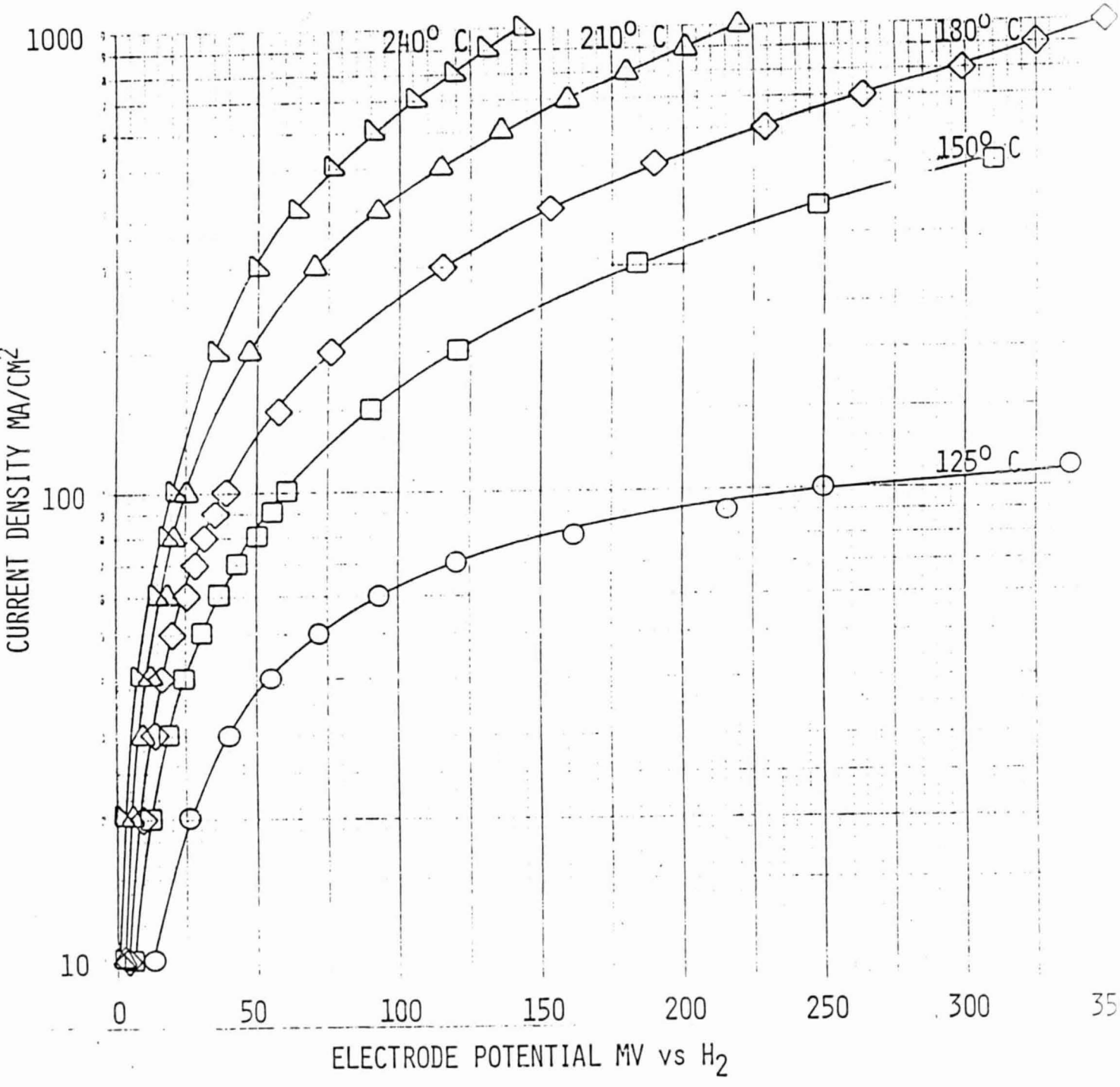

Figure 3. Polarization curves for hydrogen oxidation with 1% CO in fuel gas at various temperatures in 104% H_3PO_4. 10% Pt/Vulcan, 0.25 mg Pt/cm^2, 50% PTFE.

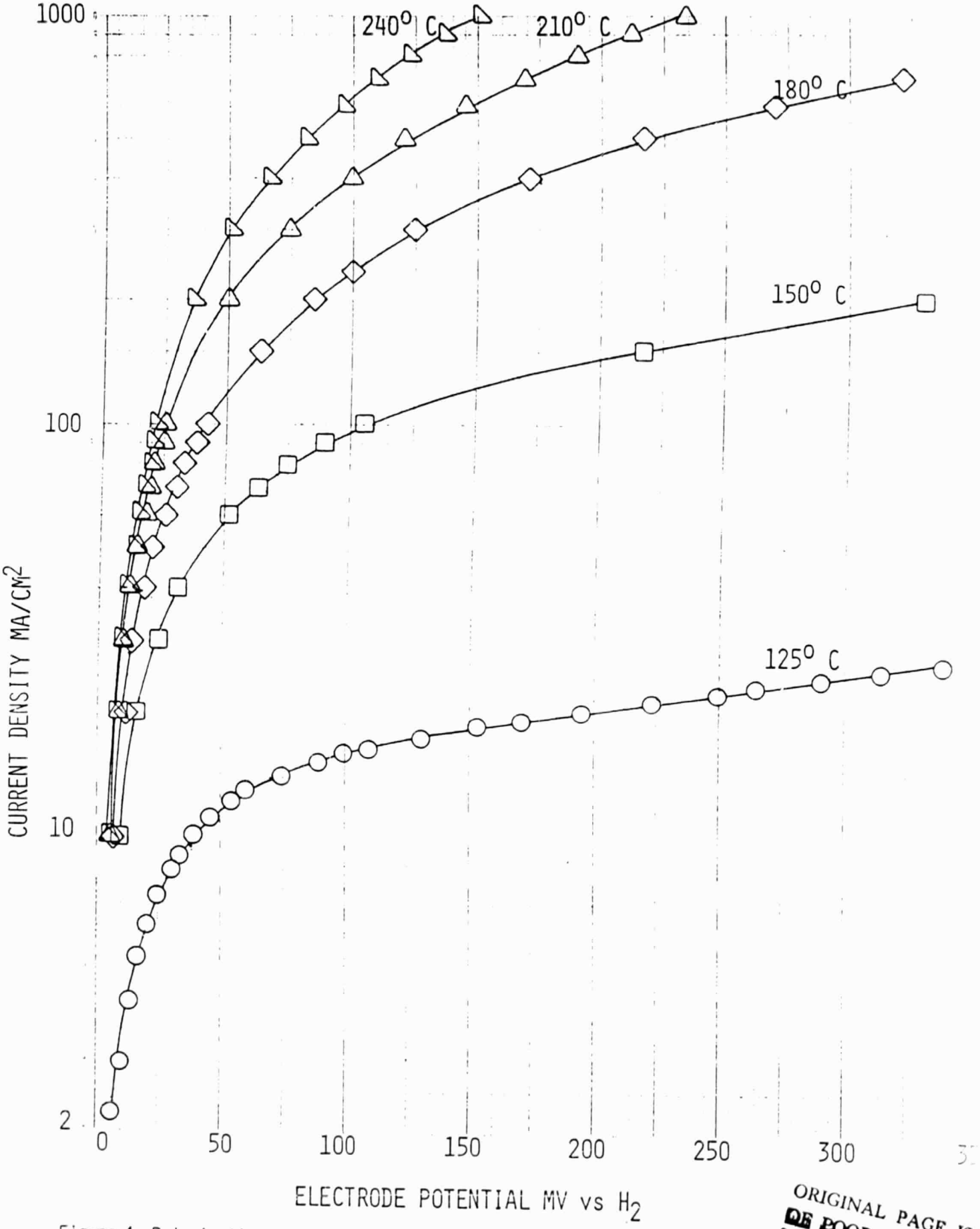

Figure 4. Polarization curves for hydrogen oxidation with 10% CO in fuel gas at various temperatures in 104% H_3PO_4. 10% Pt/Vulcan, 0.25 mg Pt/cm^2, 50% PTFE.

as-received Vulcan XC-72 with the electrode structures containing 0.5 mg of platinum are shown for the operation of the best electrodes at 120°C and 180°C (Figures 5 and 6). The performances under pure hydrogen, 1%, 2%, 10% and 30% carbon monoxide are indicated in the data set for 120°C. At 180°C, the performance is so good that we are not able to separate the 1% and 2% polarization lines. Typically, in the latter data set (180°C) we have measured the pure hydrogen polarization at 100 mA/cm^2 to be 5 mv vs the reversible hydrogen electrode. Even in the presence of 30% carbon monoxide, the total polarization is only 15 mV. That is to say that 30% carbon monoxide only contributes an additional 10 mV polarization. We are not aware that performances of this magnitude have been seen previously.

We should like to point out that the mechanism for correction of the internal resistance between the reference probe and the fuel cell electrode is critical, since at 1 amp, with 400 milliohms iR error, the exact correction is 80 mV. Consequently, if the experimental data is not corrected adequately, then it will not be possible to measure these very small polarization data.

The results shown in Figure 6 are surprising, since this would indicate that if good electrode structures can be produced, then the platinum loading can be reduced at the same time allowing the carbon monoxide level to increase. This will lower the cost of the total fuel cell system. Apparent activation energies were constructed from the polarization data using 10 mV polarization and 25 mV polarization values. The results are shown in Figures 7 and 8, respectively.

At 10 mV the reversible reaction for hydrogen evolution is still significant, since there is not a great excursion from the reversible hydrogen electrode potential. From the reversible Nernst equation for the hydrogen reaction, we can calculate that the equilibrium partial pressure of hydrogen within the pores of the electrode is 0.45 atmospheres, whereas at 25 mV the equilibrium partial pressure for hydrogen within the pores is 0.14 atmospheres. Due to the influence of the hydrogen evolution reaction, the apparent activation energy at 10 mV must be lower than the true activation energy for hydrogen molecule oxidation reaction.

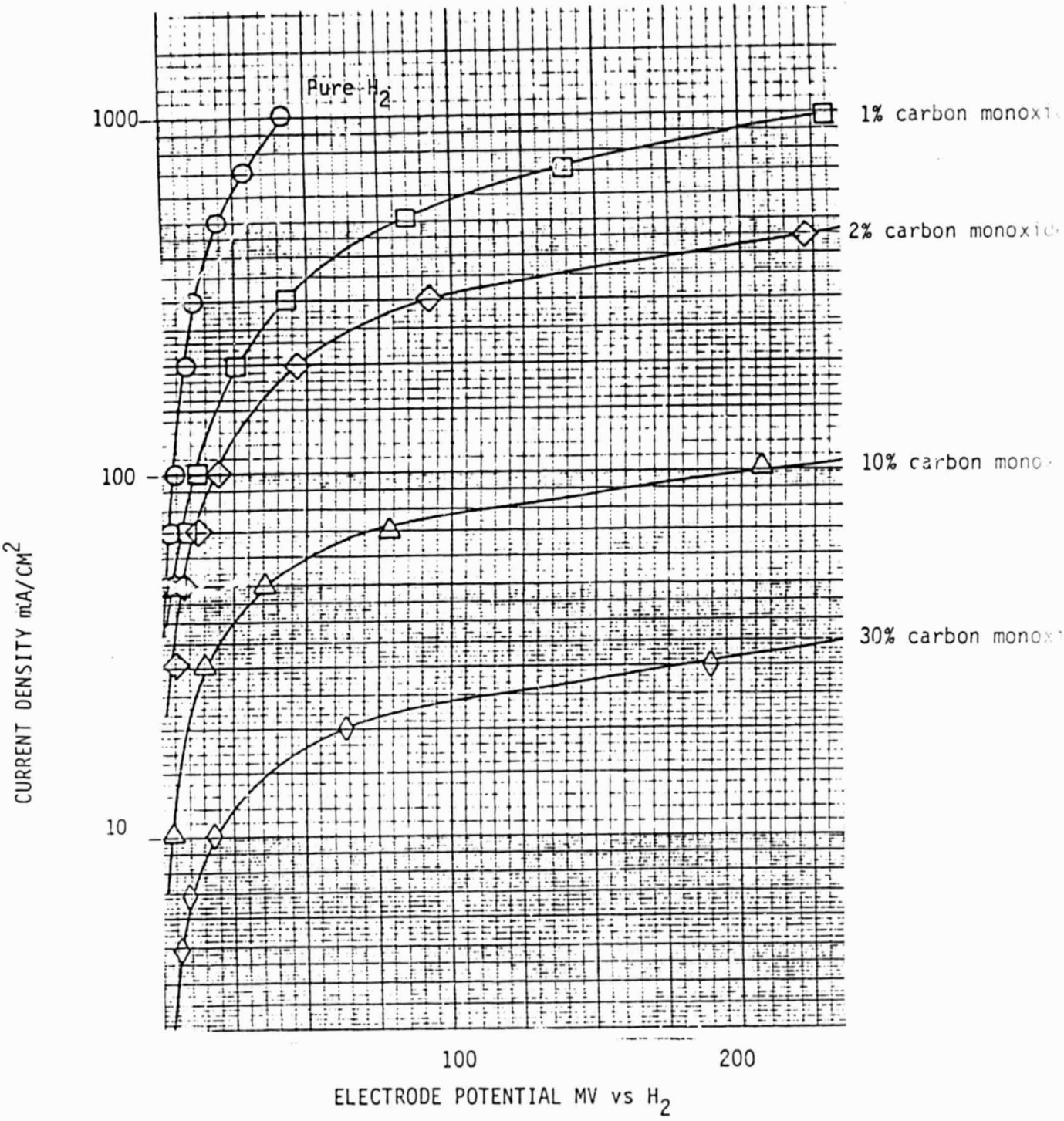

Figure 5. iR Free Polarization Curves for Hydrogen Oxidation and the Influence of Carbon Monoxide on Platinum Crystallites Supported on Vulcan XC-72R.
120°C 102% H_3PO_4. 0.5 mg Pt/cm^2

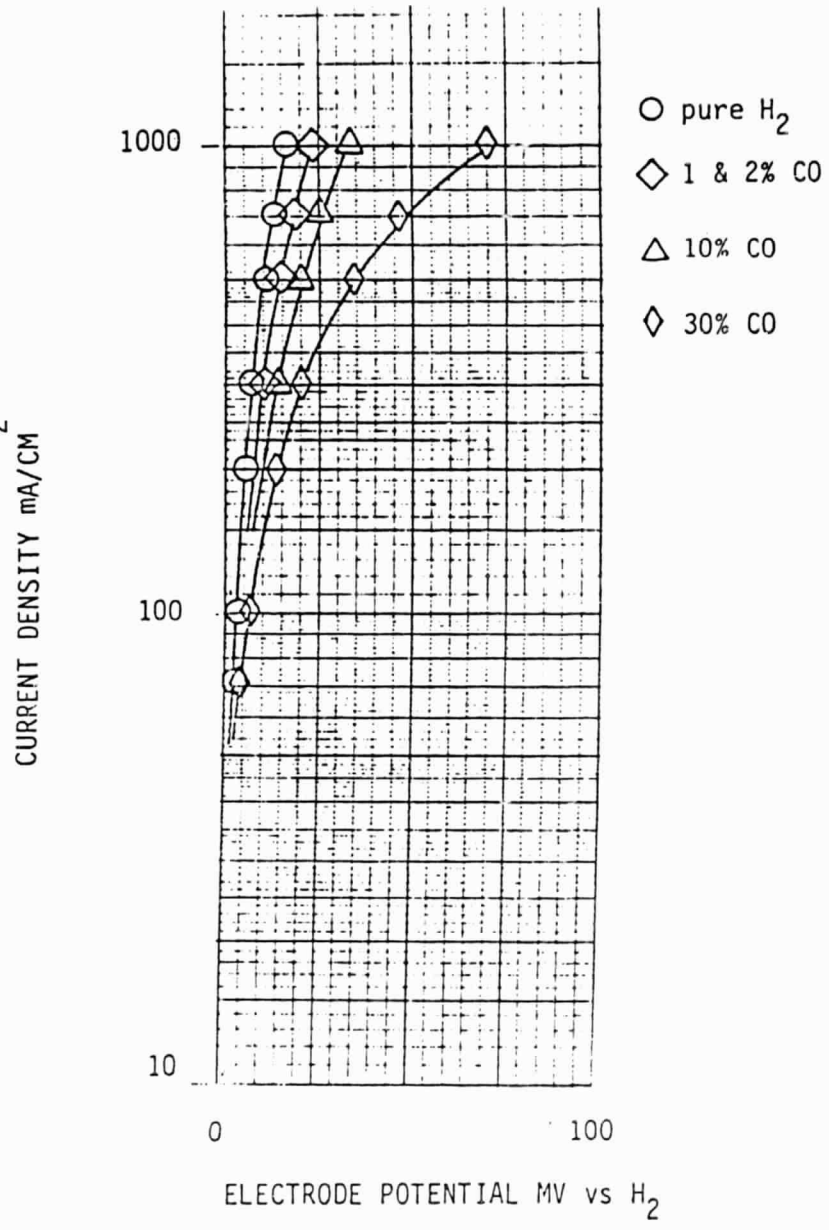

Figure 6. iR Free Polarization Curves for Hydrogen Oxidation and the Influence of Carbon Monoxide on Platinum Crystallites Supported on Vulcan XC-72R.
180°C 102% H_3PO_4
0.5 mg Pt/cm^2

Figure 7 shows that with pure hydrogen, an apparent activation energy of 4 kcal/mole is observed, whereas Figure 8 shows that at 25 mV, 7.6 kcal/mole is observed. It should be remembered parenthetically that at the reversible hydrogen potential, the apparent activation energy is Ø kcal/mole so that there must be a smooth transition between the apparent activation energy at the reversible hydrogen potential and the apparent activation energy observed at 25 mV and higher where the effect of the reverse reaction becomes negligible.

From the values shown in Figures 7 and 8, it is possible to generate the apparent adsorption isotherm for carbon monoxide on the platinum crystallites as a function of temperature and electrode potential.

This function is not simple, since the rate of the hydrogen oxidation reaction is controlled by the coverage of adsorbed hydrogen atoms as well as by the coverage of adsorbed carbon monoxide. The rate of the hydrogen oxidation reaction is governed by the availability of bare sites for the dissociation of hydrogen molecules into two hydrogen atoms, because adsorbed hydrogen is considered to be a site poison for the hydrogen molecule oxidation reaction just as the adsorbed carbon monoxide is a site specific poison.

From the foregoing discussion, Figure 9 exhibits the site availability on the platinum as a function of electrode potential and carbon monoxide partial pressure. This figure is approximately equivalent to the inverse of the carbon monoxide adsorption isotherms on platinum at these temperatures. The site availability is defined as those bare platinum sites available for dissociation of the hydrogen molecules. This availability changes with the electrode potential according to the equilibrium coverage by adsorbed hydrogen. We are, therefore, computing the carbon monoxide coverage according to the platinum surface that is not covered by adsorbed hydrogen and not according to the total platinum crystallite surface. The isotherms reflect that at 220°C with 1Ø mV polarization, 1Ø% carbon monoxide has a negligible coverage on the platinum. The separation for the carbon monoxide isotherms at 120°C between 1Ø mV and 25 mV is barely within experimental error. Apparent coverages of the platinum surface by carbon monoxide at 25 mV are higher than at 1Ø mV for the same temperatures. Since the operation of advanced anode

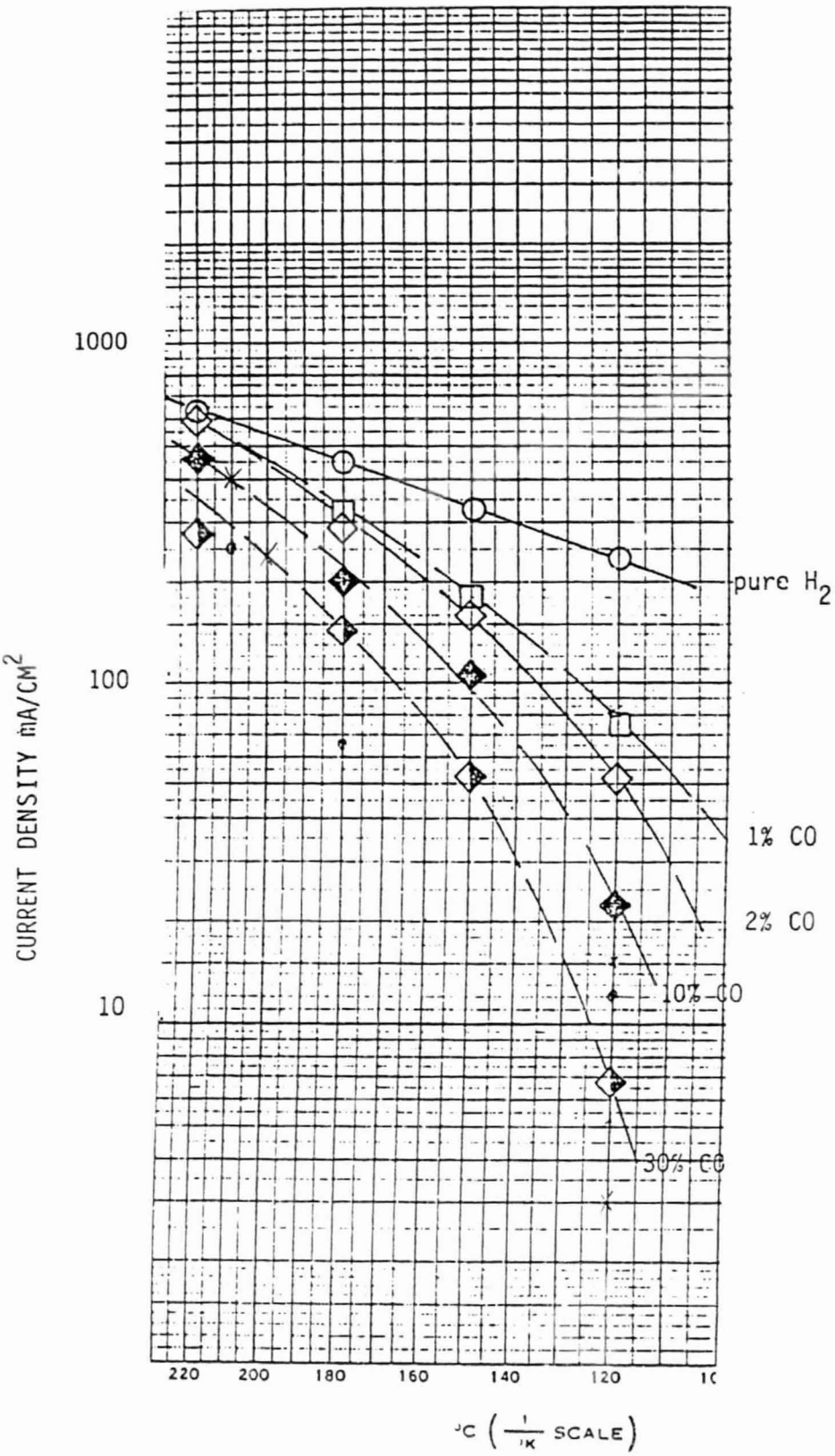

Figure 7. Activation Energies for Hydrogen Oxidation and Hydrogen Oxidation in the Presence of Carabon Monoxide. Data at 10mV Polarization vs. Hydrogen.0.5 mg Pt/cm^2

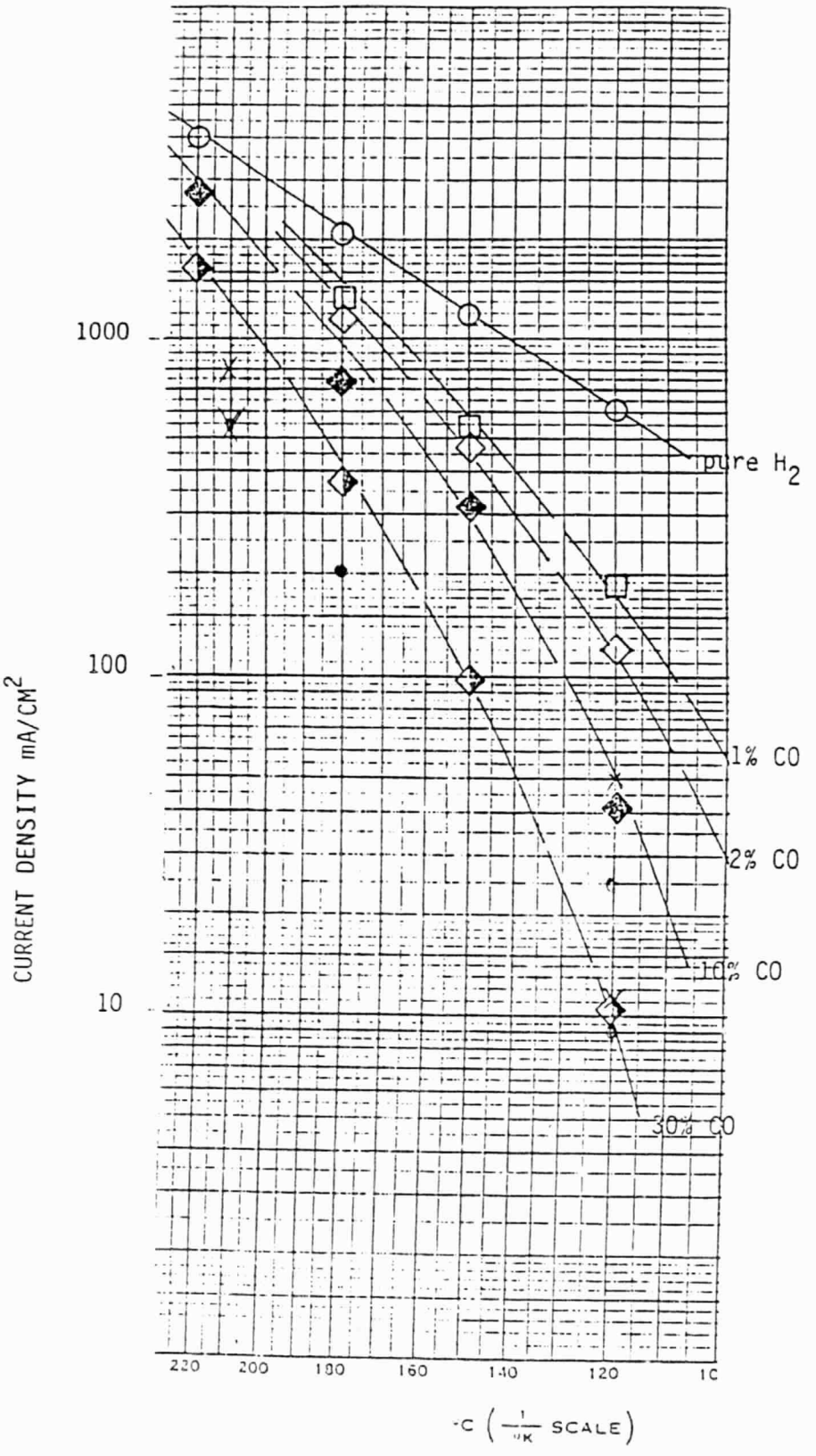

Figure 8. Activation Energies for Hydrogen Oxidation and Hydrogen Oxidation in the Presence of Carabon Monoxide. Data at 25mV Polarization vs. Hydrogen.
0.5 mg Pt/cm^2

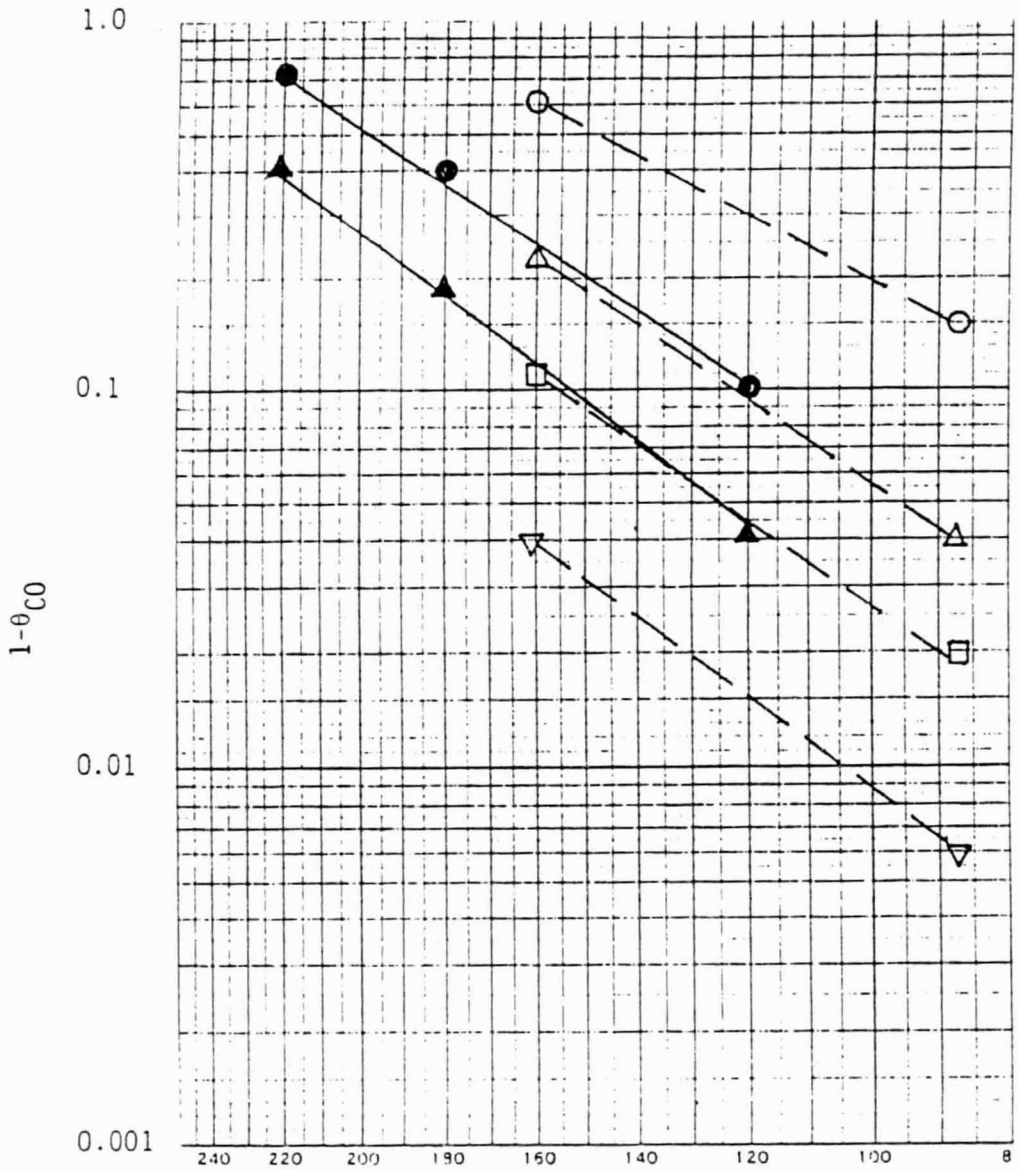

Figure 10. Apparent Arrhenius Plots for Available Platinum Surface Area Poisoned by Carbon Monoxide. Solid Points from Figure 9. Open Points from Stonehart and Ross, Electrochimica Acta, 1976. 21, 441, Figure 6.

(○) 10^{-4} atmosphere, (△) 10^{-3} atmosphere, (□) 10^{-2} atmosphere, (▽) 5×10^{-2} atmosphere, carbon monoxide with flooded electrode structures. (●) 30% carbon monoxide and (○) 10% carbon monoxide with optimized gas-diffusion electrodes, 10% .pa platinum on Vulcan XC-72R 50% PTFE.

consumed so that the carbon monoxide partial pressure at the electrocatalyst surface becomes very high. Diffusion of the carbon monoxide from the electrocatalyst surface is then inhibited when a long solution pathway is provided.

The data that were obtained in Figures 5-10 used a pure hydrogen anode feed with 0-30% carbon monoxide. The polarization data showed extremely high current densities so that kinetic limitations for hydrogen oxidation were not easily observed. In order to improve the accuracy of our measurements, polarization data were obtained using 10% hydrogen with 0-30% carbon monoxide, the balance of the gas supply being nitrogen. This had the effect of lowering the current densities at a given potential by one order of magnitude.

A series of polarization curves with flooded electrode structures as well as semi-optimized gas diffusion electrode structures were obtained on 10% Pt/Consel I over a temperature range of 120°C-210°C. A representative set of curves for the flooded electrode structures are shown in Figure 11 at 180°C. The most important feature shown by the data in Figure 11 are an offset of the open circuit potential from the reversible hydrogen potential of 45 mV which corresponds to the change in partial pressure of hydrogen in the gas supply. The current density for the 10% hydrogen curve shows a maximum at around 200 mV and is well within the capability of the instrumentation to measure and control the reaction. The observation of this maximum is thought to be original for highly dispersed platinum electrocatalysts operating on pure hydrogen. Such a maximum has, in fact, been observed previously using smooth platinum at room temperature in dilute acid solutions (see E. A. Aikasyan, A. I. Fedorova: Kokl. Akad. Nauk. USSR, 86, 1137 (1952) and G. R. Bopp,, P. Stonehart and D. M. Mason, Electrochemical Technology, 1966, 4, 416-423). With the present results, the maximum in the current density was observed to shift to more anodic potentials when the measurements were carried out in an anodic direction and towards more cathodic potentials when the curve was measured in the cathodic direction. It is probable that the maximum is due to the reversible adsorption-desorption of the phosphate ion on the platinum electrocatalyst surface. The rate constant for the peak shift was of the order of several minutes which would agree with anion adsorption-desorption kinetics. It is clear that on going to lower partial pressures of hydrogen we

have succeeeded in resolving the limiting current for the hydrogen oxidation reaction in the flooded electrode configuration.

The shapes of the curves for hydrogen oxidation in the presence of carbon monoxide show an ascending current density as the potential increases. Furthermore, the polarization lines at different carbon monoxide partial pressures are parallel. This supports our contention that desorption (or low level oxidation) of the carbon monoxide is potential dependent, so that as the potential increases, more of the platinum surface becomes available for reaction.

Electrodes formed from the same catalyst shown in Figure 11 but using higher Teflon contents were run as semi-optimized gas-diffusion electrodes. In addition, the crystallite sizes of the platinum on the Consel I were changed by subjecting some of the catalyst to a heat treatment at 935°C for one hour prior to forming into electrodes. Figure 12 shows the performance curves with 10% hydrogen and 0-30% carbon monoxide at 180°C for a platinum surface area of 80 m^2/g (post test analysis) and Figure 13 shows the equivalent performance curves on the heat-treated catalyst (60 m^2/g post test analysis). The two sets of curves shown in Figures 12 and 13 are not dramatically different. They show a small difference in current density which can be attributed to the difference in the platinum catalyst surface area. Analyses of the available platinum surface area, $(1-\theta_{CO})$, as a function of carbon monoxide gas concentration, electrode potential, and platinum crystallite surface area are given in Table 1. The overall conclusion from the tabulated data is that there appears to be no significant crystallite size effect for the carbon monoxide adsorption isotherms, although we have not yet varied the platinum crystallite size greatly. Further analyses will be carried out using a wider range of platinum electrocatalyst crystallite sizes.

A comparison of the available platinum surface from the carbon monoxide polarization data is shown for the flooded and unflooded electrodes in Figure 14. This is done as a pseudo-Arrhenius plot for comparison to Figure 10. The data show conclusively that the poisoning by carbon monoxide on flooded electrodes is significantly greater than on semi-optimized gas-diffusion electrodes. The apparent activation energy lines for all the data are

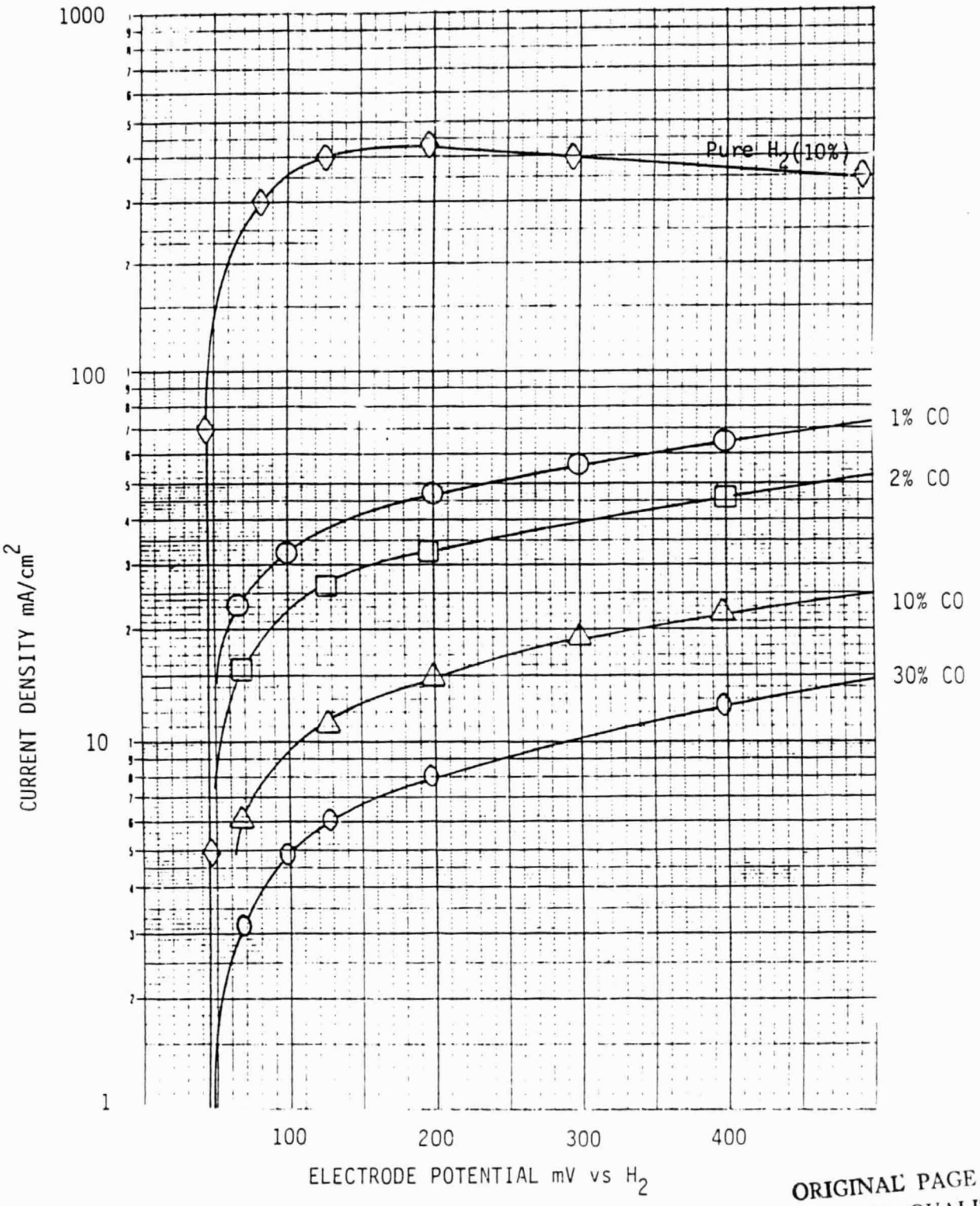

ORIGINAL PAGE IS
OF POOR QUALITY

Figure II. iR Free Polarization Curves for Hydrogen Oxidation and the Influence of Carbon Monoxide on 10% Platinum Crystallites Supported on Consel (steam-treated acetylene black). Flooded Electrode Structure.
180°C 102% H_3PO_4 10% H_2 Balance N_2. 0.51 mg Pt/cm^2. 2.5% PTFE

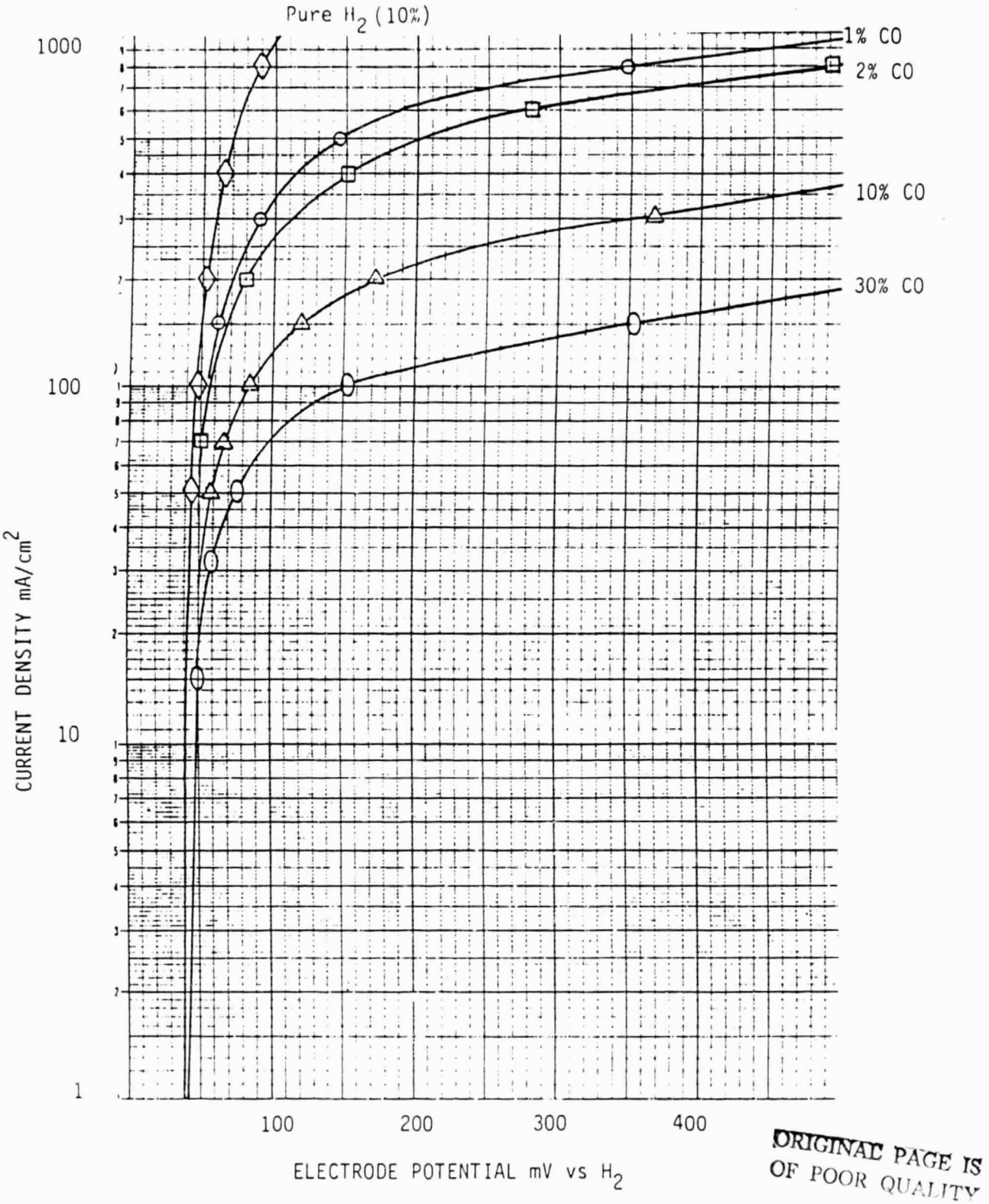

Figure 12. iR Free Polarization Curves for Hydrogen Oxidation and the Influence of Carbon Monoxide on 10% Platinum Crystallites Supported on Consel I (steam-atreated acetylene black). Semi-optimized Electrode Structure.
180%°C 102% H_3PO_4 10% H_2 Balance N_2. 0.5 mg Pt/cm^2. 30% PTFE. Platinum Surface Area 80 m^2/g post-test analysis.

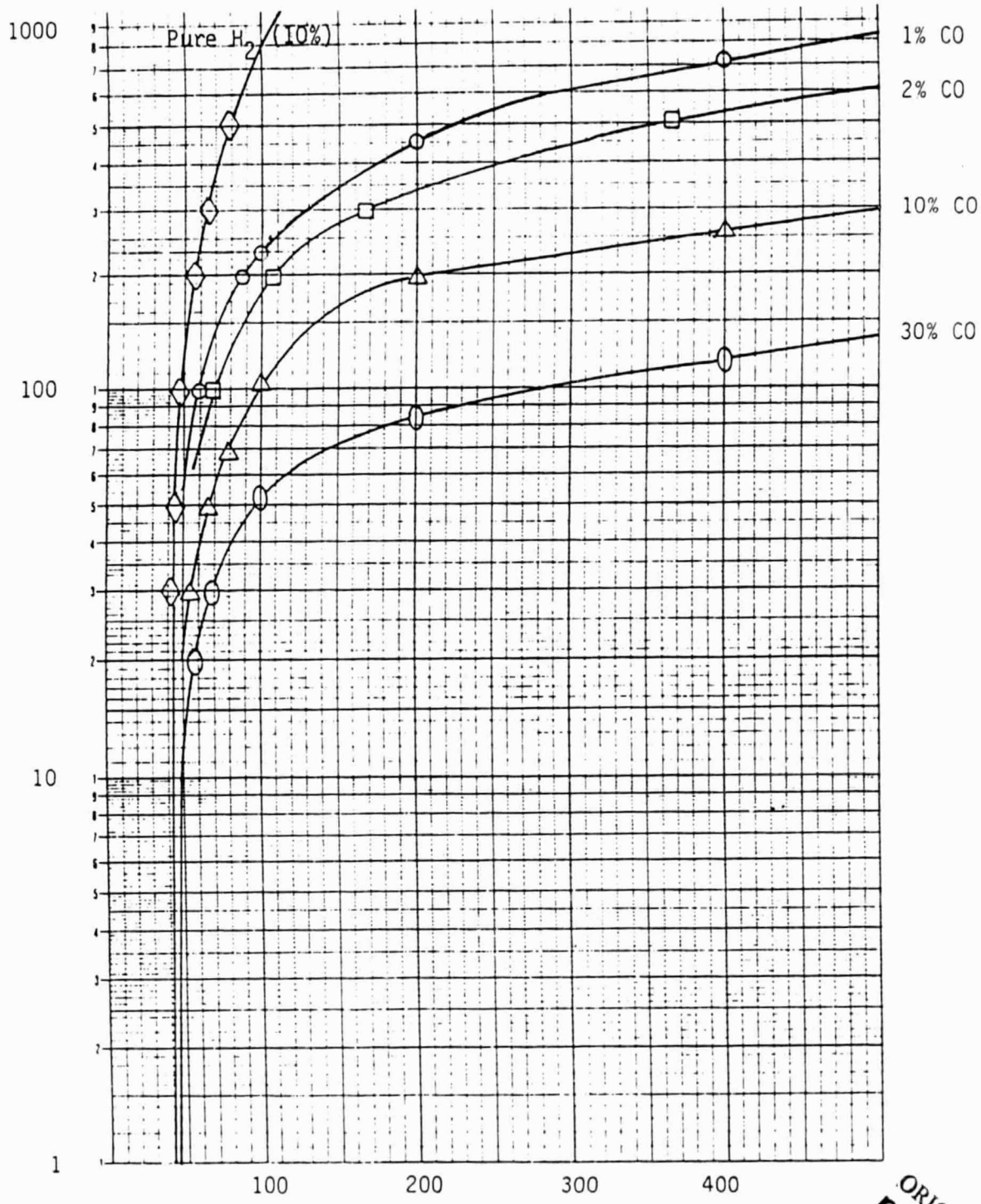

Figure 13. iR Free Polarization Curves for Hydrogen Oxidation and the Influence of Carbon Monoxide on 10% Platinum Crystallites Supported on Consel I (steam-treated acetylene black). Semi-optimized Electrode Structure.
180°C 102% H_3PO_4 10% H_2 Balance N_2. 0.5 mg Pt/cm^2. 30% PTFE. Platinum Electrocatalyst Heat Treated at 935°C for One Hour prior to Electrode Fabrication. Platinum Surface Area 60 m^2/g post-test analysis.

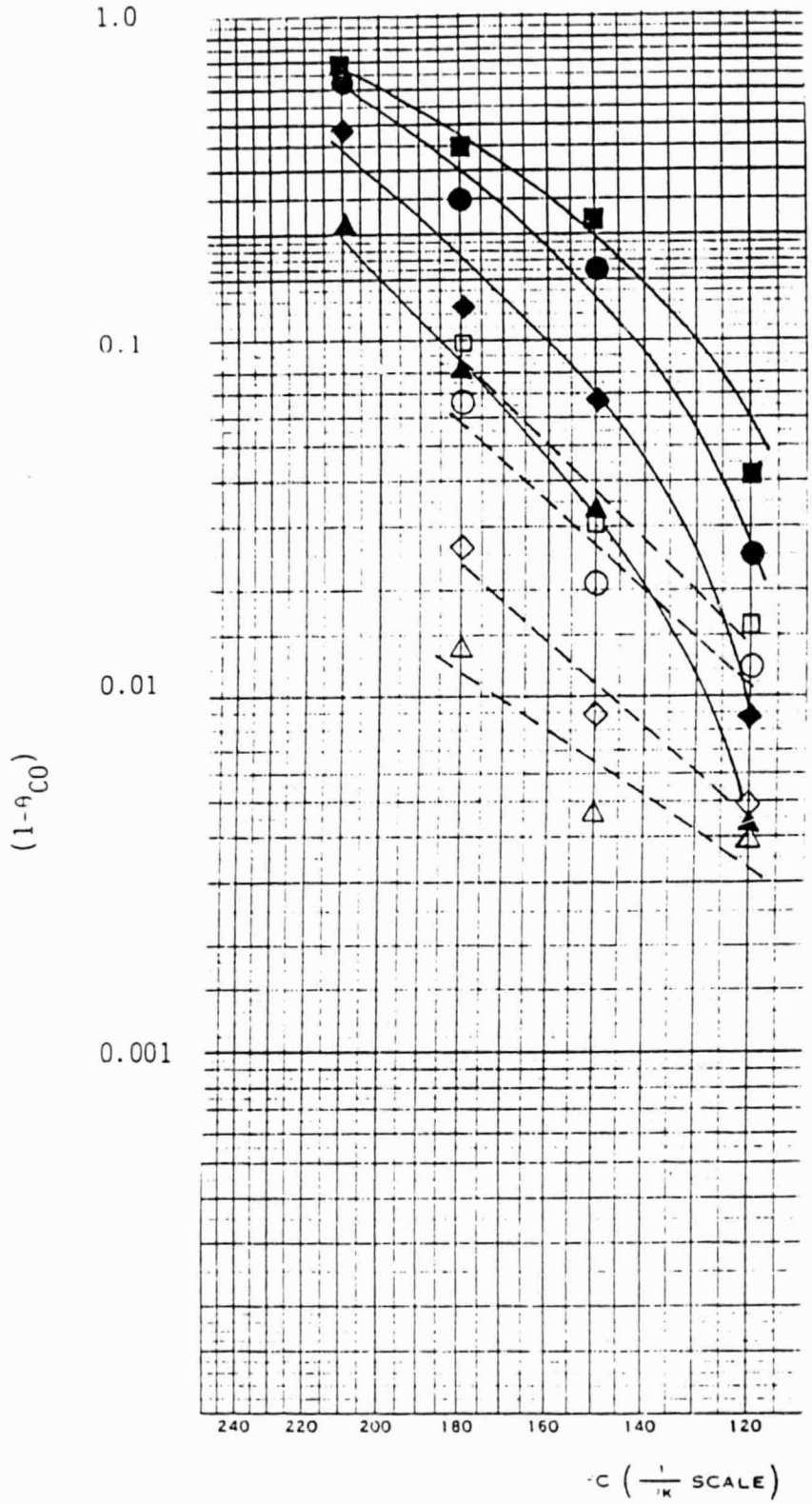

Figure 14. A Comparison of Apparent Available Platinum Surface Area for Flooded and Unflooded Electrode Structures. Solid points denote semi-optimized gas-diffusion electrode structures. Open points denote flooded electrode structures. Circles for 1% carbon monoxide, squares for 2% carbon monoxide, diamonds for 10% carbon monoxide and triangles for 30% carbon monoxide. Pt on Consel I carbon support.

constant within the limits of error. On comparing the data in Figure 14 with Figure 10, it is apparent that the electrolyte film on Consel I is thicker than the electrolyte film contained on Vulcan XC-72R.

It appears that we have a sensitive technique for the measurement of the electrolyte film within a porous electrode structure and thereby a quantitative measure of electrode structures.

A critical feature determining the performance for anodes was not so much the true adsorption isotherm for carbon monoxide on the platinum but diffusion of the carbon monoxide out of the electrode structure after the hydrogen had been oxidized. It is easy to see that the carbon monoxide levels within the porous electrode structure must increase as the hydrogen in the gas stream is electrochemically oxidized. This will set up a concentration gradient between the carbon monoxide concentration within the porous structure and carbon monoxide concentration in the bulk gas phase.

In order to further resolve the operation of porous electrodes in the presence of carbon monoxide/hydrogen mixtures, the polarization characteristics of a series of electrode structures containing different PTFE levels were determined. It should be possible to produce a smooth transition from a fully flooded electrode to a highly efficient gas diffusion electrode and measure the characteristic polarizations as a function of PTFE level. The polarization data are shown in Figures 15-18 using 2-1/2%, 10%, 20%, and 30% PTFE, respectively. In all instances the electrocatalyst was 10% platinum on steam-treated acetylene black (Consel I). Electrode performances were obtained on pure hydrogen, 10% hydrogen, and 10% hydrogen containing 1%, 2%, 10% and 30% carbon monoxide.

The data shown in Figures 15-18 show an abrupt transition in performance with PTFE level between 10% and 20%. It is possible that there are other parameters for forming the electrode structures that we do not have under sufficient control.

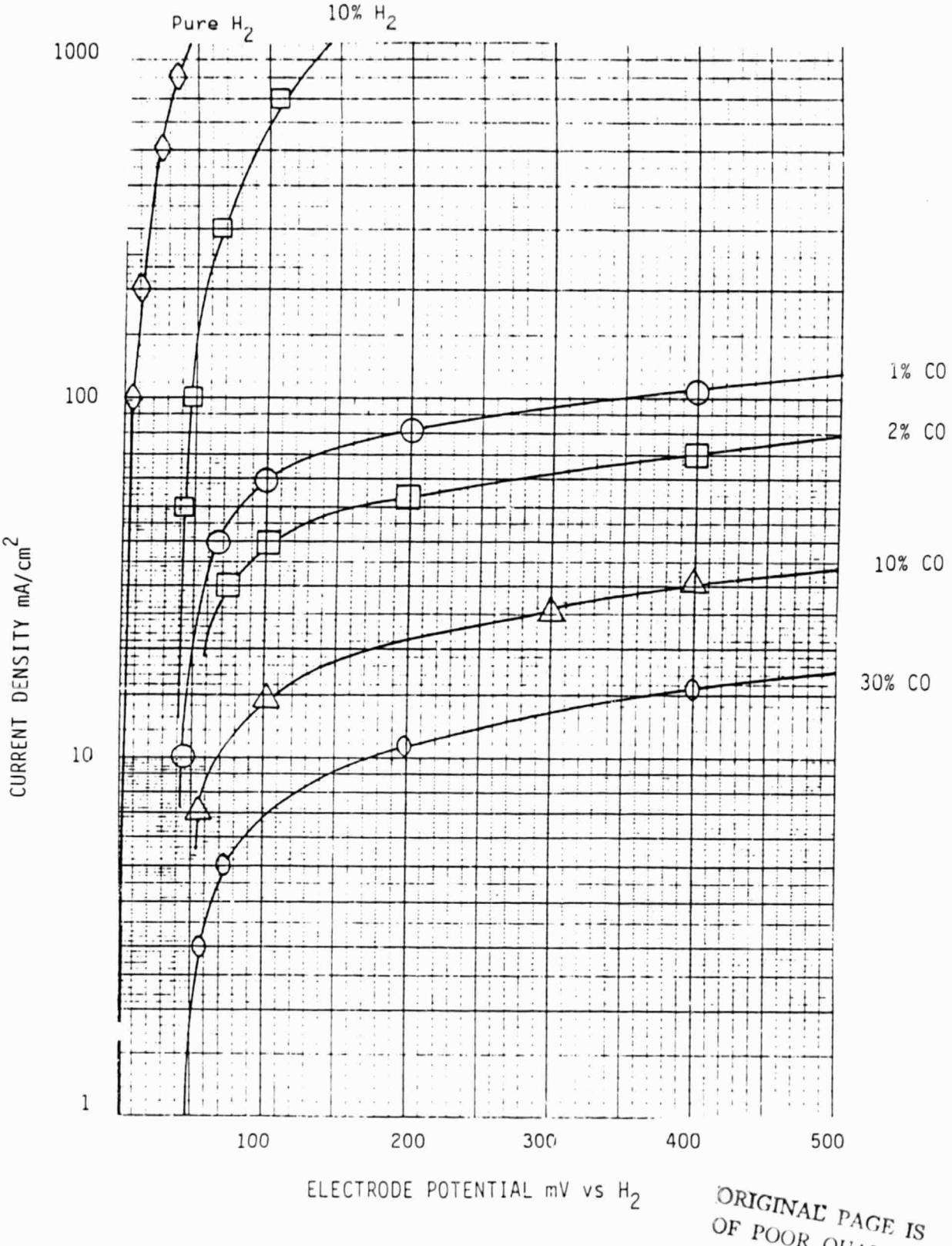

Figure 15. iR free polarization curves for hydrogen oxidation with various additions of CO to 10% H_2/N_2 fuel gas. Electrode contains 2-1/2% PTFE, 0.5 mg Pt/cm^2, was made from 10% Pt/Consel I and run at 180°C in 100% H_3PO_4.

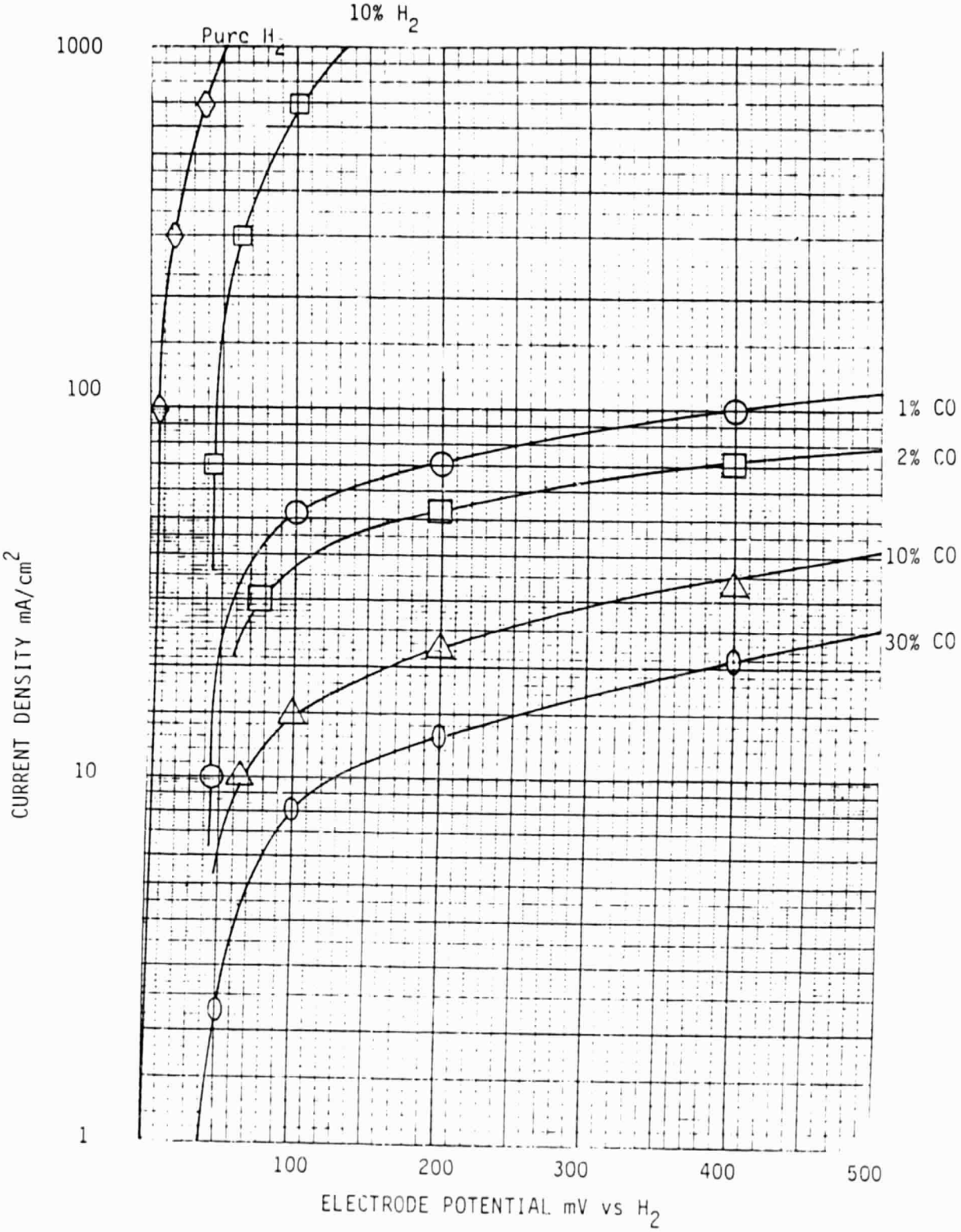

Figure 16. iR Free polarization curves for hydrogen curves for hydrogen oxidation with various additons of CO to 10% H_2/N_2 fuel gas. Electrode contains 10% PTFE, 0.5 mg Pt/cm^2, was made from 10% Pt/Consel I and run at 180°C in 100% H_3PO_4.

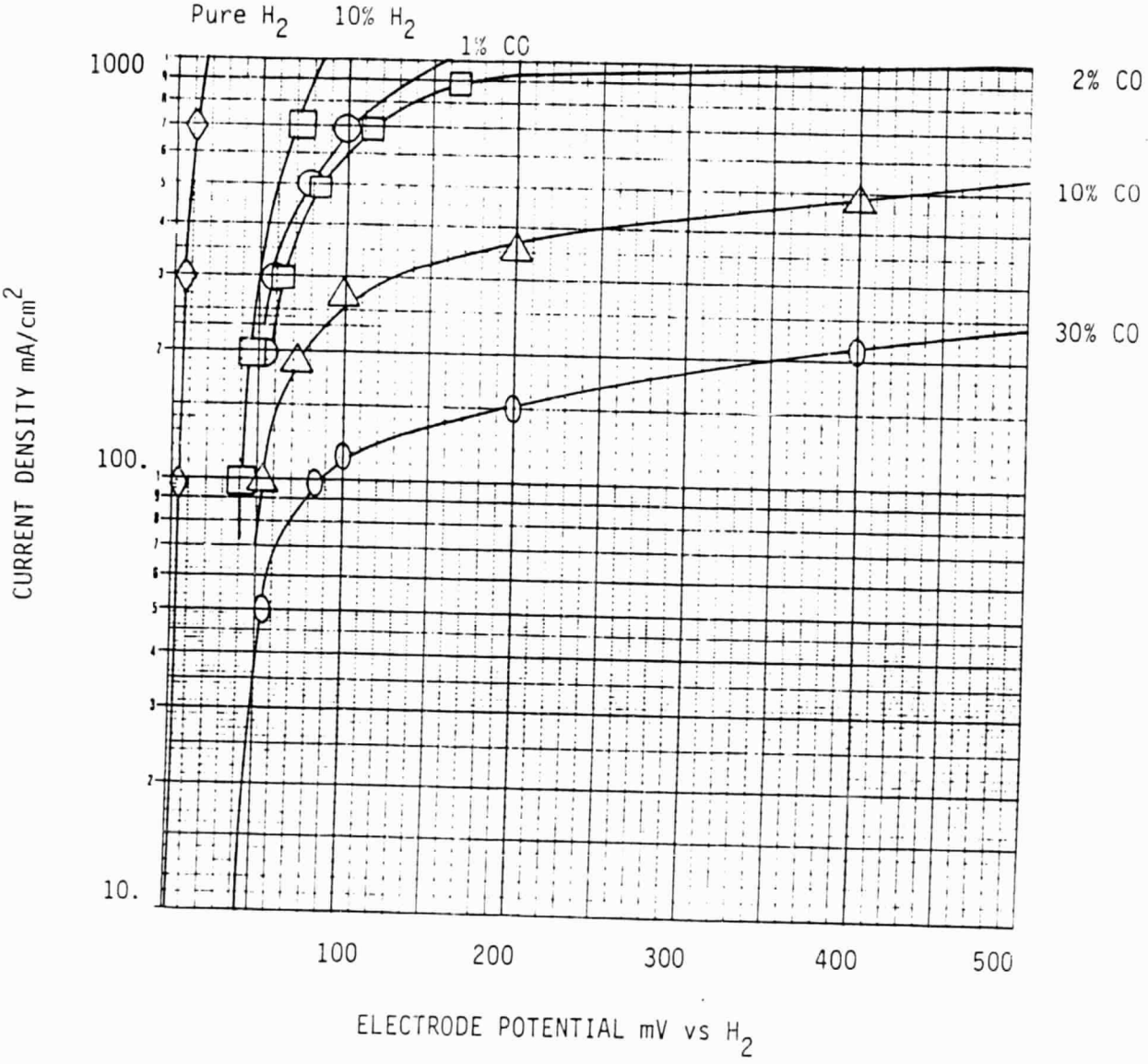

Figure 7. iR free polarization curves for hydrogen oxidation with various additions of CO to 10% H_2/N_2 fuel gas. Electrode contains 20% PTFE, 0.5 mg Pt/cm^2, was made from 10% Pt/Consel I and run at 180°C in 100% H_3PO_4.

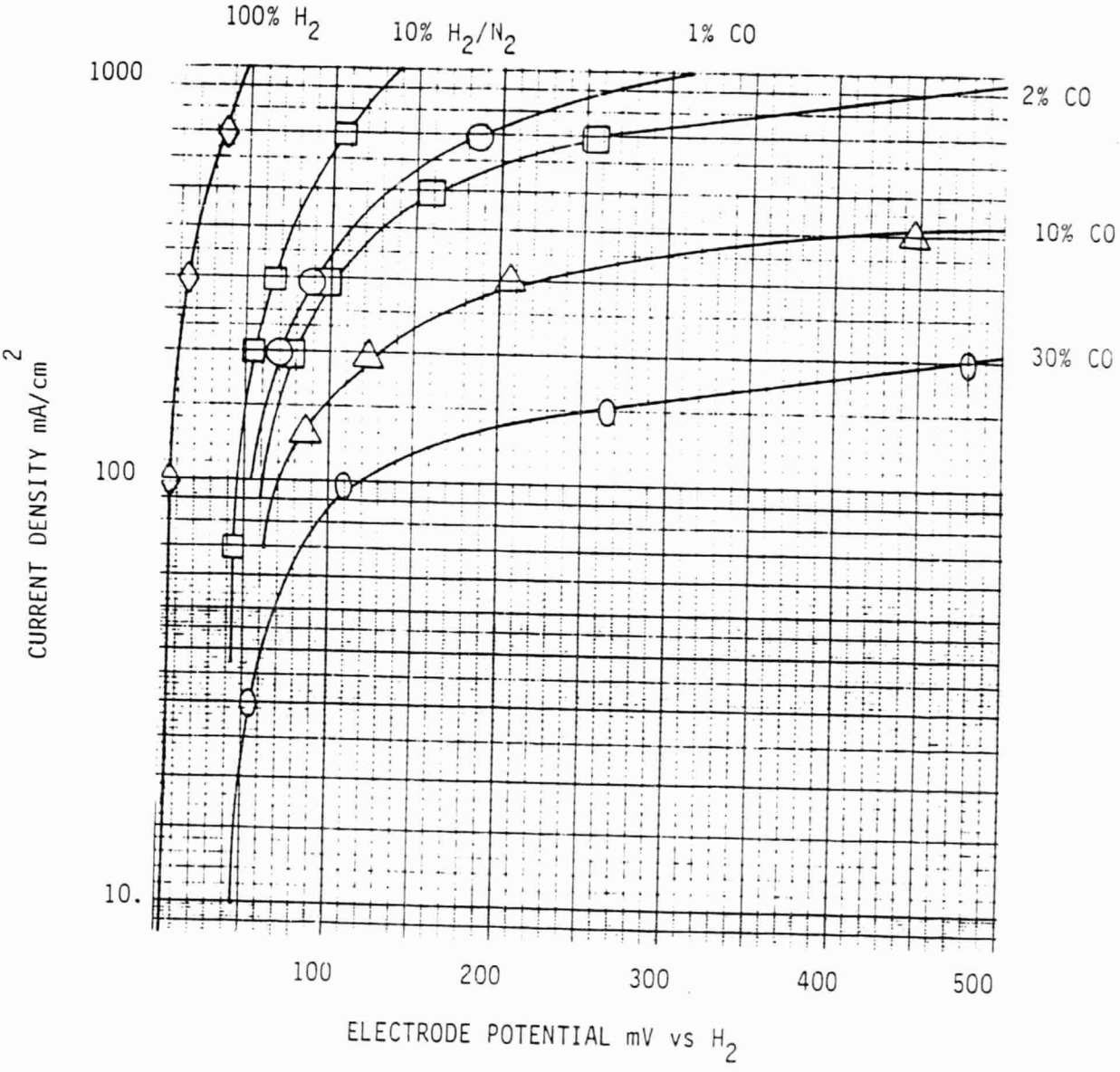

Figure 18. iR free polarization curves for hydrogen oxidation with various additons of CO to 10% H_2/N_2 fuel gas. Electrode contains 30% PTFE, 0.5 mg Pt/cm^2, was made from 10% Pt/Consel I and run at 180°C in 100% H_3PO_4.

TABLE I

Comparison of Available Platinum Surface ($1-\theta_{CO}$) as a Function of Carbon Monoxide Gas Concentration, Electrode Potential and Pt Crystallite Surface Area When Operating As an Anode

10mV Polarization

	120°C	150°C	180°C	210°C
	80 m^2/g-60 m^2/g	80 m^2/g-60 m^2/g	80 m^2/g-60 m^2/g	80 m^2/g-60 m^2/g
1% CO	0.073 - 0.092	0.22 - 0.20	0.47 - 0.47	0.54 - 0.57
2% CO	0.047 - 0.066	0.17 - 0.13	0.36 - 0.34	0.57 - 0.53
10% CO	0.017 - 0.023	0.08 - 0.07	0.18 - 0.17	0.42 - 0.41
30% CO	0.0086 - 0.010	0.04 - 0.04	0.10 - 0.12	0.20 - 0.23

25mV Polarization

	120°C	150°C	180°C	210°C
	80 m^2/g-60 m^2/g	80 m^2/g-60 m^2/g	80 m^2/g-60 m^2/g	80 m^2/g-60 m^2/g
1% CO	0.052 - 0.065	0.22 - 0.19	0.41 - 0.39	0.58 - 0.56
2% CO	0.036 - 0.045	0.16 - 0.11	0.32 - 0.30	0.59 - 0.52
10% CO	0.013 - 0.017	0.07 - 0.05	0.16 - 0.16	0.42 - 0.39
30% CO	0.006 - 0.008	0.03 - 0.02	0.09 - 0.09	0.22 - 0.24

60mV Polarization

	120°C	150°C	180°C	210°C
	80 m^2/g-60 m^2/g	80 m^2/g-60 m^2/g	80 m^2/g-60 m^2/g	80 m^2/g-60 m^2/g
1% CO	0.040 - 0.055	0.22 - 0.14	0.35 - 0.30	0.60 - 0.50
2% CO	0.025 - 0.038	0.16 - 0.085	0.26 - 0.24	0.54 - 0.43
10% CO	0.009 - 0.013	0.068 - 0.036	0.13 - 0.14	0.40 - 0.32
30% CO	0.004 - 0.007	0.032 - 0.018	0.07 - 0.07	0.21 - 0.22

In order to identify the formation and relaxation of the carbon monoxide concentration gradient within the porous electrodes, the electrode structures were subjected to a series of perturbation experiments. In these experiments the electrodes were maintained under the different gas environments and switched both potentiostatically or galvanostatically from the open circuit values to some characteristic operating value. After maintaining this operating characteristic for a short period of time, the electrode was

restored to the open circuit condition. The current and potential transients were recorded digitally using a transient analyzer. This was displayed on an oscilloscope and recorded on our XY recorder. By recording the information digitally, we were able to analyze the transients point by point.

Representative displays of the actual relaxation curves for the galvanostatic transients are shown in Figures 19 and 20. These curves were reproduced onto the paper directly from the XY recorder and have been scaled manually. The experimental conditions are defined in the legends of the figures. Analyses of the relaxation curves are given in Table II.

TABLE II

Current Pulse Relaxation Time from Steady State as a Function of PTFE Levels

Electrodes at 180°C 10% Pt On Consel I
Nominal Anode Gas Environment 2% CO; 10% H_2; 88% N_2

PTFE Level	Current Pulse	Half Time to Max. Potential	Half Time to Relax to Open Circuit
2.5%	100 mA	5.8 sec.	0.78 sec.
10.0%	100	2.0	0.84
20.0%	1000	0.05	0.015
30.0%	1000	0.008	0.007

Here we have chosen to show the half time to reach the maximum potential and the half time after removing the galvanostatic transient to relax back to open circuit conditions. Due to the very great differences in performances between the 2-1/2% and 10% on the one hand and the 20% and 30% PTFE levels on the other hand, two current densities were used. For the former electrodes, a 100 mA perturbation was used, and in the latter cases, a 1000 mA perturbation was used. The relaxations given in Table II are for gas stream containing nominally 10% hydrogen, 2% carbon monoxide and 88% nitrogen. Other relaxation curves were obtained at different carbon monoxide levels, but they are not shown in this report. Table II clearly shows the trend in relaxation times that we had expected intuitively. What is surprising is the very large differences in relaxation times between the flooded electrode structures (2-1/2% PTFE) and the electrode containing 30% PTFE. There is a thousand times difference in the characteristic half times which suggests that measurements of this sort are indeed very sensitive to the the electrode structures and

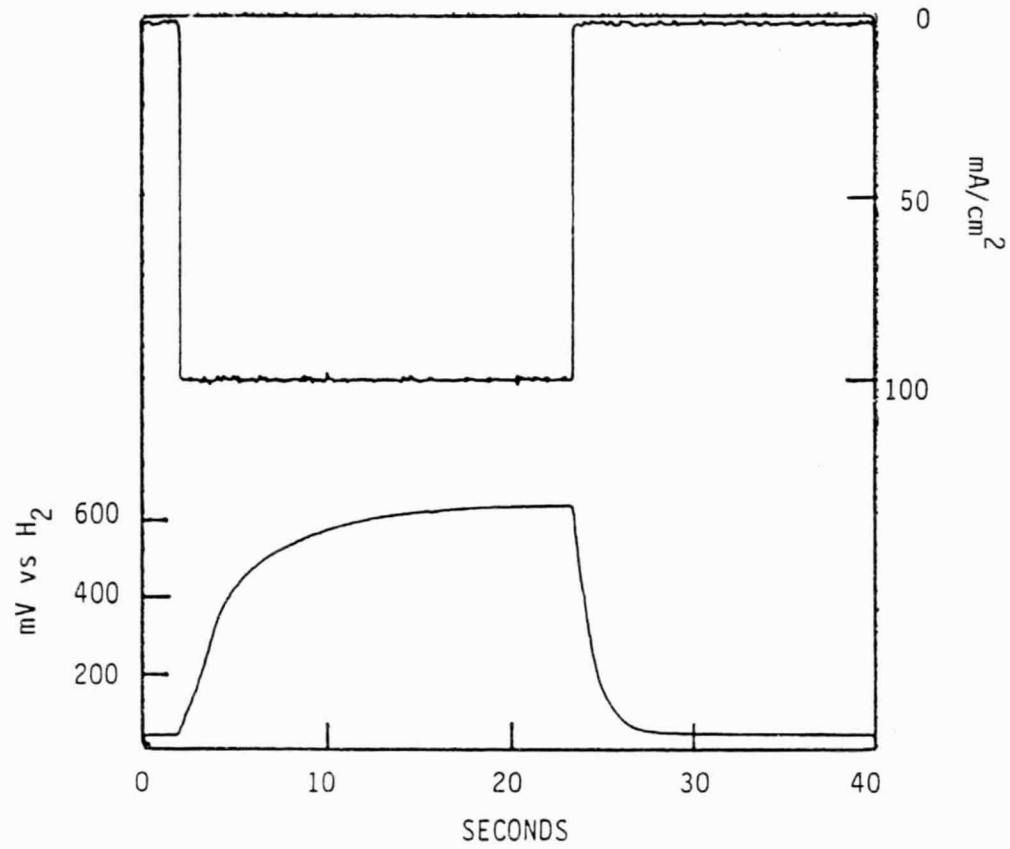

Figure 19. Response of an electrode containing 2-1/2% PTFE to a galvanostatic transient (0 to 100mA). Upper trace is applied galvanostatic transient. Lower trace is potential response. Electrode contains 2-1/2% PTFE, 0.5 mg Pt/cm^2, was made from 10% Pt/Consel I and run at 180°C in 100% H_3PO_4, on 2% CO, 10% H_2, 88% N_2.

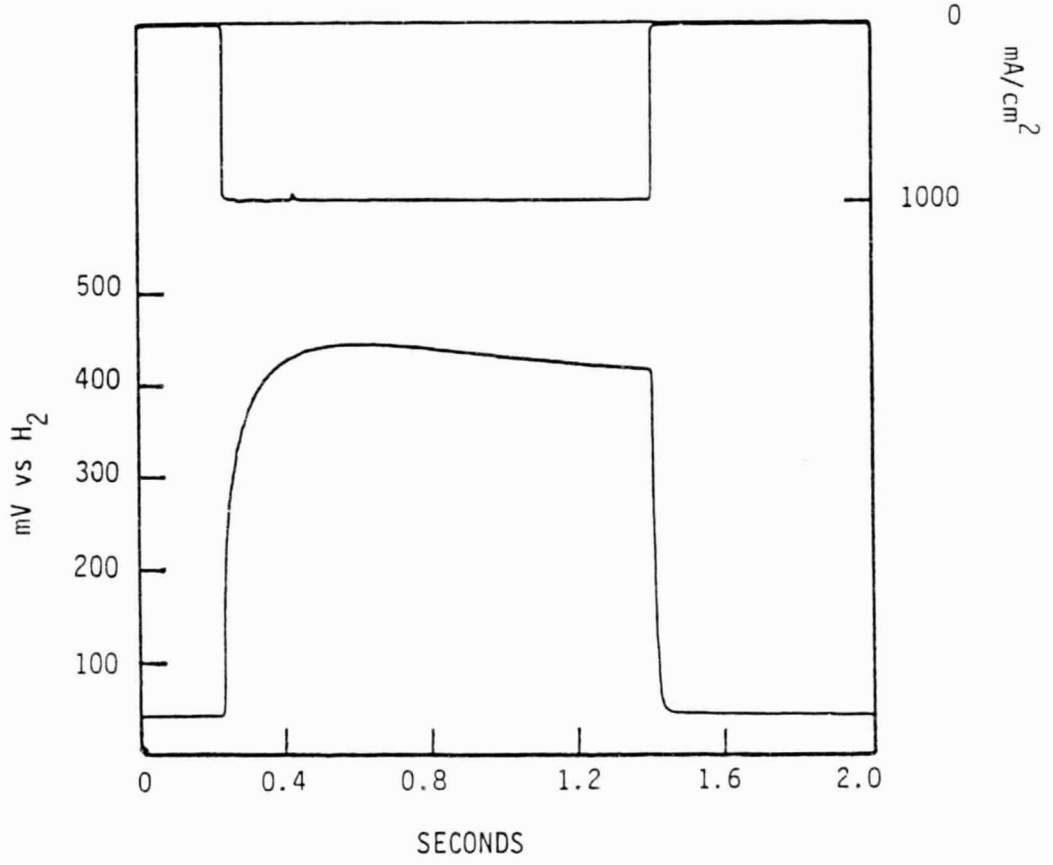

Figure 20. Response of an electrodee containing 30% PTFE to a galvanostatic transient (0 to 1000mA). Upper trace is applied galvanostatic transient. Lower trace is potential response. Electrode contains 30% PTFE, 0.5 mg Pt/cm^2, was made from 10% Pt/Consel I and run at 180°C in 100% H_3PO_4, on 2% CO, 10% H_2, 88% N_2.

electrolyte films on the electrocatalysts within the electrode structures. Following the galvanostatic relaxation curves, a series of potentiostatic transients were also obtained on these electrodes in order to provide further information regarding the carbon monoxide diffusion out of the electrode structure as the limiting factor in controlling the performance of the porous gas diffusion electrodes.

Figures 21 and 22 show representative responses of electrodes containing 2-1/2% and 30% PTFE with a potential step. The potential step was greater for the 2-1/2% and 10% PTFE electrodes since the response times were slower than the response times for the 20% and 30% PTFE electrodes. The potentiostatic transient causes an instantaneous charging of the double-layer which then decays due to the transmission line through the electrode structure. This response is shown as the upper line in Figures 21 and 22. The half times for relaxation back to open circuit are given in Table III. Only the sets of data for a nominal gas anode stream of 2% carbon monoxide, 10% hydrogen and 80% nitrogen are shown. Other relaxation curves were obtained at different carbon monoxide levels but they are not shown in this report.

TABLE III
Potential Pulse Relaxation Time as a Function of PTFE Levels

Electrodes at 180°C 10% Pt on Consel I
Nominal Anode Gas Environment 2% CO; 10% H_2; 88% N_2

PTFE Level	Potential Step Height	Half-Time To Relax to Open-Circuit
2.5%	650 mV	0.8 sec.
10.0%	700	0.7
20.0%	200	0.006
30.0%	380	0.004

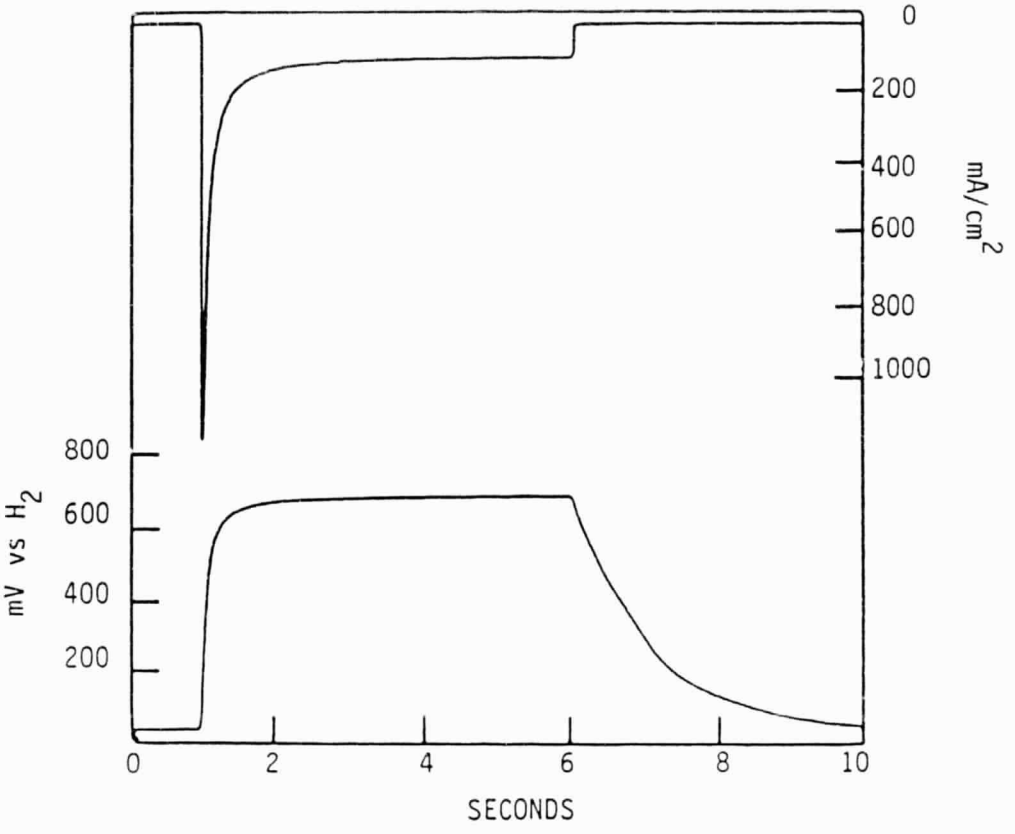

Figure 21. Response of an electrode containing 2-1/2% PTFE to a potentiostatic transient (o.c. to 650mV). Upper trace is current response. Lower trace is potential response. Electrode contains 2-1/2% PTFE, 0.5 mg Pt/cm^2, was made from 10% Pt/Consel I and run at 180°C in 100% H_3PO_4, on 2% CO, 10% H_2, 88% N_2.

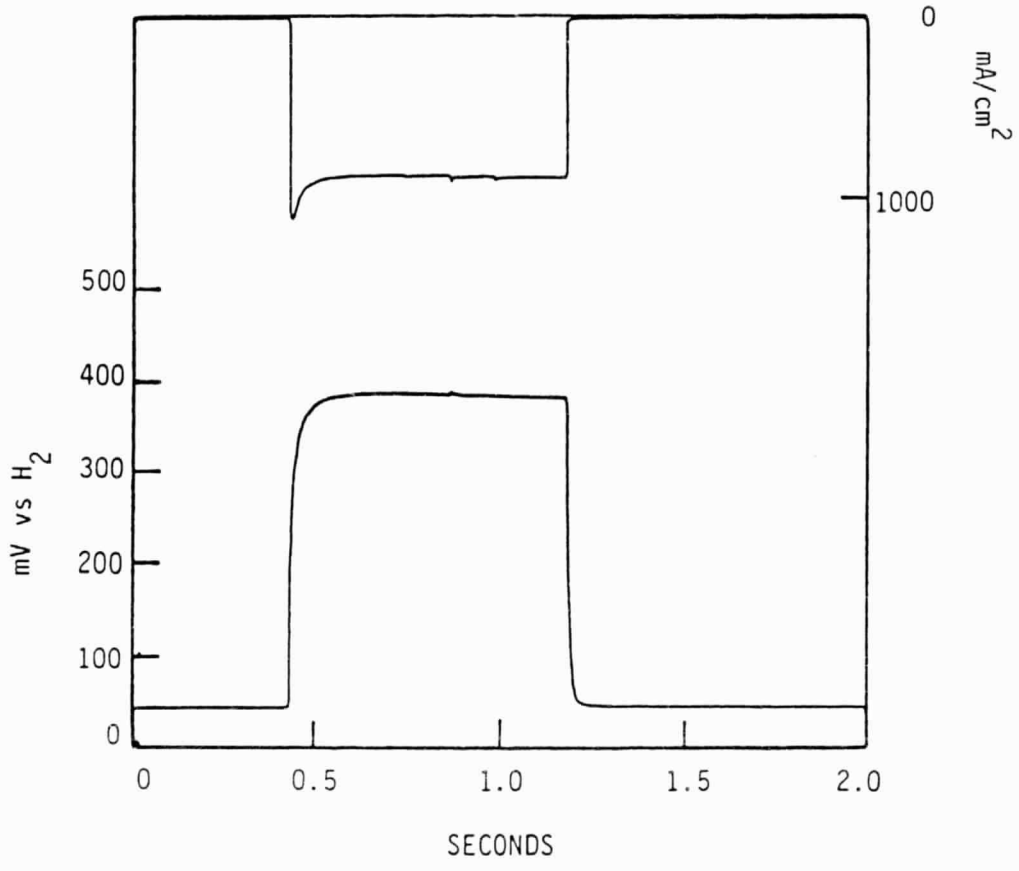

Figure 22. Response of an electrode containing 30% PTFE to a potentiostatic transient (o.c. to 380mV). Upper trace is current response. Lower trace is potential response. Electrode contains 30% PTFE, 0.5 mg Pt/cm^2, was made from 10% Pt/Consel I and run at 180°C in 100% H_3PO_4, on 2% CO, 10% H_2, 88% N_2.

Task 3 - Cathodic Activity of Platinum-Carbon Electrocatalysts

Some of the experimental electrocatalysts produced under Task 1 were formed into electrode structures with low amounts of PTFE in order to fabricate fully flooded structures. An important characterization of any electrocatalyst is the polarization characteristic of the electrocatalyst under load. An unequivocal determination of catalytic performance is not possible using gas diffusion Teflon bonded electrodes. In addition to the activation polarization, which we want to measure, there is always included some gas diffusion polarization. The activation polarization measures the activity of the catalyst, but the diffusion polarization measures the efficiency of the structure. It is not always possible to measure the catalytic activity free of electrode structural effects.

Several models have been proposed to explain the operation of a supported platinum gas diffusion electrode. The theory modified by Kosinski as explained by Kunz and Gruver (J. Electro. Chem. Soc. 122, No. 10, p. 1279, 1975) predicts that under activation control, an electrode shows a single Tafel slope region where the current at a given potential varies linearly with the catalyst loading. Under diffusion control, a double Tafel slope occurs where the current at a given potential varies as the square root of the loading.

This model was felt to be a good tool for determining whether an electrode is operating under diffusion or activation control. We have previously shown a linear relationship with loading for gas diffusion electrodes containing 50% PTFE. In order to prove the theory, one must show a square root relationship between current density at a given potential versus loading. The purpose for forming electrodes with flooded structures is to develop a tool for determining the difference between a "good" or a "poor" electrode structure, and thereby, a quantitative determination of electrocatalytic activity for these experimental electrocatalysts.

In order to be sure that the electrodes were "flooded", only 2.5% PTFE was used to bond the electrode structure together. These electrodes were placed on a wetproofed carbon paper substrate and run in hot phosphoric acid at

180°C, Ø.6V under air for 64 hours in order to fully flood the electrode structures. It was found that the electrode performance was invariant over the 64 hour period in question. The performances of these electrodes under air and under oxygen conditions (neither gas humidified) is shown in Figure 23 for oxygen and in Figure 24 for air over a temperature range between 120°C and 210°C. Remarkably straight lines are obtained for all the data extending over two orders of magnitude in the logarithm of the current axis. If the electrode structures are indeed flooded, then the electrocatalysts must be operating in the kinetics + diffusion mode. As a consequence, the observed slopes for the change in electrode potential as a function of decade change in the logarithm of the current density would be exactly twice the true Tafel slope in the absence of any influence for diffusion. The results of the "double" Tafel slopes shown in Figures 23 and 24 are tabulated in Table IV.

TABLE IV

Comparison of "Double" and Single Tafel Slopes for Oxygen Reduction as a Function of Temperatures

Temperature °C	Oxygen DTS mV	Oxygen (TS) mV	Air DTS mV	Air (TS) mV	Tafel Slope on Air
122	215	107	-	-	-
122	-	-	190	95	-
139	-	-	-	-	100
152	208	104	-	-	-
152	-	-	185	92	-
157	-	-	-	-	105
180	200	100	180	90	115
200	-	-	-	-	100
210	200	100	190	95	-
228	-	-	-	-	90

Table IV shows the double Tafel slope and the derived singular true Tafel slope for the electrodes shown in Figures 23 and 24 together with the Tafel slopes obtained on air from Figure 5, Technical Report #14 (DE-AC03-78ET15365). The agreement is quite remarkable. Several features should be noted and they are: i) The derived Tafel slope on oxygen is greater than the derived Tafel slope on air for flooded electrode structures. This is probably due to the influence of water formation at the higher current densities under oxygen reduction skewing the Tafel slopes. ii) The derived Tafel slope on air is most probably closest to the correct value and it is significant that it does not appear to change with temperature. This means that the transfer

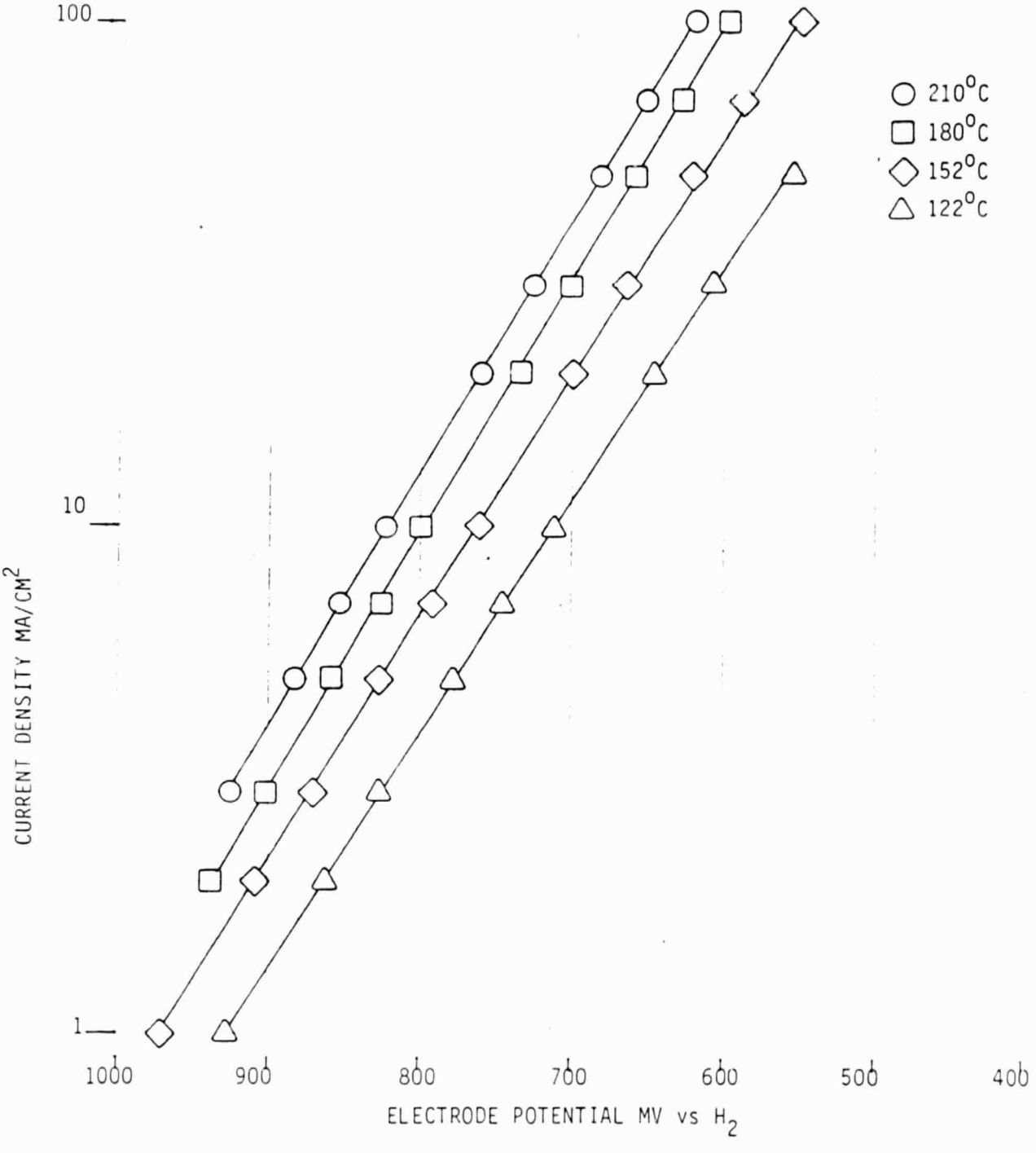

Figure 23. Polarization curves for oxygen reduction at various temperatures in 100% H_3PO_4. Catalyst is 10% platium on acetylene black. Electrode contains 2.5% PTFE and 0.50 mg Pt/cm^2. The electrode was tested on 100% dry O_2.

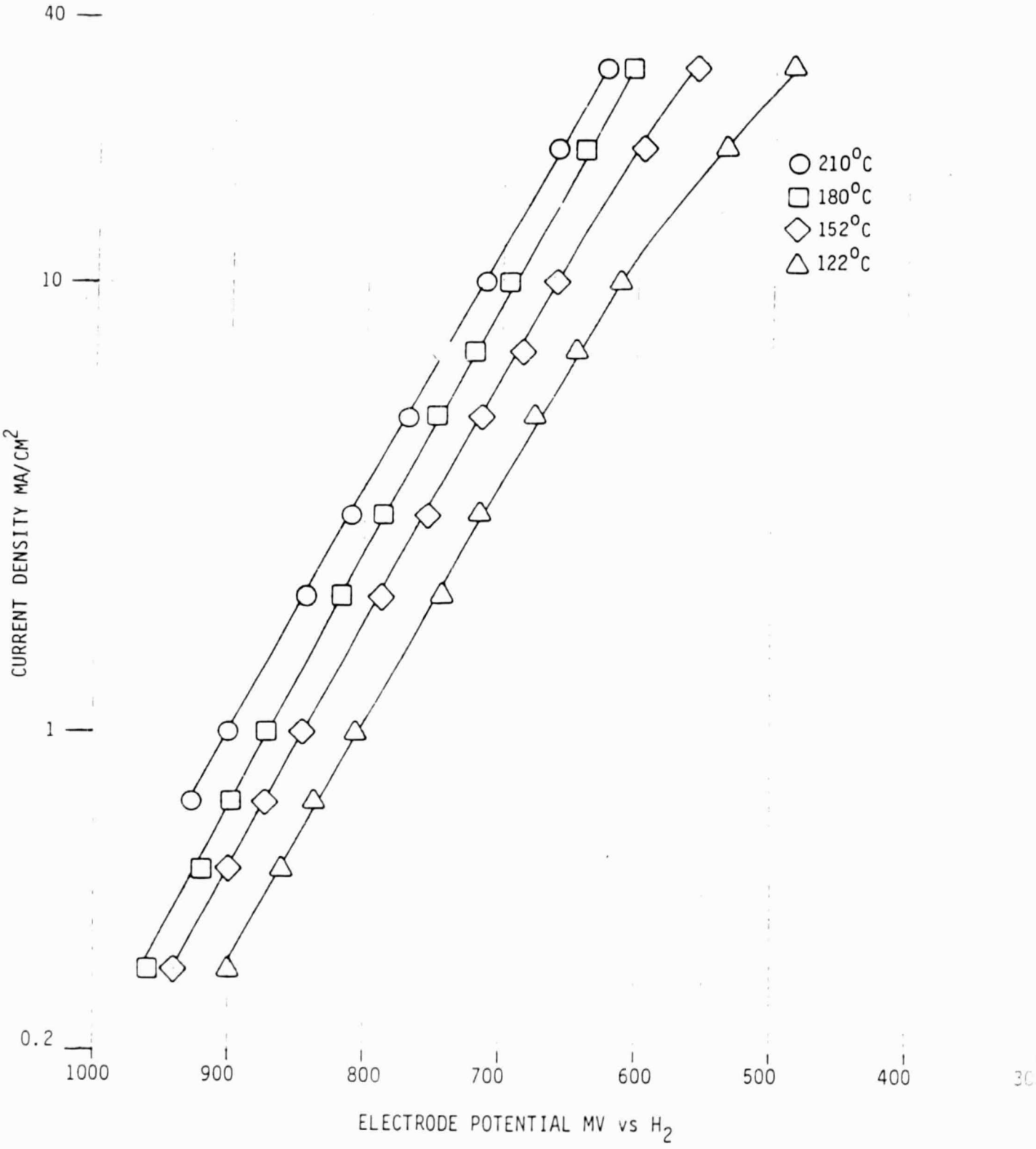

Figure 24. Polarization curves for oxygen reduction at various temperatures in 100% H_3PO_4. Catalyst is 10% platinum on acetylene black. Electrode contains 2.5% PTFE and 0.50 mg Pt/cm^2. The electrode was tested on dry air.

coefficient is not independent of temperature or that there are multiple pathways acting in a compensating mode. iii) The Tafel slopes obtained with high PTFE concentrations are greater than the derived Tafel slopes obtained in air on the flooded electrode structures. This confirms our belief that there was a diffusion contribution to the gas-diffusion electrode structures used previously and, therefore, we have not observed the true kinetic rate for the electrocatalytic materials. iv) The ratios of the apparent current densities under oxygen and under air in the flooded electrode structures are not the 5:1 ratios that one would expect from the differences in concentrations of oxygen in the gas streams. This is due probably to the influence of water vapor pressure since the observed ratios are approximately 4:1.

The apparent activation energies for oxygen reduction and the reduction of oxygen in air are shown in Figure 25 from Figures 23 and 24 using the potential of 700 mV vs the reversible hydrogen electrode in both instances. The apparent activation energy is of the order of 5 K cal, which is approximately the value that we would expect if the diffusion activation energy and the apparent kinetic activation energies are similar. Since we are most interested in the activity as a function of the overvoltage for oxygen reduction, we have replotted Figures 23 and 24 into Figures 26 and 27, taking into account the changing oxygen reversible potential with temperature and water concentration. Figures 26 and 27 should be compared to DE-AC03-78ET15365, Tech. 14, Figure 10. Activation energies are then derived from Figures 26 and 27 in Figure 28 at a constant overpotential of 500 mV. The activation energy is of the order of 11 K cal which is lower (as expected) than the 15 K cal shown in DE-AC03-78ET15365 Tech. 14, Figure 11.

There are several considerations to be taken into account when running electrode structures in concentrated acid solutions where one of the products of the electrode reaction is water.

In the first instance, it is important to confirm that the apparent true Tafel slope obtained for oxygen in air reduction is invariant with temperatures over the range of 120-230°C and is about 92 mV per decade change in current density. Kunz and Gruver (JECS, 1975, 122, 1284, Figure 12) showed that for their experimental data up to 160°C, an invariance in the apparent Tafel slope

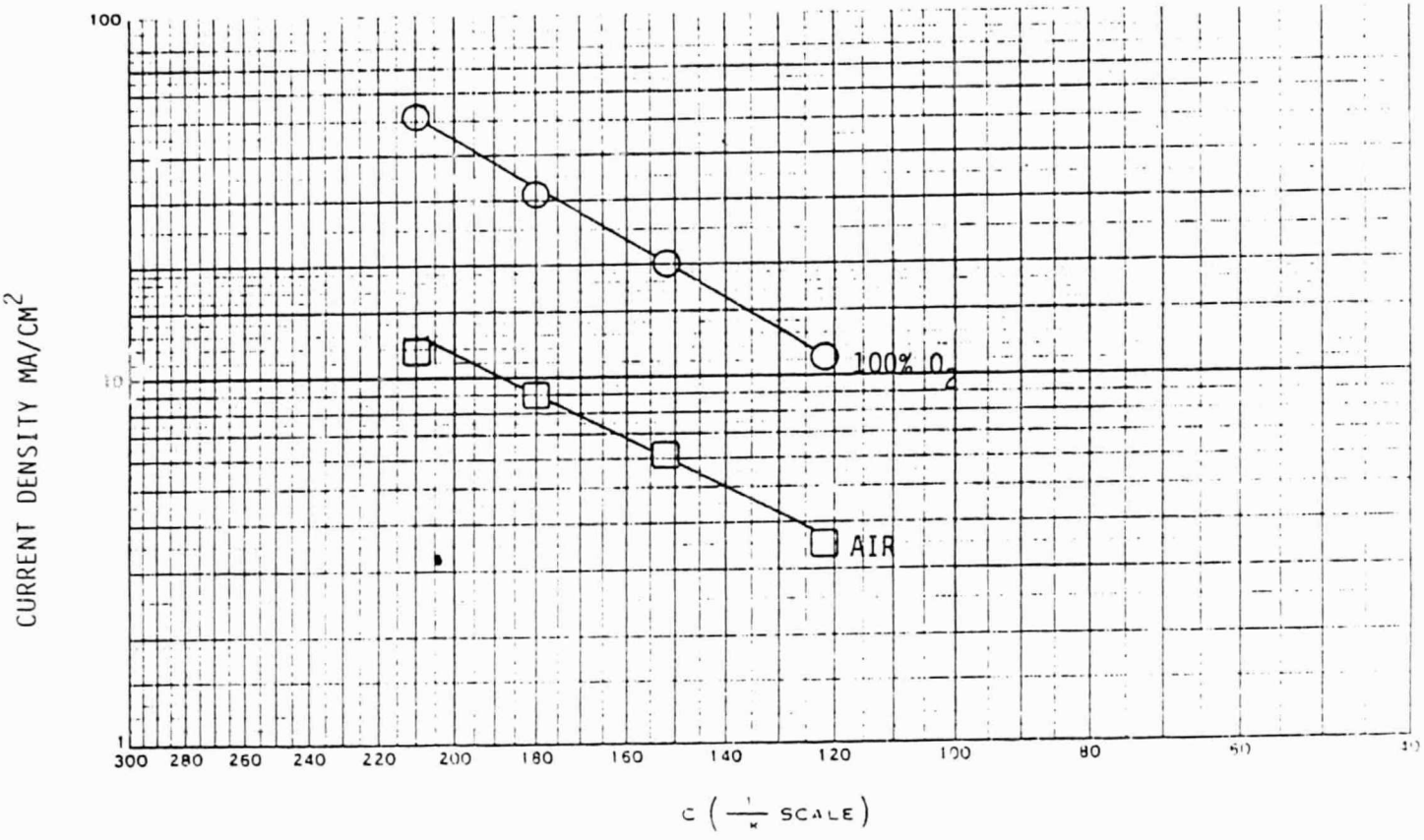

Figure 25. Current density as a function of 1/T for oxygen reduction at 700 mV vs H_2 electrode potential in 100% H_3PO_4. Catalyst is 10% platinum on acetylene black. Electrode contains 2.5% PTFE and 0.50 mg Pt/cm^2.

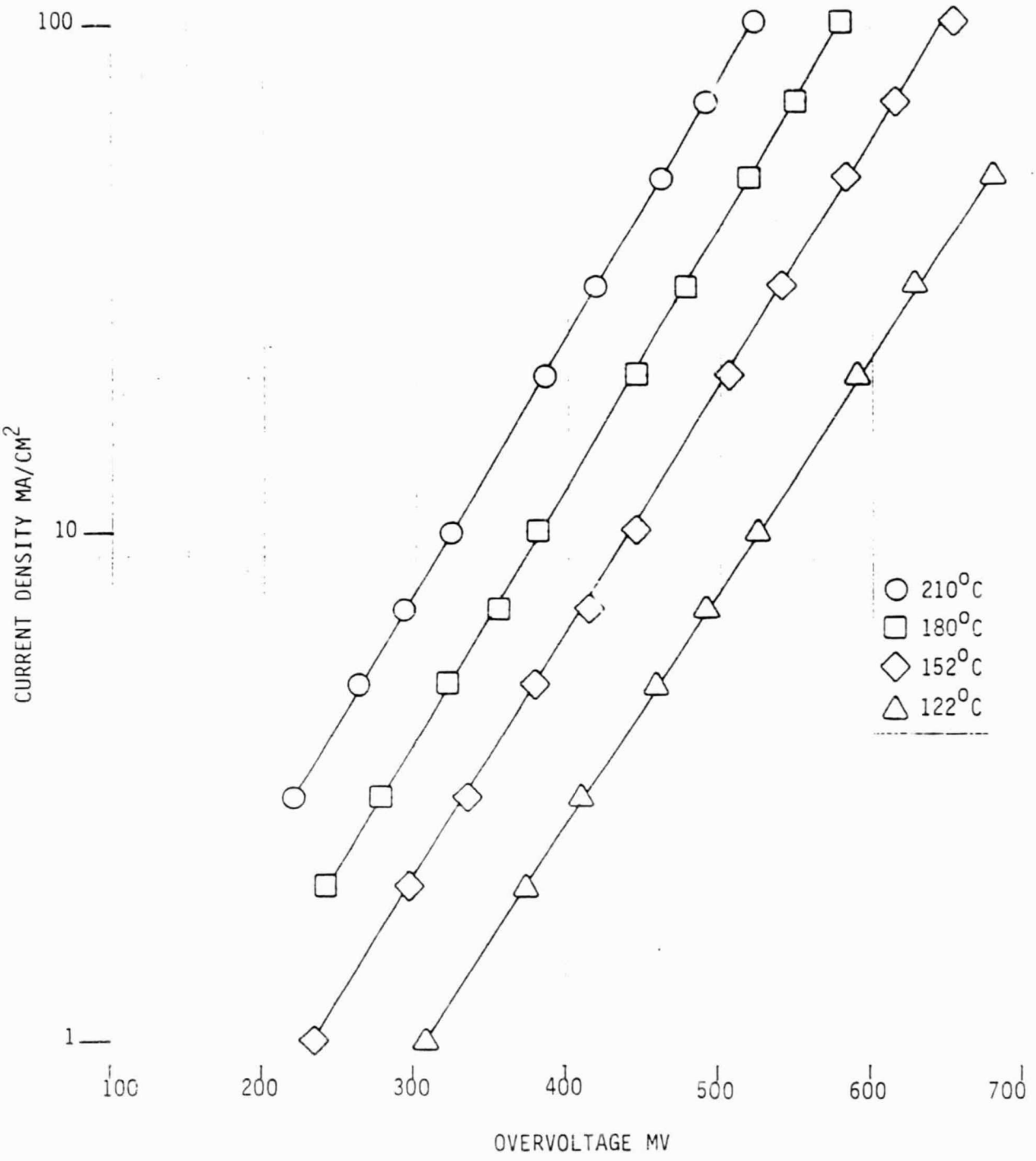

Figure 26. Current density as a function of overvoltage at various temperatures for oxygen reduction in 100% H_3PO_4. Catalyst is 10% platinum on acetylene black. Electrode contains 2.5% PTFE and 0.50 mg Pt/cm^2. The electrode was tested on dry 100% O_2.

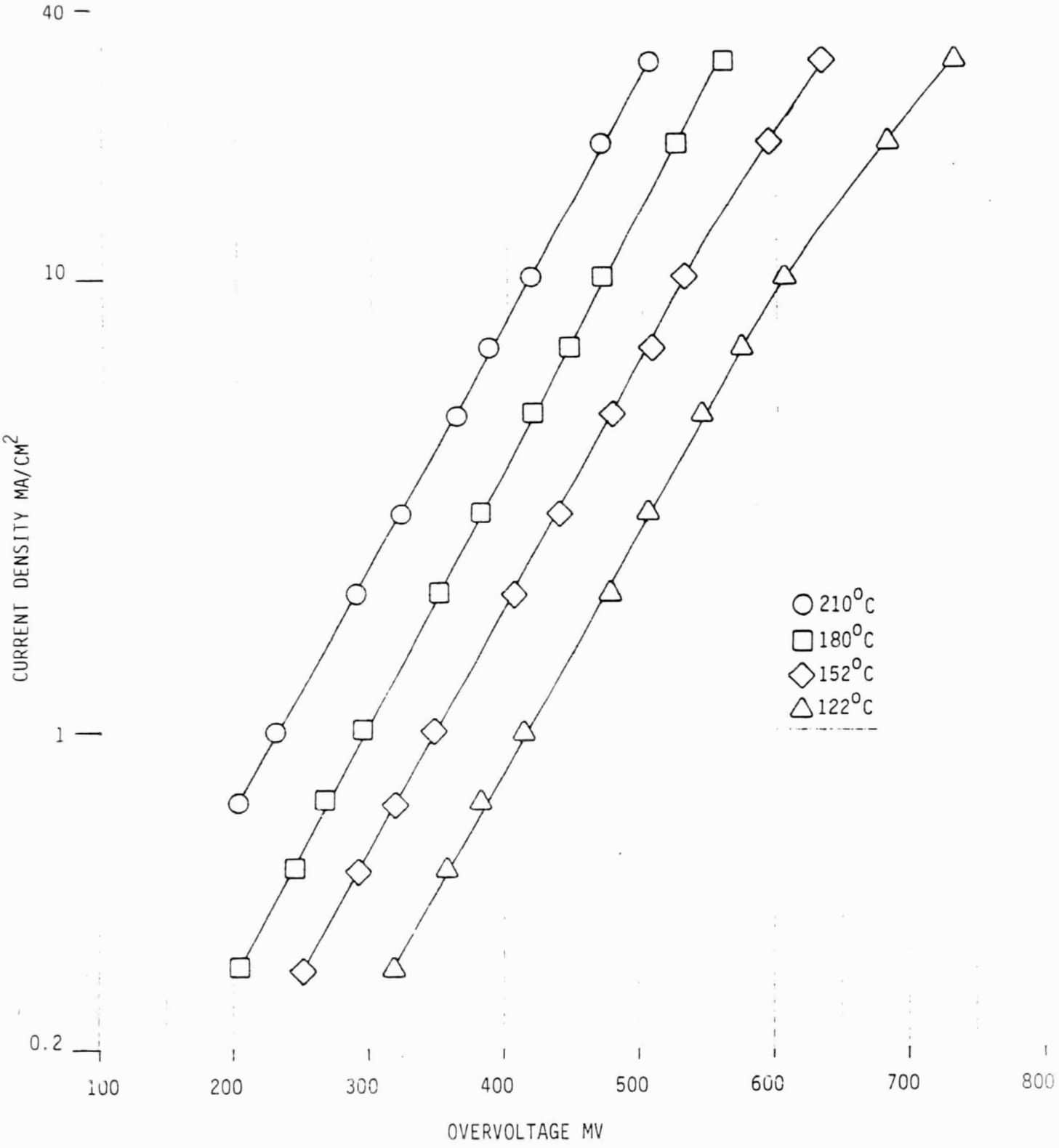

Figure 27. Current density as a function of overvoltage at various temperatures for oxygen reduction in 100% H_3PO_4. Catalyst is 10% platinum on acetylene black. Electrode contains 2.5% PTFE and 0.50 mg Pt/cm^2. The electrode was tested on dry air.

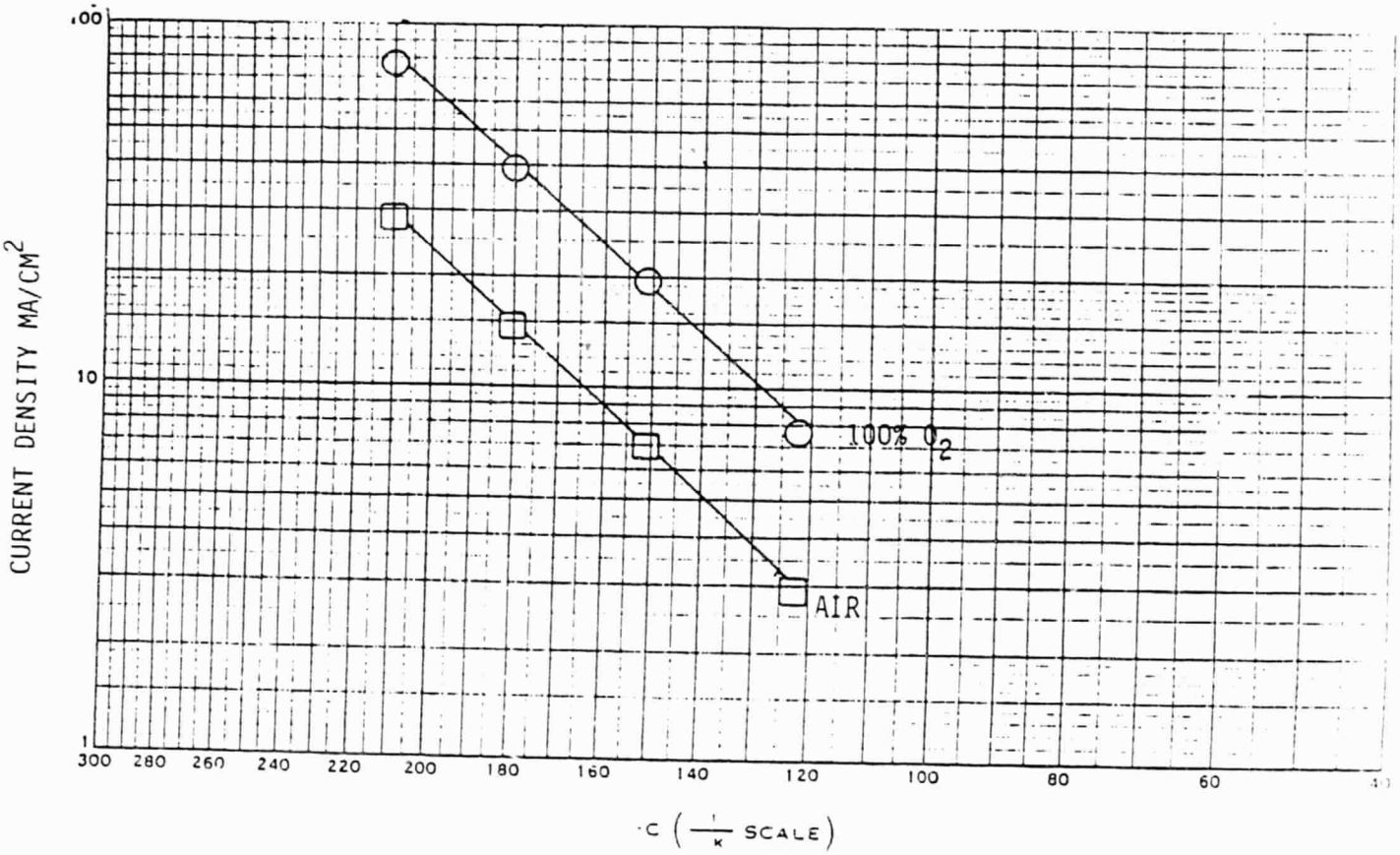

Figure 28. Current density as a function of 1/T for oxygen reduction at an overvoltage of 500 MV in 100% H_3PO_4. Catalyst is 10% platinum on acetylene black. Electrode contains 2.5% PTFE and 0.5 mg Pt/cm^2.

was shown for platinum dispersed on a furnace black (96% phosphoric acid). Appleby (JECS, 1970, 117, 328) had shown a similar invariance on smooth platinum, provided the electrolyte was unpurified but had obtained an RT/F dependence in purified phosphoric acid. It should be noted that there was considerable scatter in the experimental data presented by Kunz and Gruver.

Taking the apparent Tafel slope of 92 mV and inserting it into the data previously obtained for oxygen reduction on platinum supported on acetylene black (Tech. Status Report #14, Contract DE-AC03-78ET15365, Figure 15), we obtain the polarization in the absence of diffusion over the range 139-228°C shown in Figure 29. This figure indicates the overvoltage as a function of current density. Based on these calculations, it is possible to generate the projected performance for oxygen reduction on platinum supported on acetylene black at the 100 ASF(amps per square foot) and 200 ASF levels as a function of temperature.

At first glance, we would expect a ratio of about 5:1 in the current densities for the reduction of oxygen and the reduction of air at the same temperature in the same electrolyte provided that the oxygen reaction is first order, since with Tafel kinetics, Equation 1 is expected to apply for porous electrocatalyst layers:

$$I = i_0 L \gamma \exp(-2.303\eta/b) \qquad (1)$$

where i_0 is the usual standard exhange current, L is the thickness of the electrode structure, and α is the surface area of active electrocatalyst per volume of electrode structure (real cm^2 electrocatalyst/cm^3 electrode structure). I, n, and b (Tafel slope) have their usual electrochemical significance. The concentration of oxygen is contained in the exchange current term since:

$$i_0 = nFk_0C_0 \qquad (2)$$

where k_0 is the specific rate constant and C_0 is the oxygen concentration in solution. If the electrocatalyst layers are influenced by mass transport, then the current density/potential relationship will have the form:

$$I = (nFDC_0 i_0 \gamma)^{1/2} \exp(-2.303\eta/2b) \qquad (3)$$

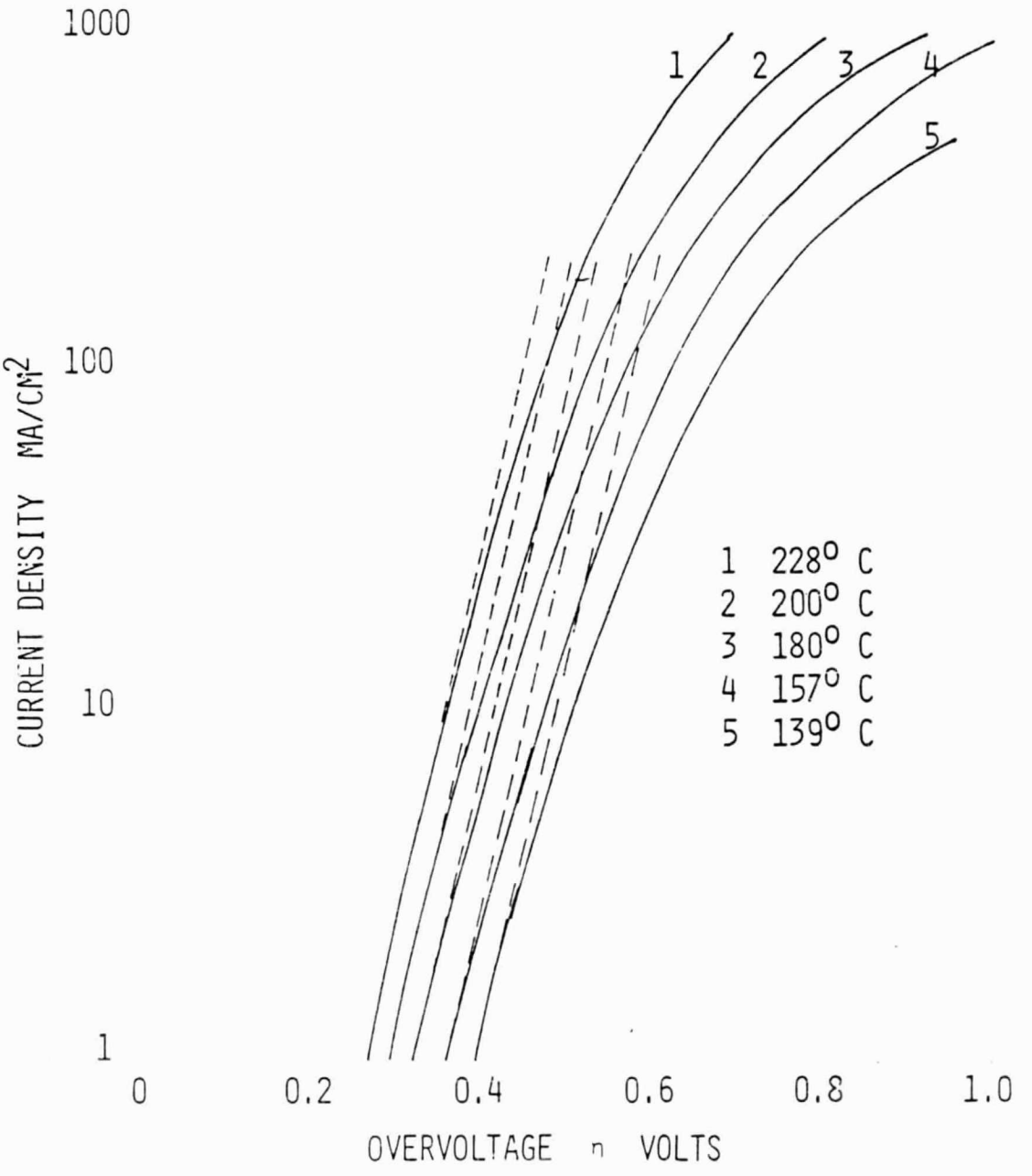

Figure 29. Current density as a function of overvoltage for oxygen reduction at various temperatures. Electrode is 0.53 mg Pt/cm^2 on acetylene black with 30% TFE. Run on air in 104.6 w/o H_3PO_4. (---) polarization in the absence of diffusion.

where D is the diffusivity of oxygen in the electrolyte.

At first glance, it would seem that the current density will vary according to the square root of the diffusivity-solubility product for oxygen in the electrolyte. Since the solubility term is already contained in the exchange current, then the current density must change as the square root of the diffusivity but remains first order in the solubility. It is to be expected, therefore, that with flooded layer structures, one should observe approximately the 5:1 ratio in current density between oxygen reduction and oxygen in air reduction at the same potential and at the same temperature. This is not necessarily so. As the current density increases for oxygen reduction, more water is formed. The oxygen partial pressure within the porous electrode structure will decrease and this will be in direct proportion to the current density. In addition, the theoretical open circuit potential must change according to Equation 4:

$$E = E_o + \frac{RT}{4F} \ln \frac{[pH_2O]^2}{[pO_2][pH_2]^2} \qquad (4)$$

In Equation 4 the observed open circuit potential changes by the logarithm of the square of the water vapor pressure and the oxygen partial pressure term is $(1-pH_2O)$.

At low temperatures, the water vapor pressure is small but at high temperatures, it is quite considerable and represents a significant fraction of the gas volume in the electrode structure. It can be seen that the apparent Tafel slope must be influenced throughout the current density range due to the formation of water in the electrode structure and that the Tafel slope obtained on pure oxygen will be lower due to the greater formation of water than the Tafel slope obtained for oxygen reduction in air over the same temperature range and the same potential range.

An Interpretation for the Activity of Highly Dispersed Platinum Crystallites on Carbon for Oxygen Reduction in Hot Phosphoric Acid

One of the concerns expressed in the present technology is that when platinum is dispersed more highly on a carbon support, there has not been a

corresponding benefit in increased activity as reflected by the increased surface area of the platinum electrocatalysts. Stonehart Associates presented experimental results for the specific oxygen reduction rate on a variety of platinum on carbon electrocatalysts in the Quarterly technical Progress Report No. 4, June 1, 1979 - August 31, 1979, Contract DE-AC03-78ET15365, Figure 2. The activity results of Bregoli (L. J. Bregoli, Electrochimica Acta, 1978, 23, 489, Figure 3) were replotted since Bregoli had not provided a distinctive fit to the data and a least squares linear regression analysis of Bregoli's results was carried out. The result is shown as the upper solid line in the Figure 30. A similar least squares linear regression for platinum crystallites supported on acetylene black is shown as the lower solid line in Figure 30 with the latter results obtained on contract DE-AC03-78ET15365.

One feature now needs to be explained and understood, and that is: What are the relationships exhibited by the solid lines and are there interdependencies between the crystallite sizes and the specific oxygen reduction activities? In our further analyses of the data we have developed our understanding of the structure of the electrocatalysts by computing the inter-crystallite distances for both the platinum supported on Shawinigan acetylene black and for platinum supported on the XC72-R. In order to carry out these calculations we have assumed (reasonably) that the Shawinigan acetylene black carbon particles are not porous and that the surface area available for catalyzation is the BET surface area of 65 m^2/g. In the case of the XC72-R, this material has a BET surface area of 250 m^2/g but a significant portion of that surface area is not available for either catalyzation or diffusion of the oxygen since it is contained within the prime particle (microporous internal porosity of the carbon). From an examination of the pore volumes of this carbon and detailed examination of the isotherms for nitrogen adsorption we have removed from consideration those pores having a diameter of less than 20 Å since they are not considered to be available surface. This then reduces the prime particle surface area for the XC-72R to be in the vicinity of 180 m^2/g. (It may be slightly less but 180 m^2/g seems reasonable to us). Using a 10% platinum loading and knowing the platinum crystallite surface area, we have calculated the platinum inter-crystallite distances on both the Shawinigan acetylene black and the Vulcan XC-72R. There is an exact correspondence between the specific activity for platinum crystallites supported on Shawinigan acetylene

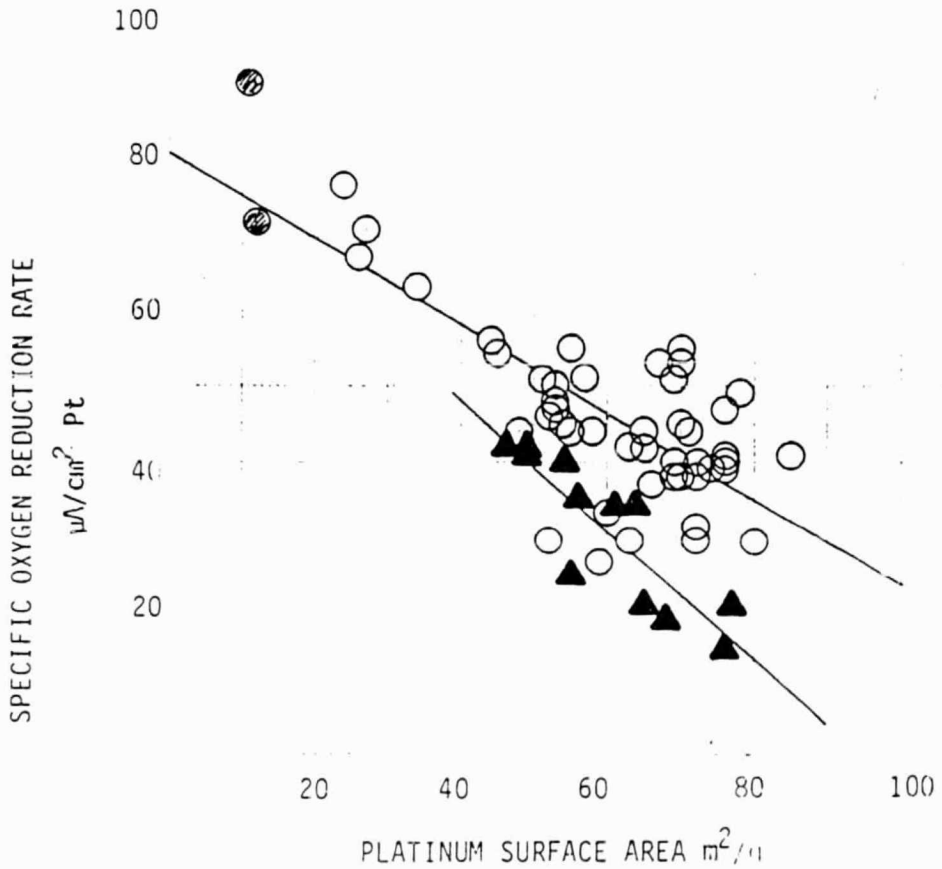

Figure 30. Specific oxygen reduction rate as a function of surface area at 180°C in 100% H_3PO_4 at 900 mV.

▲ Platinum on acetylene black. DEAC03-78ET 15365

○ Platinum on Vulcan XC-72 from Bregoli

● Platinum Black Mixed with Carbon

black to the specific activity for platinum crystallites supported on Vulcan XC-72R when the separation of the crystallites on the carbon surfaces is identical. That is to say smaller platinum crystallites on Vulcan XC-72R have the same specific activities as larger platinum crystallites on Shawinigan acetylene black when they have the identical crystallite separations. Typical values are plotted as horizontal bars in the modified Figure 31 and the values that we have calculated are given in Table V.

TABLE V

(i)

Estimation of Carbon Particle Surface Areas After Ignoring Microporous Surface

	Carbon Type	
	Shawinigan	XC-72R
BET SA	65 m^2/g C	250 m^2/g C
Prime particle BET	65	180

TABLE V(ii)

Specific Activity of Platinum Crystallite for O_2 Reduction at Constant Crystallite Separations

At 10% Pt Specific O_2 Activity	Pt SA (Shaw)	Separation Spheres	Hemispheres	Pt SA (XC-72R)
64 microA/cm^2	20 m^2/g Pt	1340Å	948 Å	28 m^2/g Pt
52	35	580	410	49
40	50	340	240	70
22	70	200	141	100

(For hemispheres, surface area is the same as spheres. Crystallite base is the same. Height is 1/2 diameter and number of particles is x2.)

It really doesn't matter whether one computes spheres or hemispheres since the availability of the platinum surface per gram of platinum does not change, provided that the interface between the hemisphere and the carbon support is not available for reaction. The inter-crystallite distance shown in Figure 32 is reduced and is that value for spheres divided by the square root of 2. Admittedly, this approach is simplistic, but therein lies its elegance in that it supplies an answer for the apparent "crystallite size" effects. The crystallite size effects are not truly dependent on the dimensions of the

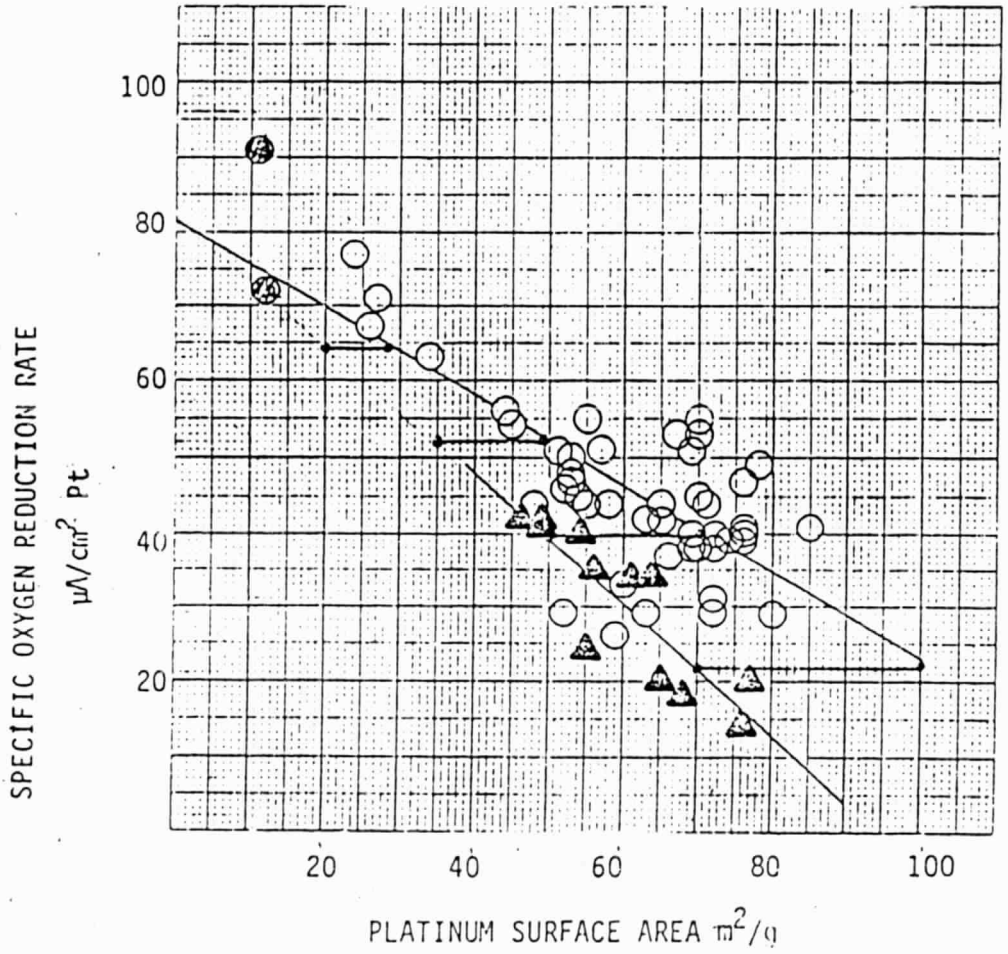

Figure 31. Specific oxygen reduction rate as a function of surface area at 180°C in 100% H_3PO_4 at 900 mV.

▲ Platinum on acetylene black. DEAC03-78ET 15365

○ Platinum on Vulcan XC-72 from Bregoli

● Platinum Black Mixed with Carbon

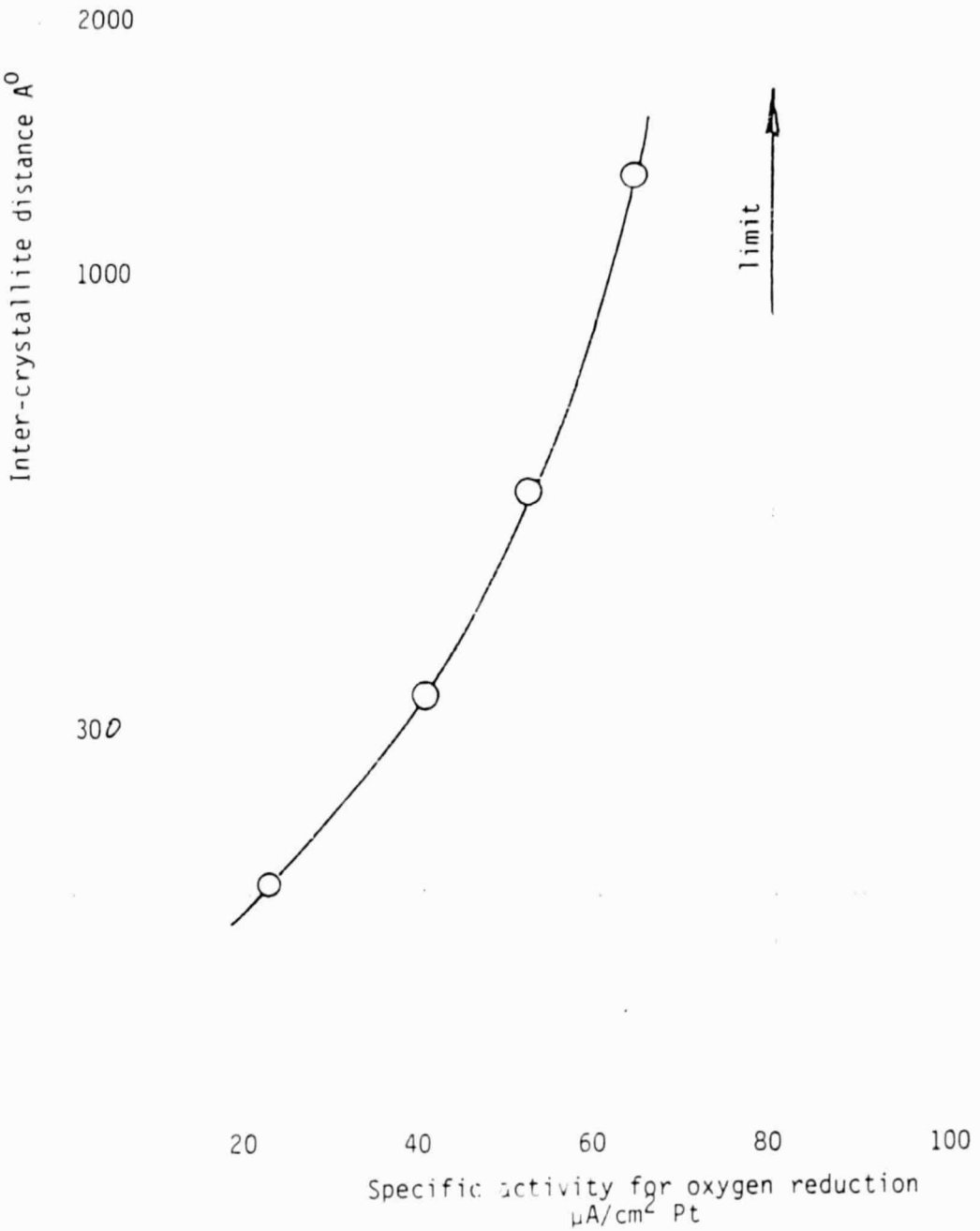

Figure 32. Specific Activity for Platinum Crystallites Supported on Vulcan XC-72R and on Shawinigan Acetylene Black as a function of inter-crystallite distance.

platinum crystallites but are dependent on the availability of oxygen diffusing through a thin liquid film to react at the crystallite surfaces. Diffusion is through a thin liquid film to give spherical diffusion at each individual crystallite. If the crystallites are too close together they will rob each other of their spherical diffusion field. Since mutual crystallite interferences will be a function of the thickness of the electrolyte film, we should see that the electrolyte film will be described as a dimension of half the crystallite separation (e.g. about 50-200 Å). Further calculations have been done to compare the ratios of inter-crystallite distances to the diameter of the platinum crystallites and the ratios of the carbon free surfaces to the platinum crystallite surfaces. These are shown in Table VI.

TABLE VI

Pt Crystallite Separation on Two Carbon Supports-Shawinigan Ac Blk and Vulcan XC-72R

i) 65 m^2/g Carbon (Shawinigan Acetylene Black)

Pt SA	Hemisphere Distances	Dist/Dia. of Pt Cryst.	Ratio of Carbon Free Surface to Pt Cryst. Surface
20 m^2/g	948 Å	6.8	29.25
30	516	5.5	19.50
40	335	4.8	14.61
50	240	4.3	11.72
60	182	3.9	9.70
70	-	-	-
80	118.5	3.4	7.3
90	-	-	-
100	85	3.0	5.9

ii) 180 m^2/g Carbon (XC-72R Prime Particles)

Pt SA	"Specific Activity" microA/cm^2Pt	Hemisphere Distances	Dist/Dia. of Pt Cryst.	Ratio of Carbon Free Surface to Pt.Cryst.Sur
20	70	1578	11.3	81.0
40	58	558	8.0	40.5
60	46	304	6.5	27.1
80	35	197	5.6	20.2
100	23	141.1	5.0	16.2

The implications of this theory are that we should be able to define the thickness of the electrolyte film and describe how catalysts should be designed in order to utilize the platinum most effectively. The indications are that one should increase the surface area of the carbon and not decrease it as it is presently being done by United Technologies. Secondly, we should go to lower platinum loadings than are currently being used.

Task 4 - Electrocatalyst Literature Survey and Selection

The purpose of this task is to review the technical and patent literature to identify platinum based materials that will be suitable for use as phosphoric acid fuel cell catalysts. In particular, the chosen materials must be capable of being prepared in a high surface area form and to be resistant to corrosion. With regard to the cathode, promising materials should have more activity for oxygen reduction than the activities so far exhibited for platinum. For the anode, the activities should be more active than platinum when operating on hydrogen and carbon monoxide mixtures. Another consideration is the lifetime of the electrocatalysts. They must be considered for use in practical fuel cell power plants and this requires an operating life of 40,000 hours. The characteristics for anode electrocatalysts are considerably different from the characteristics of the cathode electrocatalysts, particularly when alloys or intermetallic compounds are being considered. That is to say, materials that have a high activity for hydrogen oxidation in the presence of catalyst poisons may be unstable or inactive for oxygen reduction.

The emphasis for phosphoric acid fuel cell electrocatalyst technology has been on platinum supported on a carbon for both the anode and the cathode electrocatalyst materials. Clearly, the emphasis for future electrocatalyst development must be on substituting for the platinum in the fuel cell system with equally active but lower cost materials.

Phase diagrams are shown in Figure 33 for some of the most promising materials that have been developed for oxygen electrocatalysts (see P. N. Ross, Jr., U.S. DOE Contract W-7405-ENG-48, EPRI RP-1200-5, LBL-10799). The thrust of

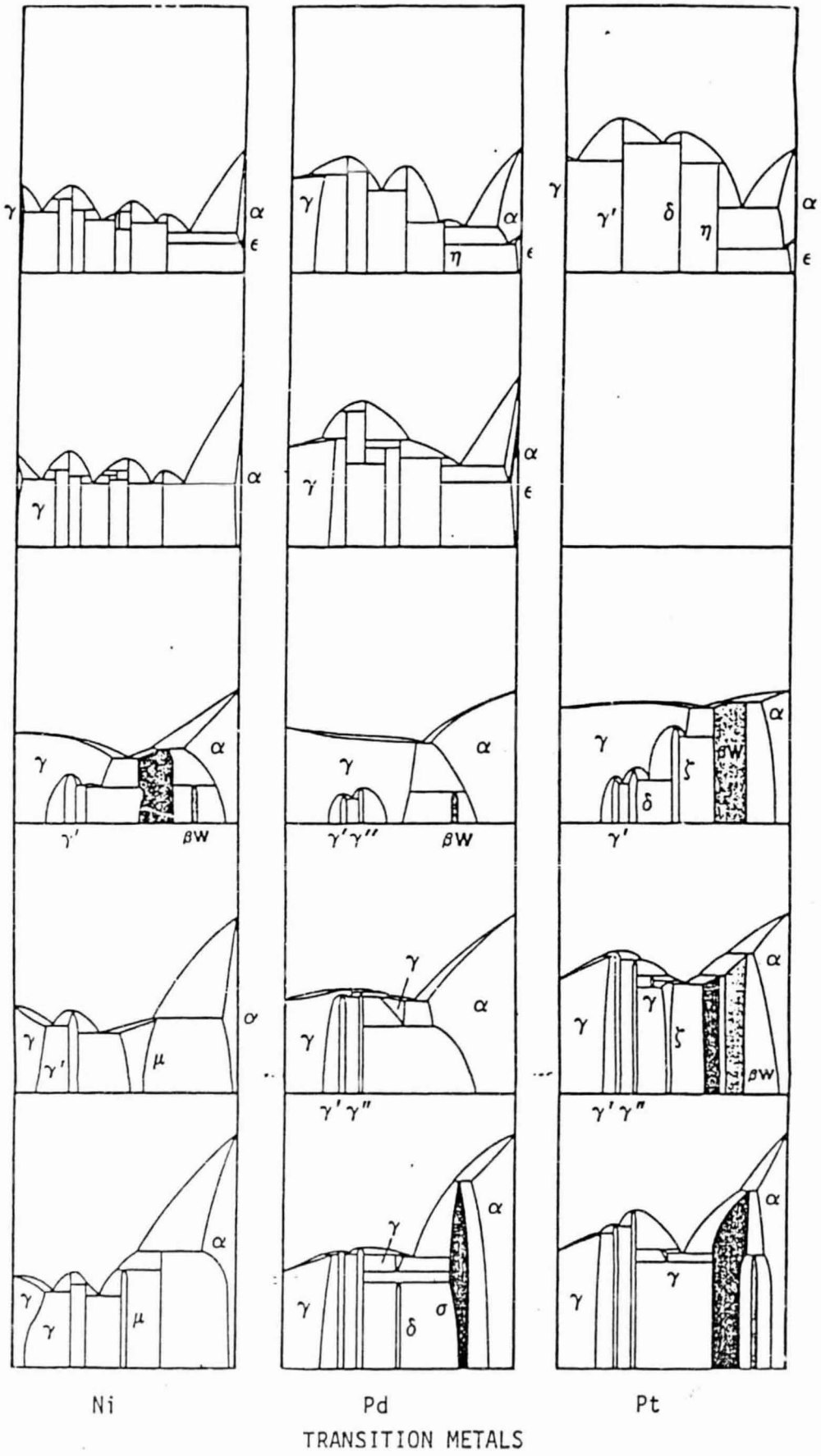

Figure 33. Phase Diagrams of Nickel, Palladium and Platinum Transition Metals with Refractory Metals.

that work has been to develop noble metal-refractory metal intermetallics. The noble metals have been either platinum or palladium and the refractory metals have been from the carbide-forming refractory materials, principally Zr, Hf, V, Nb and Ta. The most interesting feature about the phase diagrams of the latter materials with both platinum and palladium is that a series of well-identified intermetallics are formed. The carbide-forming refractory metals occur with body-centered cubic structures, whereas the transition metals (nickel, palladium and platinum) have face-centered cubic structures. As such, the transition metals have a high electrocatalytic activity for both hydrogen oxidation and oxygen reduction by having a "close-packed" structure. Clearly, an intermetallic formed between the transition metals and the refractory metals should have a corresponding "close-packed" structure.

The most promising intermetallics are: $ZrPt_4$, $HfPt_4$, VPt_3, $NbPt_5$ and $TaPt_5$. Figure 33 shows the best phase diagrams that have been obtained to date for the nickel, palladium and platinum metals with the refractory metals. In this figure, the transition metal is plotted on the left hand side of the phase diagram and the refractory metal on the right hand side. The vertical dimension in the phase diagram is a temperature axis, going from 500-3500°C. Phases are marked as α (BCC), γ (FCC) and ε (HCP). The similarities and trends between the nickel, palladium and platinum phase diagrams with the same refractory metal become obvious. Of the intermetallics so far reported, the VPt_3 and $TaPt_5$ are the most promising, (P. Ross LBL-10799 EPRI RP1200-5) in that they appear to out-perform platinum for oxygen reduction in hot phosphoric acid (180°C), whilst at the same time they do not appear to corrode significantly. An unknown is the degree of demetallization (losing the refractory metal) at the particle surfaces.

For the anode, the most important consideration is that the electrocatalyst should be capable of oxidizing hydrogen in the presence of carbon monoxide rather than the oxidation of hydrogen in the absence of this poison. Alloying of platinum with rhodium (J. Electroanal. Chem., 1975, 59, 177-189) showed increased activities over that of platinum alone but during extended operation of the electrocatalyst, the rhodium (which is far more expensive than platinum) segregated to the insides of the alloy crystallites and the platinum to the surfaces. This had the effect of removing the most expensive component

from beneficial operation. In an attempt to use a cheaper element to replace platinum, the platinum-ruthenium alloy combinations were examined (J. Electroanal. Chem., 1975, 63, 97-110). No great beneficial effects were identified. At various times, platinum-gold alloys have been examined as electrocatalysts but they are clearly inferior for hydrogen oxidation. At low temperatures, segregation occurs between a platinum-rich phase and a gold-rich phase, with the gold-rich phase at the electrocatalyst surface. Since gold is not active for the dissociation of hydrogen molecules, this electrocatalyst alloy combination is not satisfactory. On the other hand, substituting palladium for the platinum does produce an active electrocatalyst for hydrogen oxidation in the presence of carbon monoxide since palladium and gold form a continuous series of solid solutions (see Hansen Constitution of Binary Alloys, Second Edition, McGraw-Hill, p. 224). It is clear that sufficient palladium will be surface segregated on the palladium-gold alloy to confer electrocatalytic activity for hydrogen oxidation and yet carbon monoxide poisoning would not be overly significant. Fishman (U.S. Patent 3,510,355) produced palladium-gold alloys as metal blacks and operated them in 85% H_3PO_4 at 75°C. Although the fuel only contained 0.1% carbon monoxide, he claimed that an active electrocatalyst was produced.

From an examination of binary alloy phase diagrams, it can be seen that a preferred anode catalyst combination might be that of platinum-palladium (see Hansen in Constitution of Binary Alloys, Second Edition, McGraw-Hill, p. 1121) where it is stated that platinum and palladium form an uninterrupted series of solid solutions. Since we know that the adsorption of carbon monoxide on platinum occurs as a single site process (one carbon monoxide molecule adsorbed at each surface platinum atom) and the adsorption of carbon monoxide on palladium occurs through a bridged structure (one carbon monoxide molecule adsorbed on two surface palladium atoms), it would be expected that the equilibrium adsorption isotherm for carbon monoxide on palladium would be lower than that on platinum at a given temperature and partial pressure of carbon monoxide. The foregoing patent shows that palladium is indeed active for hydrogen oxidation in the presence of carbon monoxide but there is no evidence that platinum-palladium alloys have ever been supported on carbon and operated in hot phosphoric acid fuel cell environments with high carbon monoxide concentrations. Due to the surface energy considerations, we would

expect the palladium-rich alloy to be surface segregated with the platinum-rich alloy in the interior of the crystallite. Palladium alone is thought not to be attractive as an anode electrocatalyst under real fuel cell conditions since it is a soft metal and undergoes rapid surface area loss. The addition of a minor atomic amount of platinum to the palladium electrocatalyst causes significant metallurgical hardening of the electrocatalyst particle with consequent reduction in the loss of electrocatalyst surface area with time. It goes without saying that such a catalyst combination is financially attractive since the price of palladium is one third of the price of platinum. The activity of palladium for hydrogen molecule oxidation is comparable to the activity of platinum.

Platinum sulphide is a promising cathode candidate. Transition metal sulphides have been shown to be stable electrochemically and to have substantial oxygen reduction activity in acid solution (Behret, Binder, and Sandstede, Symposium on Electrocatalysis, 319, 1974). Chromium and cobalt sulphides and certain thiospinels have also been reported as being stable with the cobalt thiospinels being the most active (Barasel, et al., Ber. Bunsengessellschaft Phys. Chem., 78, 608, 1974). In particular, $FeCo_2S_4$ retained moderately good activity in sulphuric acid; however, stability was lacking as the transition metal eventually dissolved in the electrolyte. Nickel sulphide also exhibits good electrocatalytic activity (Behret, Binder, and Sandstede, Electrochimica Acta., 20, 111, 1975). Although these materials hold future promise, none have been prepared in high surface area form, and none exhibits oxygen reduction activity close to platinum. Platinum sulphide, on the other hand, shows considerable stability and activity, and it can be prepared in high surface area form. The divalent sulphide is very resistant to both acid and alkali environments (Kida, Bull. Chem. Soc. Jap., 38, 1804, 1965). Dramatically enhanced activities have been reported for the anodic oxidation of formic acid (Binder, Koehling, and Sandstede, Fuel Cell Systems II, 1969) and methanol (Janssen and Moolhuysen, Electrochimica Acta., 869, 1976) when sulphur adsorption layers were used to modify the catalytic properties of platinum surfaces. Platinum sulphide, however, has not been effectively utilized as an oxygen reduction catalyst.

This material warrants investigation as a cathode electrocatalyst due to the

stability and activity characteristics cited here. High surface area supported catalyst preparation techniques for PtS are well known in the petroleum industry (Heard, U.S. 2,659,701).

Another interesting material which warrants attention is rhenium. The stability of platinum-rhenium alloy electrocatalysts is excellent; the alloy is inert in acid, base, and aqueous carbonate environments (Holt, U.S. 3,287,171). Increased activity has been reported for methanol oxidation using platinum-rhenium as opposed to platinum anode electrocatalysts (Cathro, Electrochimica Acta, 5, 441, 1967). Rhenium powder has been reported as showing some activity for hydrogen oxidation in 1M H_3PO_4 at room temperature (Bennett, et al., Materials for Fuel Cells, DOE Annual Report, 1977). Platinum-rhenium, however, has not been investigated as a hydrogen oxidation catalyst at 180°C in acid media. This bimetallic may also be an outstanding candidate for use at the anode because of its ability to tolerate poisons. Carbon monoxide adsorption behavior on rhenium is similar to that observed on tungsten (Ford, Adv. Cat., 21, 51, 1970). Tungsten carbide is known to be insensitive to carbon monoxide poisoning in fuel cell operation (von Sturm, XXIVth Int. Cong. Pure and Applied Chem., 1, 1973). Furthermore, rhenium is capable of tolerating high sulphur concentrations (Davenport, Kollonitsch, and Kling, Ind. Eng. Chem., 60, 10, 1968).

The relative rates of the gas phase H_2-D_2 equilibration reaction on the transition metals Pt, Rh, Ni, Fe, W, Mo, and Cr are remarkably similar (Stonehart and Ross, Cat. Revs., 12, 1, 1975). When operating in the presence of an acid electrolyte, however, the less noble of these elements, i.e. Ni, Fe, W, Mo, and Cr, perform poorly as hydrogen dissociation catalysts. Examinations of electrochemical equilibria data indicate that the surfaces of these elements are more characteristic of the oxides as opposed to the metals at hydrogen potentials. It is known that metal oxides are poorer hydrogen dissociation catalysts relative to the parent metal (Bond, Catalysis by Metals, Academic Press, 1962 and Clark, Ind. Eng. Chem., 45, 1476, 1953) so these materials are not expected to be promising candidates for anode electrocatalyst structures. Nevertheless, the transition metals should not be rejected out of hand. Some transition metal carbides, e.g. WC and Mo_2C, exhibit almost metallic activity as hydrogen electrodes. It has been

postulated that the effect of carbon is to stabilize the transition metal against oxidation (Ross and Stonehart, J. Cat., 48, 42, 1977). Furthermore, WC has the same electronic structure as platinum and exhibits many of the same catalytic properties (McNicol, Catalysis, V. 2, 243, 1978).

Platinum-molybdenum and platinum-tungsten alloys have been investigated for the electrochemical oxidation of methanol in acid electrolyte (Janssen and Moolhuysen, Electrochemica Acta, 21, 869, 1976). The Pt-Mo electrocatalyst exhibited activity 2-3 times that of platinum while the Pt-W electrocatalyst exhibited activity comparable to platinum. More importantly, the voltammetry for both alloys showed extended hydrogen adsorption peaks compared to platinum, and the hydrogen adsorption was stable. Hobbs and Tseung previously investigated hydrogen oxidation in acid electrolyte for Pt supported on WO_3. A maximum in specific electrocatalytic activity was reported in the range 0.02 to 0.1 mg Pt/cm^2 (Hobbs and Tseung, J. Electrochem. Soc., 120, 766, 1973).

There is already extant evidence that molybdenum and tungsten in combination with platinum can be used at both the anode and cathode in phosphoric acid fuel cells. Platinum sodium tungsten bronzes (Niedrach and Zeliger, J. Electrochem. Soc., 116, 152, 1969), platinum molybdenum oxide, and platinum tungsten oxide (Niedrach and Weinstock, J. Electrochem. Soc., 3, 270, 1965) all show increased activity for H_2 + CO oxidation. McKee and Pak have also reported increased activity for H_2-CO mixtures in phosphoric acid (McKee and Pak, J. Electrochem. Soc., 116, 516, 1969).

Since both tungsten and molybdenum do not chemisorb carbon monoxide to any appreciable extent (Ford, Adv. Cat., 31, 51, 1970), the ability of these electrodes to operate better than platinum is not surprising. Platinum is severely poisoned at the low temperatures used in the aforementioned research efforts. It is not clear whether this performance will hold up under current fuel cell operating temperatures (180-200°C). Rhenium is a member of the same family as tungsten and molybdenum and exhibits similar CO adsorption properties. Both tungsten and molybdenum are better carbide forming materials, however, so they should not be prejudged on the basis of the rhenium formulations.

The molybdenum-platinum and tungsten-platinum alloys are also promising cathode materials. WC and $MoSi_2$ have been used as cathodes on air and oxygen (Thompson and Heath, U.S. 3,346,421, 1967). Of particular interest is the ability of molybdenum to stabilize supported platinum. Pt surface area retention has been demonstrated for the Mo^{2+} ion (Eimakov, et al., Kinet. Katal., 15, 1093, 1974). In addition to surface area retention, improved Pt activity has been reported for addition of MoO_3 to Pt/Al_2O_3 catalysts (Esso, Ger. Patent 1,028,266, 1958). Since the carbides are apparently very stable, similar behavior should be expected for carbon supported electrocatalysts.

Alloy catalysts have been of interest to workers in heterogeneous catalysis for some time. Much of the early work in this area was conducted with conventional metal alloys prepared in a form suitable for catalytic studies and it is now clear that alloying has a marked effect on the physicochemical properties of the constituent metals. A major theme of the work conducted has been the investigation of the relationship between catalytic activity and the electronic structure of metals (Schwab, Disc. Far. Soc., 8, 166, 1950 and Dowden and Reynolds, Disc. Far. Soc., 8, 184, 1950). The general approach for these studies is to correlate catalytic activity with alloy composition, the latter determining the electronic properties of the alloy. Alloys consisting of Group VIII and Group IB have received particular attention in this regard (Sinfelt, et al., J. Cat., 24, 283, 1972). The Group VIII metals have unfilled d-orbitals, and by varying the alloy compositions, the effect of d-orbital occupancy on catalytic activity could be observed. The d-electrons have been suggested frequently as playing an important rôle in the determination of catalytic properties.

The Engel-Brewer valence bond theory (Brewer, in Phase Stability in Metals and Alloys, P. Rudman, J. Stringer, and R. Jaffee, eds., McGraw-Hill, N.Y., 1967) has been remarkably successful in predicting the structure and stability of d-electron transition metals and alloys. The theory suggests that bonding between these elements occurs primarily through metal ligand bonds involving d-orbital overlap. More bonding orbitals are formed, hence a more stable structure is maintained due to donation of two paired electrons to unfilled d-orbitals. Changes in the d-orbital structure of platinum-transition metal compounds might be expected to produce dramatic changes in the catalytic

properties of the constituent metals. It is this possibility which led Ross to investigate the Pt-Group IVB and Pt-Group VB intermetallic compounds for use as cathode electrocatalysts (Ross, EPRI EM 1553, 1980). Vulcan supported electrocatalysts were prepared by precipitating the base metal hydroxide onto a Prototech (Pt/Vulcan) catalyst. Subsequent heat treating to > 900°C resulted in stable intermetallic compounds having 30-50 Å crystallites. The vanadium, zirconium, and tantalum intermetallics all showed better cathode performance than the Pt standard at 110°C. At 170°C, only the vanadium intermetallic was superior. It was proposed that the intermetallic compound formation altered the heat of adsorption for oxygen, leading to a change in the rate of oxygen reduction. Preliminary stability testing indicated that those compounds having the Cu_3Au structure were the most stable. Both the vanadium and zirconium intermetallics were resistant to surface area loss under gas phase conditions, suggesting long-term stability, even though surface area loss in liquid phase environments has been shown to be far different than for the same catalyst in the gas phase (Bett, et al., J. Cat., 35, 307, 1974 and Bett, et al., J. Cat., 41, 124, 1976). In later work (Ross, EPRI RP 1676-2, 1980), it was shown that the tantalum intermetallic was actually a two phase Pt_4Ta/Ta system. This catalyst exhibited better activity than the standard Prototech catalyst at 180°C. Furthermore, there was no appreciable change in the Pt cluster size after 1000 hr at 0.8V in 98% H_3PO_4 at 180°C. Palladium was also substituted for the platinum to form a series of Pd-Group IV and Pd-Group V intermetallic compounds. The Pd_3Nb intermetallic was of particular interest because it is isomorphic to Pt_3V. Reasonable dispersions for this catalyst could only be obtained for 5 w/o Pd loading, however, and the peformance of these compounds was poorer than both Pt and Pt intermetallics.

The majority of performance testing of Pt intermetallics has been conducted below fuel cell operating conditions. Further testing of these materials is required at 180°C and above. It should be pointed out that the catalytic activity may be supplied only by the platinum. Previous work has been performed using Pt loadings identical to standard Pt/C electrocatalysts, and the kinetic parameters reported for the intermetallics are essentially the same as for platinum alone (Ross, EPRI EM 1553, 1980). Since all the transition elements form stable carbides, the role of the transition metal may

be one of stabilizing the Pt crystallites.

Task 5 - Preparation of Platinum-Based Carbon-Supported Electrocatalysts

The purpose of this task is to prepare electrocatalysts that have been identified as promising candidates from the literature survey carried out in Task 4. It is intended that two platinum group metal (PGM) compounds shall be selected and three platinum group metal alloys. Selection of the compounds or the alloys is determined by the application of the material as an anode electrocatalyst or a cathode electrocatalyst. In addition, the electrocatalyst shall be cost effective with regard to providing an equivalent performance to a pure platinum catalyst but without having that cost attributed to the platinum.

i. Noble Metal Alloys

Following the discussion in Part 4, two catalysts were prepared and supported on Vulcan XC-72R. The first catalyst contained Ø.5 mg PGM loading with a 5Ø/5Ø weight percent distribution between platinum and palladium. Due to the differences in atomic weights between platinum and palladium this alloy has a 2:1 ratio of palladium atoms to platinum atoms. A second electrocatalyst was prepared with a Ø.3 mg PGM loading on Vulcan XC-72R with a 46/54 weight percent ratio between platinum and palladium. These electrocatalysts were bonded with PTFE and tested at 18Ø°C in 1ØØ% phosphoric acid.

In order to provide a rigorous evaluation of the catalytic activity, it was decided that performance data would be obtained for hydrogen oxidation in the presence of 1Ø% carbon monoxide and 3Ø% carbon monoxide since these are the most difficult conditions for an anode electrocatalyst. The results with the platinum-palladium alloys were compared to a good Ø.5 mg per cm^2 platinum on Vulcan electrode. Results are shown in Figures 34 and 35. It can be seen that the platinum-palladium alloys (Code EC 1Ø1) are very close to the performance of the good platinum electrodes, even though the PGM loading is Ø.3 mg per cm^2 versus Ø.5 mg per cm^2 for the platinum alone electrocatalyst.

A detailed characterization of the Pt/Pd alloys as electrocatalysts for

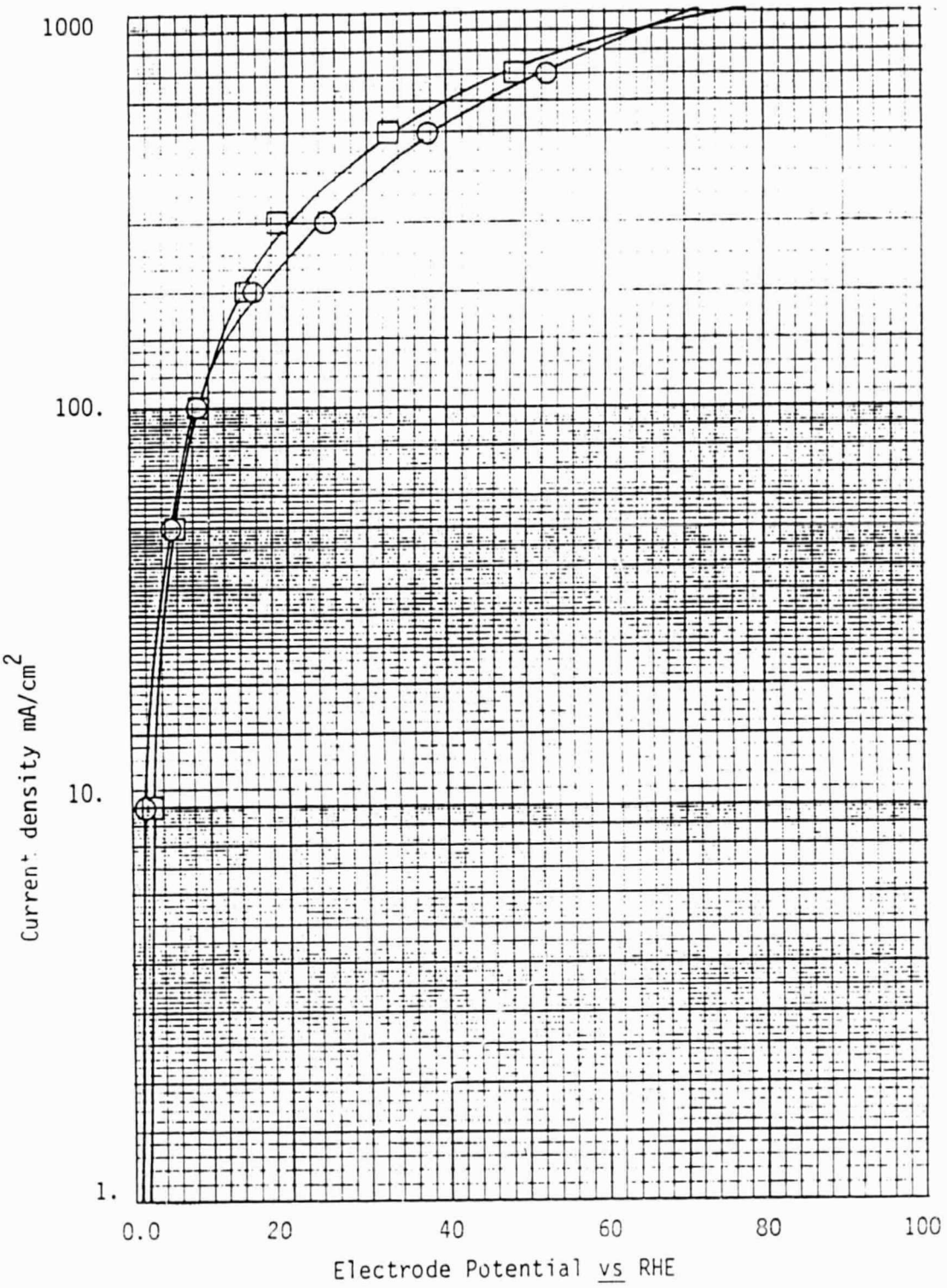

Figure 34. Anode performance for 0.5mg Pt on Vulcan XC-72R (squares) and 0.3mg PGM on Vulcan XC-72R(circles). Nominal 90% H_2+10% CO. 180°C and 100% H_3PO_4.

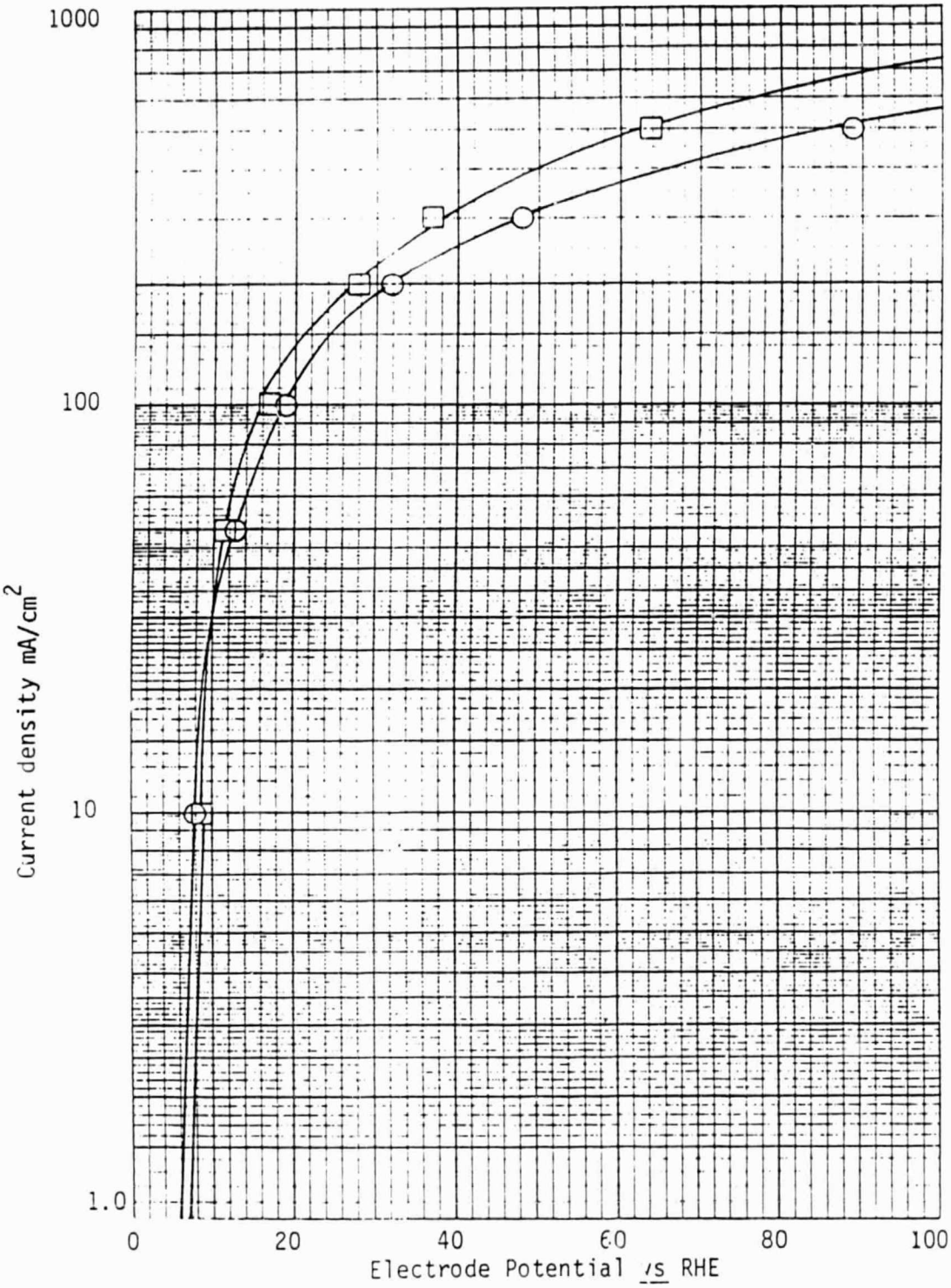

Figure 35. Anode performances for 0.5mg Pt on Vulcan XC-72R (squares) and 0.3mg PGM on Vulcan XC-72R (circles). Nominal 70% H_2+30% CO. 180°C and 100% H_3PO_4.

ORIGINAL PAGE IS
OE POOR QUALITY

hydrogen oxidation requires the preparation of a number of catalysts in which the Pt to Pd ratio is varied. One of the most important factors which determines the performance of these catalysts is the surface layer composition. The hydrogen oxidation mechanism, and therefore the reaction rate, will be influenced by the catalyst surface composition. Furthermore, the effect of carbon monoxide poisoning on the reaction rate must certainly be influenced by the surface composition since it is known that palladium chemisorbs CO in a bridged form whereas platinum chemisorbs CO in the linear form (Ford, Adv. Cat., 20, 51, 1970). The surface composition is related to the bulk composition although it is not likely to be identical because of surface segregation (Burton and Garten, Adv. Mat. in Cat., 33, 1977). Catalysts were prepared, therefore, with different ratios of platinum to palladium. Electrocatalysts containing 0, 35, 65, and 100 a/o Pt were prepared at 4 w/o PGM loading. The carbon support was Consel I.

Alloy catalysts at the 35 a/o Pt level were prepared at loadings of 2, 4 and 10 w/o PGM to examine the influence of electrode structure on performance of PGM electrocatalysts. Previously reported results in this contract clearly demonstrated that structure has a dramatic effect on carbon monoxide tolerance.

In addition, a small number of electrocatalysts were prepared in order to investigate the influence of PGM loading on the electrode performance. At this time there are two types of carbon supports that have been investigated. These are Vulcan XC-72R, a turbostratic furnace black that is easy to catalyze and to form into electrode structures, and the Consel I, which is a steam-treated acetylene black having a partially "graphitized" surface layer. The latter carbon is more difficult to catalyze and to form into electrode structures due to the graphitic nature of the carbon surface. In order to maintain approximately the same PGM particle sizes, the carbons were catalyzed using our standard colloidal technique. All of the catalyst formulations were treated in the same manner. The electrocatalyst designations, electrode numbers and compositions are given in Table VII.

TABLE VII
Composition of Designated Electrocatalyst in Preparation

Catalyst #	Electrode #	
EC-123	P-116	50/50 a/o Pt-Pd on Consel I 4 w/o PGM 0.2 mg PGM/cm^2 electrode
EC-161	P-117	1 w/o Pt on Vulcan XC-72R 0.05 mg Pt/cm^2 electrode
EC-162	P-118	4 w/o Pt on Vulcan XC-72R 0.2 mg Pt/cm^2 electrode
POWERCAT 1000	P-91	10 w/o Pt on Vulcan XC-72R 0.5 mg Pt/cm^2 electrode

ii. Noble Metal - Refractory Metal Mixtures

High surface area platinum-rhenium alloy catalysts were prepared by a modified colloidal technique. This is the same technique we have been using to produce high surface area platinum and platinum-palladium alloy catalysts for this contract. It was found necessary to increase the acidity of the solution to 6N with HCl in order to produce colloidal particles of rhenium for deposition on the carbon support.

For electrocatalysts containing platinum with a refractory metal, electrocatalyst preparation focused on high surface area platinum tungsten and platinum molybdenum bimetallics supported on Consel I. These formulations were all prepared by an impregnation technique. The salt solutions were prepared to yield electrocatalysts containing 10 w/o Pt in the form of an alloy composed of 66 a/o Pt. Typically, about 1 g Consel I was added to the solution and the resulting slurry dried overnight at about 75^{o}C. The dried catalyst was reduced in 10% H_2/N_2 at reduction conditions reported in Table VIII.

The 400^{o}C treatment was recommended by Kehl et al. (U.S. 3,639,647) for Ni/W or Ni/Mo catalysts to obtain superior alloy formulation and higher surface area.

TABLE VIII

Heat Treatment Conditions for Pt-refractory Metal Catalysts

Catalyst	Reduction Condition
14.7% Pt/W	400°C for 2 hrs.
12.6% Pt/Mo	400°C for 2 hrs.
14.7% Pt/W	900°C for 1 hr.

Based upon the information described in the literature, several intermetallic compounds were prepared for evaluation as oxygen reduction catalysts. Palladium-tantalum, palladium-niobium, and platinum-tantalum intermetallic preparations were attempted by co-impregnating Consel I with the appropriate metal chlorides. After drying the impregnated Consel I at 70-80°C for approximately 24 hours, the dried material was heat treated at 900°C in a H_2/N_2 atmosphere to effect reduction of the chlorides and intermetallic formation.

The development of techniques for the preparation of platinum intermetallic catalysts was also initiated with the preparation of a platinum-vanadium intermetallic. This initial catalyst preparation consists of impregnation of a 10% platinum on Consel I catalyst with vanadium chloride, and heat treating the dried catalyst at 900°C in a 10% H_2/N_2 atmosphere. This heat treatment should both reduce the vanadium chloride to vanadium and facilitate alloying of the platinum and vanadium.

As reported previously, a superior support material was developed in the EPRI 1200-2 program. The usefulness of this material as a catalyst support was further investigated by depositing platinum on the surface. In order to achieve maximum dispersion of the platinum, a colloidal method was used to deposit the platinum and after drying, the resultant material was split and one portion was heat treated in a H_2/N_2 atmosphere at 200°C while the remainder was heat treated at 900°C for 1 hour in a H_2/N_2 atmosphere.

Investigation of platinum-vanadium intermetallic as electrocatalysts for oxygen reduction continued with the preparation of Pt-V on Consel I and Pt-V on Vulcan XC-72R supports. Both of these catalysts were prepared by

impregnating an existing platinum catalyst with vanadium chloride and heat treating at 900°C in H_2/N_2 to effect alloying.

The catalyst preparations report are summarized in the following Table.

TABLE IX

Compositions and Treatments of Noble Metal (Refractory Metal) Electrocatalysts

Catalyst #	Metals	Alloy Mix w/o	Total Load w/o	Support	Heat Treatment
EC-150	Pd/Nb	10.0/2.91	12.9	Consel I	900°C H_2/N_2
EC-151	Pd/Ta	10.0/4.25	14.3	Consel I	900°C H_2/N_2
EC-152	Pt/Ta	10.0/2.32	12.3	Consel I	900°C H_2/N_2
EC-214	Pt/V	9.9/0.9	10.8	Consel I	900°C H_2/N_2
EC-215	Pt/V	9.9/0.9	10.8	Vulcan XC-72R	900°C H_2/N_2
EC-154	Pt/V	9.9/0.9	10.8	Consel IV	
EC-155	Pt	—	5	Consel I	
EC-156	Pt	—	5	Consel IV	
EC-157	Pt/V	4.96/0.43	5.4	Consel IV	

A number of additional electrocatalysts were prepared, investigating the preparation of platinum-vanadium intermetallics on Consel. In addition, the formation of platinum-tungsten compounds was carried out by forming tungsten carbide on the surface of Consel I, and then catalyzing with platinum. The tungsten carbide was formed by impregnating the Consel I with ammonium tungstate, heating to 700°C and passing a small amount of carbon monoxide (see D. E. Fornwalt, E. J. Felton and P. Stonehart, Micron 1975, 6, 147-152). After the carbon monoxide treatment, the tungsten carbide on the carbon support was heat treated for a further 16 hours at 700°C in argon. After heat treatment, the tungsten carbide on carbon was catalyzed with platinum using a colloidal technique.

iii. Noble Metal Sulphides

The preparation of high surface area platinum sulphide on carbon catalysts using the techniques of Heards (U.S. Patent #2,659,701) was attempted. The procedure is to add ammonium sulphide dropwise to a solution of chloroplatinic acid to form a colloidal suspension of platinum sulphide. Adding the carbon support material to this colloidal platinum sulphide suspension and drying the

resultant slurry deposits the platinum sulphide on the support. Final treatment of the catalyst consists, so far, of either calcining in air at 200°C or heat treating in 5-10% H_2/N_2 at 150-350°C. Five electrocatalysts have been made using this technique with a PtS_2 loading of 10% on Consel I support.

The preparation of a carbon supported platinum sulphide electrocatalyst consists of first forming a platinum sulphide colloid in H_2O, adding ammonium sulphide to a solution of chloroplatinic acid. Deposition of the platinum sulphide on a carbon support is then accomplished by adding a carbon black to the solution and stirring to produce a slurry. This slurry is then dried at 70-80°C in air for approximately 24 hours. The dried material is then heat treated at 200°C for one hour in a H_2/N_2 atmosphere. Since the platinum sulphide colloid forms almost immediately after addition of the ammonium sulphide to the chloroplatinic acid solution, and the colloid particles grow rapidly, obtaining a high surface area catalyst depends greatly on how quickly the carbon support is added to the solution after the ammonium sulphide is added. Several preparations of platinum sulphide were made keeping the above considerations in mind, and a higher surface area electrocatalyst was produced with improved activity for oxygen reduction.

Task 6 - Characterization of Platinum-Based Carbon-Supported Electrocatalysts

i. Noble Metal Alloys

Characterization of high surface area, supported alloy catalysts is a difficult and challenging problem. With non-alloy supported catalysts, physical characterization is fairly complete when the crystallite size distribution and morphology have been determined. This is not to imply, however, that these determinations are always a simple matter. Electron microscopy may be used to obtain the morphology and crystallite size distribution. Gas phase adsorption methods such as CO slug flow and hydrogen titration provide estimates of noble metal active areas. Active surface area estimates can also be obtained by electrochemical techniques. In this

procedure, the area under the hydrogen atom adsorption peaks in the voltammogram is measured to give an estimate of the total coulombic charge required for hydrogen deposition. The active metal area is related to this charge. Finally, x-ray line broadening can also be used to determine both crystallite size and lattice dimensions. The latter has been used to determine bulk alloy compositions (Sinfelt, in Adv. Mat. in Cat., 1, 1977).

Since alloying introduces an additional parameter, i.e. surface composition, interpretation of data obtained from the previously mentioned analytical techniques is difficult. Electron microscopy, for example, would still be capable of providing crystallite morphology and size distribution information, but this technique cannot resolve the surface composition of small crystallites. Gas phase adsorption techniques require knowledge of the nature of chemisorption. The quantity of gas adsorbed is related to the number of available surface atoms, which when coupled with the chemisorption stoichiometry and the metal atom cross section, can be used to estimate the active surface area metal catalysts. Complications may arise when using this method for determination of supported alloy catalyst surface areas. The CO chemisorption stoichiometry is different for each element of the platinum-palladium binary, for example. Carbon monoxide chemisorbs in the linear form on platinum and in the bridged form on palladium. As a result, the quantity of adsorbed carbon monoxide cannot be directly related to surface area without prior knowledge of the surface composition. Cyclic voltammograms are unique to the metal which is potential cycled. The voltammogram of platinum, for example, is clearly understood so that determination of the active metal area is straightforward.

Addition of an alloying element, however, may sufficiently alter the voltammogram to obscure the interpretation. X-ray line broadening can be used to determine average crystallite size down to about 50 Å. The alloy catalysts prepared in Task 5 should have crystallites on the order of 25-30 Å. The determination of lattice constants of alloys by x-ray techniques have been used to determine bulk alloy compositions (Sinfelt, Carter and Yates, J. Cat., 24, 283, 1972) by the correlation developed by Vegard (Dekker, Solid State Physics, 104, 1957). Since the lattice constants for platinum (0.39158 nm) and palladium (0.38825 nm) are similar (Hartley, The Chem. of Platinum and

Palladium, 6, 1973), very accurate lattice constant determination is necessary. This procedure has been successful for large crystallites and bulk alloys. It is not known if this method can resolve the composition of high surface area supported alloy catalysts.

Based on this discussion, three techniques have been chosen to characterize alloy catalysts. The first method is the CO slug flow technique which has been used to determine surface areas of platinum catalysts in previous tasks. The difficulties encountered with the application of the CO slug flow method for determination of alloy surface areas have already been described previously. In addition, it is now clear that a colloidal procedure used to make the alloy catalysts in Task 5 yields catalysts with high impurity coverages which impair adsorption of CO. A more rigorous cleaning technique for the alloy catalysts has been formulated and details of the procedure will be reported at a later date. The second technique is the electrochemical adsorption method. Since little is known concerning the characteristics of alloy ECA's, we are in the process of identifying the location of oxidation and reduction peaks on the voltammograms of both platinum and palladium. These results are used to interpret voltammograms for the alloy compositions so that a methodology for estimating alloy surface areas can be defined. The final area of characterization employed in this task is the temperature programmed method. A test stand has been constructed that is capable of performing temperature programmed adsorption, desorption, or reaction. The apparatus is under control of a 16 bit 8086 digital microprocessor which allows input of any temperature program by means of software modifications. Since this hardware and software is quite general, it is capable of programming any heating/cooling system. Some timing sequences may have to be adjusted according to the thermal characteristics of the reactor, but that is trivial. The hardware (digital circuitry and analog control circuitry) were coupled to the micro-computer, the program loaded and the total system performed in the required manner.

The ability of palladium to absorb hydrogen usually makes it impossible to determine the surface area of palladium or palladium containing alloys by cyclic voltammetry. Surface area determination by voltammetry depends upon measuring the pseudocapacitance of monolayer hydrogen adsorption. When

palladium is present and accessible to adsorbed hydrogen, the internal palladium atoms will absorb the surface adsorbed hydrogen. This creates a clean surface site for additional hydrogen adsorption. Monolayer equilibrium hydrogen coverage is not obtained until internal absorption of hydrogen is satisfied. At this point, the total measured pseudocapacitance is due to adsorbed plus absorbed hydrogen. Since the two phenomena cannot be separated on the voltammogram, a surface area determination is not possible. In the hydrogen adsorption region equilibrium hydrogen coverage is not obtained before hydrogen evolution occurs. It is impossible to determine the surface area of this particular catalyst by voltammetry. The measured pseudocapacity is not indicative of monolayer hydrogen coverage.

For very small crystallites of palladium, however, internal absorption of hydrogen is minimal or non-existent since very few internal absorption sites are present. By decreasing the concentration of palladium to 4%, very small crystallites are obtained. These crystallites are small enough to have very little, if any, internal absorption of hydrogen, and the pseudocapacity due to hydrogen adsorption can be measured. In fact, the electrochemical adsorption peak of hydrogen on palladium is so characteristic that it can be seen to be distinct from the hydrogen on platinum adsorption peaks on a voltammogram of small crystallite size platinum-palladium alloys.

Since the charge for hydrogen adsorption on platinum and palladium is nearly the same (210 micro coul./cm^2 for platinum and 214 micro coul./cm^2 palladium), the surface areas of these alloy catalysts can be estimated from the adsorption pseudocapacitance (Stonehart, Power Sources, 514, 1966).

Surface areas for these catalysts are given in Table X, before and after testing in phosphoric acid at 180°C for five hours.

TABLE X

Pt and Pd Anode Electrocatalyst Formulation with Surface Area Changes

Catalyst	Composition	Surface Area (m^2/g) Pre-Test	Post-Test	% SA Lost
4% Pt/Consel I		190	90	53
4% Pd/Consel I		260	190	27
4% PGM/Consel I	25 a/o Pt/Pd	125	37	71
4% PGM/Consel I	35 a/o Pt/Pd	145	32	78
4% PGM/Consel I	50 a/o Pt/Pd	160	45	72
4% PGM/Consel I	75 a/o Pt/Pd	166	60	64

Except for a small peak on the 75 a/o Pd - 25 a/o Pt catalyst post-performance test voltammogram, none of these catalysts shows a hydrogen adsorption peak due to palladium. The hydrogen adsorption peak on the 75 a/o Pd - 25 a/o Pt voltammogram is considerably smaller on the post-test voltammogram than on the pre-test voltammogram.

The reason for the disappearance of this peak could be due to palladium segregation to the interior of the crystallite, palladium loss from the support, or change in the nature of hydrogen adsorption caused by testing in 180°C, 100% H_3PO_4.

Characterization of platinum-palladium alloy catalysts by cyclic voltammetry proved to be unexpectedly useful for obtaining information on both the surface area and composition of these catalysts. Palladium metal will absorb hydrogen atoms up to a H/Pd ratio of about 0.6 at room temperature (Palacyewska, Advances in Catalysis, 24, 248, 1975) in the presence of hydrogen.

As can be seen from Table X, the alloys show much greater surface area loss than either the platinum or palladium alone. The high surface area retention shown for palladium (190 m^2/g post-test) is surprising, since sintering of palladium on carbon is usually assumed to be very fast and severe. We have

experienced the rapid surface area loss for palladium on Vulcan XC-72 where the observed performance deteriorated too rapidly to allow a reproducible polarization curve.

Consel I is an excellent support material for palladium crystallites. Very high surface areas can be obtained on this material. A palladium preparation on Consel I had an initial surface area of 345 m^2/g or 14.5 Å crystallites. Contrary to expectations, these high surface areas seem to be stable. Very good bonding between palladium and Consel I seems to have been achieved.

Work on this contract produced several hydrogen oxidation binary alloy electrocatalysts which performed exemplarily, especially in the presence of carbon monoxide. The platinum-palladium electrocatalysts showed superior performance over pure platinum catalysts and were able to perform with minimal loss due to carbon monoxide poisoning even with carbon monoxide levels as high as 30%. At the request of NASA and DOE, patent disclosures have been written and a patent application (DOE Case S-55,310) has now been submitted.

At that time, the only technique available for characterizing the surface areas of these catalysts was electrochemical. Voltammetry was used extensively in an attempt to obtain crystallite size information. Since palladium will absorb hydrogen as well as adsorb it, then surface area determinations by this method are ambiguous. The voltammetric data needed to be verified by additional techniques. The gas phase carbon monoxide adsorption technique provided no aid, since it produced data which was both incomprehensible and non-reproducible. An explanation for this has not been found.

High resolution electron microscopy was used as a preferred technique. The platinum-palladium system was of sufficient interest to warrant the investment of time and resources to produce the required high magnification photomicrographs. Figures 36 and 37 are examples of this work. The magnification on these photomicrographs is 2×10^6 times (2,000,000X). Each millimeter is equivalent to 5 Å.

Figures 36 and 37 are quarter tone reproductions of photographic prints, so

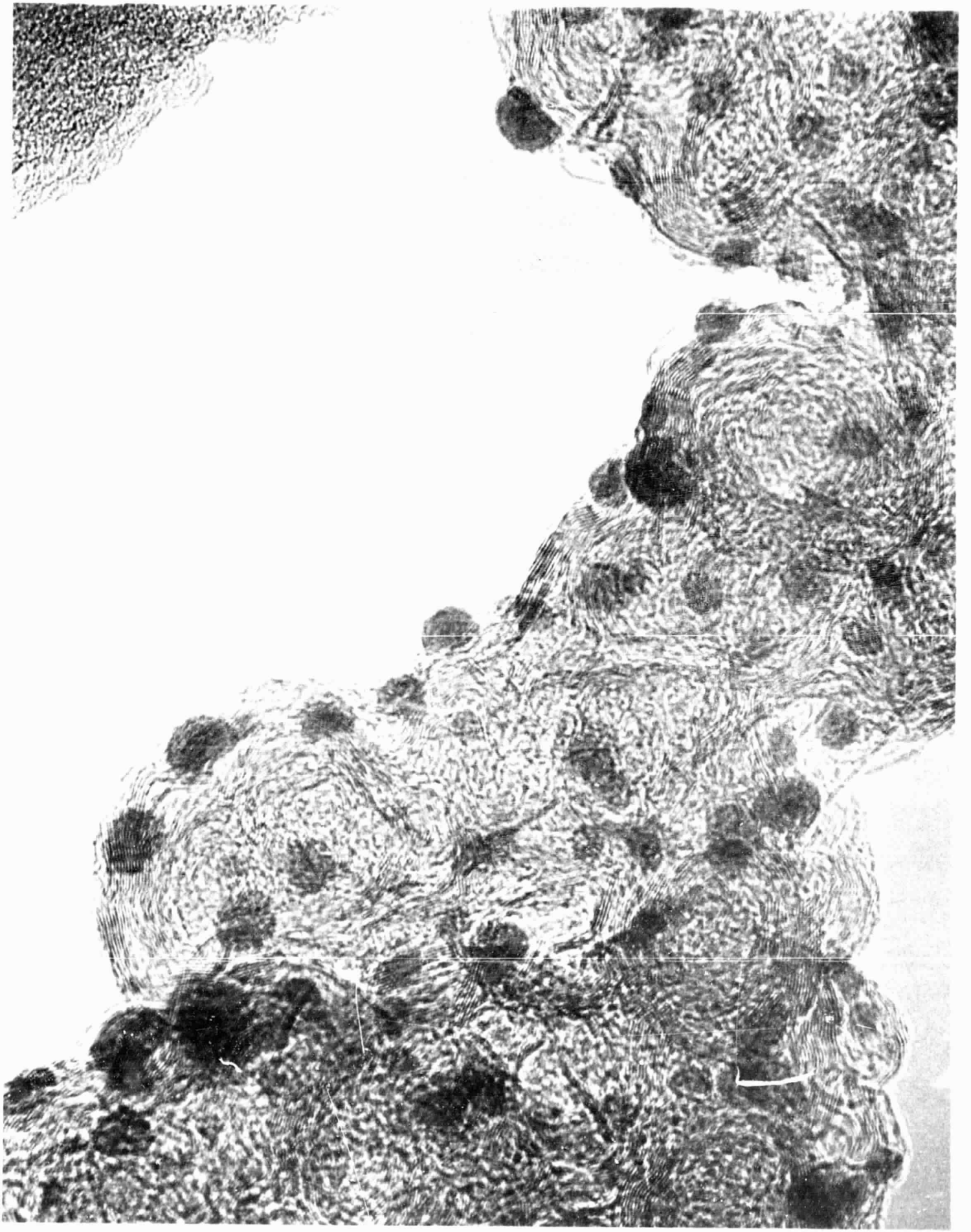

Figure 36. EC 125 4 w/o Pd on Consel I. 2,035,000X mag.

Figure 37. EC 123 4 w/o Pt-Pd (50 a/o Pd) on Consel I. 2,035,000X mag.

some of the fine resolution in the original photographic print is lost. The transmission electron micrograph plates were obtained at a magnification of 400,000X and then 5X enlargements were produced from selected areas of the plates to the prints. It can be seen by comparison of Figures 36 and 37 that the metal crystallite sizes of the Pd particles in Figure 36 are larger than the Pt-Pd alloy particles of Figure 37. (Table XI shows that our catalyst preparation techniques produce a higher dispersion for platinum than palladium.) These electron micrographs demonstrate that the addition of platinum to the palladium (Figure 37, EC 123, is a 50/50 a/o Pt/Pd alloy) confers a significantly higher dispersion to the palladium than for palladium alone. Based on the transparency of the metal particles to the electron beam, some idea can be gained for the metal particle thickness. Figure 36 (EC 125) shows uniform densities for the particles, arguing that the apparently spherical particles are of approximately equal size and thickness. The metal particles in Figure 37 (EC 123) on the other hand, show significant variation in size and electron transparency, suggesting thin platelets.

One further feature of the electrocatalysts is exhibited by these electron micrographs. Close examination of the carbon support surface shows distinct evidence for graphitic layers. (Parallel lines 3.5 Å width separation). This demonstrates that the Consel I support that is so beneficial, has the surface graphitic character that is required for both corrosion resistance in the hot phosphoric acid and for stabilizing the PGM crystallites. The interior of the carbon particle remains untouched in a more turbostratic form to preserve the integrity of the carbon agglomerate.

Table XI summarizes the data obtained for these photomicrographs.

TABLE XI
Electrocatalyst Crystallite Sizes

Catalyst #	Catalyst	Crystallite Size (Å) ECA	Microscopy
EC 127	4% Pt/Consel I	15 Å	17 ± 3 Å
EC 125	4% Pd/Consel I	19 Å	40 ± 10 Å
	4% PGM/Consel I		
EC 122	a. 25 a/o Pt/Pd	33 Å	50 ± 25 Å
EC 123	b. 50 a/o Pt/Pd	21 Å	25 ± 3 Å
EC 128	c. 75 a/o Pt/Pd	18 Å	30 ± 15 Å

The crystallite size determinations by voltammetry and microscopy are in very good agreement for 4% Pt/Consel I as would be expected. The voltammetry underestimates the crystallite size when palladium is present. This is due to the absorption of hydrogen by internal palladium to form palladium hydride. In fact, the hydrogen to palladium absorption ratio can now be determined. Equation (5) below (see Appendix for derivation) relates the charge measured under the hydrogen region for the palladium voltammogram with the crystallite size, assuming spherical geometry.

$$d = \frac{B(1-R)}{Q-AR}$$

where Q is the charge (per gram of palladium) measured under the cathodic hydrogen peak on a voltammogram; A and B are constants, ($A = 9.07 \times 10^2$, $B = 1.10 \times 10^4$); R is the atomic ratio of hydrogen to palladium atoms interior to the crystallite; and d is the diameter of the crystallite in angstroms. The surface H/Pd ratio is assumed to be 1. Using 40 Å as d and 546 coul/gram Pd measured previously, the ratio R is equal to 0.43.

During voltammetry, then, the H/Pd ratio interior to a crystallite is equal to 0.43 (subject to further experimental verification) which is somewhat lower

than 0.6 reported by Palcyewska (Advances in Catalysis, 24, 247-253) for bulk palladium in the gas phase. This is, perhaps, an example of the strangeness in the properties of small particles versus the properties of the bulk material, where the surface energy of the particle is affecting the bulk properties of the material. The value of R needs to be verified by further correlations of voltammetry and microscopy on other crystallite sizes of palladium, but once that is done, Equation (5) can be used to determine palladium crystallite size by voltammetry.

Of the three platinum-palladium catalysts reported in Table XI, the 50 a/o Pt/Pd catalyst has the smallest average crystallite diameter with the most uniform dispersion (Figure 37). This may, in part, explain the fact that a 50 a/o Pt/Pd ratio also gives the best performance with the highest CO poisoning tolerance.

A 50 a/o Pt/Pd ratio would also be expected to give the most homogeneous alloy composition. Perhaps the non-uniformity of the 25 a/o and 75 a/o Pt/Pd catalysts is due to an excess of Pt or Pd producing unalloyed Pt or Pd crystallites when Pt or Pd is in excess over a 50 a/o mix. Such an inhomogeneous catalyst would not be expected to take full advantage of the synergism which seems to exist between platinum and palladium for CO tolerance.

ii. Noble Metal - Refractory Metal Mixtures

Rhenium does not have a hydrogen adsorption pseudocapacitance, and hence, presents a problem. Similar characteristics for rhenium powder have been previously reported (Bennett, et al., Materials for Fuel Cells, DOE Annual Report, 1977). Hydrogen adsorption pseudocapacitance, therefore, cannot be used to estimate the surface area of rhenium. Since rhenium also does not adsorb CO (see Task 4 above), CO chemisorption cannot be used to estimate particle size. Lack of superior performance of rhenium and platinum-rhenium alloys so far makes the effort and expense involved in determining the surface area of these materials by transmission electron microscopy unwarranted. The presence of rhenium does not seem to interfere with the hydrogen adsorption of the platinum in the alloys, so the surface area of the platinum in these alloy

catalysts can be determined by electrochemical scanning and the results are summarized in Table XII.

TABLE XII
Platinum-Rhenium Alloy Electrocatalyst Surface Areas

Catalyst	Composition	Surface Area (m^2/g) Pre-Test	Post-Test	% SA Lost
4% Re/Consel I		—	—	—
4% Pt-Re/Consel I	49 a/o Pt	72	48	33
10% Pt-Re/Consel I	24 a/o Pt	94	70	26
10% Pt-Re/Consel I	49 a/o Pt	142	71	50
10% Pt-Re/Consel I	74 a/o Pt	150	72	52
10% Re/Consel I		—	—	—
10% Pt/Consel I		140	62	56

Initial attempts to characterize platinum-tungsten and platinum-molybdenum catalysts were made using cyclic voltammetry. There are no obvious features on the Pt/W voltammogram which show the presence of tungsten in the catalyst surface layer.

On the platinum-molybdenum voltammogram, the hydrogen adsorption on platinum region of the curve is not as well defined, and an additional couple seems to appear at 500 mV (anodic) and 470 mV (cathodic).

Further investigation of the voltammetry of molybdenum and tungsten with platinum needs to be done in order to fully interpret these voltammograms. Measurement of the pseudocapacity under the hydrogen adsorption peaks, however, should give an indication of the surface area of platinum exposed and the crystallite size. These values for pre- and post-performance electrodes are tabulated in Table XIII.

TABLE XIII

Platinum-Refractory Metal Electrocatalyst Surface Areas

Catalyst	Treatment	Pt Surface Area (m^2/g Pt) Pre-Test	Post-Test
10% Pt + 4.7% W/Consel I	400°C - 2 hrs.	16	16
10% Pt + 2.6% Mo/Consel I	400°C - 2 hrs.	23	14
10% Pt + 4.7% W/Consel I	900°C - 1 hr.	30	13
10% Pt + 2.6% Mo/Consel I	900°C - 1 hr.	31	31
9.9% Pt + 0.9% V/Consel I	900°C - 1 hr.	77	44

If this measurement is any indication of the crystallite size, then these catalysts do not have high surface areas and are not expected to perform as well as cathodes in phosphoric acid. The apparent increase in the surface area from 400°C heat treat to the 900°C heat treat is due probably to a surface rearrangement of the platinum-tungsten and platinum-molybdenum atoms, with subsequent exposure of more platinum atoms. Obviously, additional surface characterization techniques need to be pursued before the surfaces of these catalyst crystallites can be fully understood.

The voltammogram of supported platinum-vanadium electrocatalysts was obtained. Additional peaks have appeared at high potentials (700-1100 mV) but little if any effect is seen at the lower potentials. The pre-performance test surface area of the platinum-vanadium catalyst is 77 m^2/g Pt, and the post-test surface area is 44 m^2/g Pt. These areas are lower than the surface area of the platinum on Consel I precursor used to make this catalyst which was 110 m^2/g Pt. Addition of vanadium has decreased the platinum surface area from 110 m^2/g to 77 m^2/g. This surface area loss may be due to the severe heat treatment (900°C) needed to react the platinum with vanadium.

Voltammetry can only give an estimate of the surface area of alloy catalysts and tells nothing of the surface composition when the alloying element does not produce a measurable feature on the voltammetric curve. Further characterization of these alloy catalysts must proceed with microscopy or surface spectroscopy. Even these techniques are often stretched to their limits when applied to highly dispersed supported catalysts.

The following table summarizes the voltammetry results.

TABLE XIV

Surface Areas of Platinum-Refractory Metal Alloy Electrocatalyst Obtained by Voltammetry

Catalyst	Composition/Support	Surface Area (m^2/g) Pre-Test	Post-Test	% SA Lost
	Consel I	82		
EC-150	12.9% Pd-Nb/Consel I	88	54	38
EC-151	14.3% Pd-Ta/Consel I	128	95	26
EC-152	12.3% Pt-Ta/Consel I	20	10	50
EC-216	10% Pt/Consel IV	125	80	36
EC-217	10% Pt/Consel IV	60	60	0
EC-214	10.8% Pt_3V/Consel I	75		
EC-215	10.8% Pt_3V/Vulcan	100		

iii. Noble Metal Sulphides

The voltammogram of platinum sulphide does not show any presence of sulphur. Since the hydrogen adsorption region of the voltammogram seems unaffected, the surface area of the platinum may be estimated. It must be remembered that the presence of sulphur may distort the surface area determination. If necessary, the surface area estimate by voltammetry can be supported with transmission electron microscopy. Table XV summarizes the platinum surface area found for five PtS_2/Consel I preparations.

TABLE XV

Platinum Sulphide Electrocatalyst Surface Areas

Catalyst	Surface Area (m^2/g)	Final Treatment
10% PtS_2/Consel I	29	None
10% PtS_2/Consel I	42	Calcined in air @ 200°C
10% PtS_2/Consel I	41	Reduced in 5-10% H_2/N_2 @ 200°C
10% PtS_2/Consel I	39	Reduced in 5-10% H_2/N_2 @ 150°C
10% PtS_2/Consel I	51	Reduced in 5-10% H_2/N_2 @ 350°C

Along with the preparation and testing of platinum sulphide catalysts as cathodes, some initial studies were made to find a method for determining the

crystallite size. The voltammogram for platinum sulphide appears to be similar to that of platinum.

If sulphur is present in the crystallite, which observation of the preparation procedure seems to indicate, it either does not have electrochemical activity which the cyclic voltammetry could detect, or sulphur is not present at the surface of the crystallite.

Determination of the crystallite size of supported platinum sulphide may not be accomplished by either gas phase or electrochemical adsorption techniques. Thus far, no specific adsorbents which could be used for surface area determination of platinum sulphide have been found in the literature.

Qualitatively, the hydrogen adsorption charge of the voltammogram can be used as an indication of the surface area since the surface platinum present probably indicates the relative crystallite size. Pre- and post-test platinum surface areas are given in Table XVI for four platinum sulphide preparations.

TABLE XVI
Surface Area of Platinum Sulphide Electrocatalysts

Catalyst No.	Surface Area (m^2/g) Pre-Test	Post-Test	% SA Lost
EC-137	29	17	41
EC-138	42	21	50
EC-139	41	15	63
EC-141	51	19	62

Interest in further characterization of this catalyst will be dependent on its performance as an oxygen reduction catalyst in phosphoric acid.

Task 7 - Catalytic Activity of Platinum-Based Carbon-Supported Electrocatalysts

i. Noble Metal Alloys - Anodes

The performances for two platinum-palladium electrocatalysts for hydrogen oxidation were reported previously (Figures 34 and 35). Both of these catalysts contained approximately 10% metal loading and a Pt/Pd ratio of approximately 50 w/o (35 a/o) Pt. The performances of gas diffusion electrodes prepared from these catalysts compare favorably to the performance of a platinum supported catalyst. These performances for hydrogen oxidation and carbon monoxide tolerance are very promising, especially when one considers that even partial replacement of platinum by palladium would result in a reduction of material cost since palladium is about 1/3 to 1/2 the cost of platinum. As a result, further investigation of the platinum-palladium alloy system as anode catalysts was conducted. Results are reported below for the platinum-palladium alloy catalysts in the ratio 0 to 100% Pt/Pd and catalyst loadings of 2, 4 and 10%. Also, since structure has been shown to influence the sensitivity of a platinum on carbon electrocatalyst to carbon monoxide poisoning some preliminary work was done to investigate the extent of structural sensitivity of platinum-palladium alloy catalyst electrodes to

carbon monoxide poisoning.

The alloy catalysts prepared in Task 5 at the 35 a/o Pt level and 2, 4 and 10 w/o PGM were fabricated into gas diffusion electrodes and tested for performance as anodes under H_2, 10% CO/H_2 and 30% CO/H_2. The performance results were obtained and then used to construct Figure 38 which summarizes the performance data at 25 mV polarization. The data would suggest that these electrodes are operating in a diffusion limited regime; however, it should be noted that electrocatalyst surface area has not been factored into the analysis. As a result, this interpretation of Figure 38 is not conclusive.

The apparent activation energy for hydrogen oxidation with and without carbon monoxide in the fuel gas is determined by plotting the reaction rate as a function of temperature.

The data reported here can be compared to similar data obtained for platinum on Vulcan XC-72R as reported previously. In Figure 39 the anode performance of electrode P-54 is shown as a function of temperature while operating on 100% H_2. Electrode P-54 was made from a 10% PGM (50 w/o Pt/Pd) catalyst, and has a loading of 0.5 mg PGM/cm^2. Comparing the hydrogen oxidation performance of electrode P-54 (0.5 mg PGM/cm^2) with electrode P-55 (0.2 mg PGM/cm^2) (Figure 40) it is apparent that at a current density of 200 mA/cm^2 (approximately the fuel cell operating current density) only an additional 1-4 mV polarization is incurred by dropping the loading from 0.5 mg PGM/cm^2 to 0.2 mg PGM/cm^2. The lack of significant performance loss seen on the 0.2 mg PGM/cm^2 electrode versus the 0.5 mg PGM/cm^2 electrode is due probably to a decrease in crystallite size achieved on the lower loaded catalyst, which of course increases the surface area available for reaction. The performance of the Pt/Pd catalysts compares most favorably with performance data generated for 100% Pt catalysts. Performance data usually agree within 5 mV at 200 mA/cm^2. Optimization of the electrode structure could eliminate even this small difference and probably improve the performance of this alloy over the performance of pure platinum. The temperature variation of the reaction rate for 100% H_2 for these catalysts (4% PGM/Consel I and 10% PGM/Consel I) are plotted in Figures 41 and 42. Measurements of the slopes at 10 and 25 mV gives an apparent activation energy of 4 kcal/mole at both potentials for the

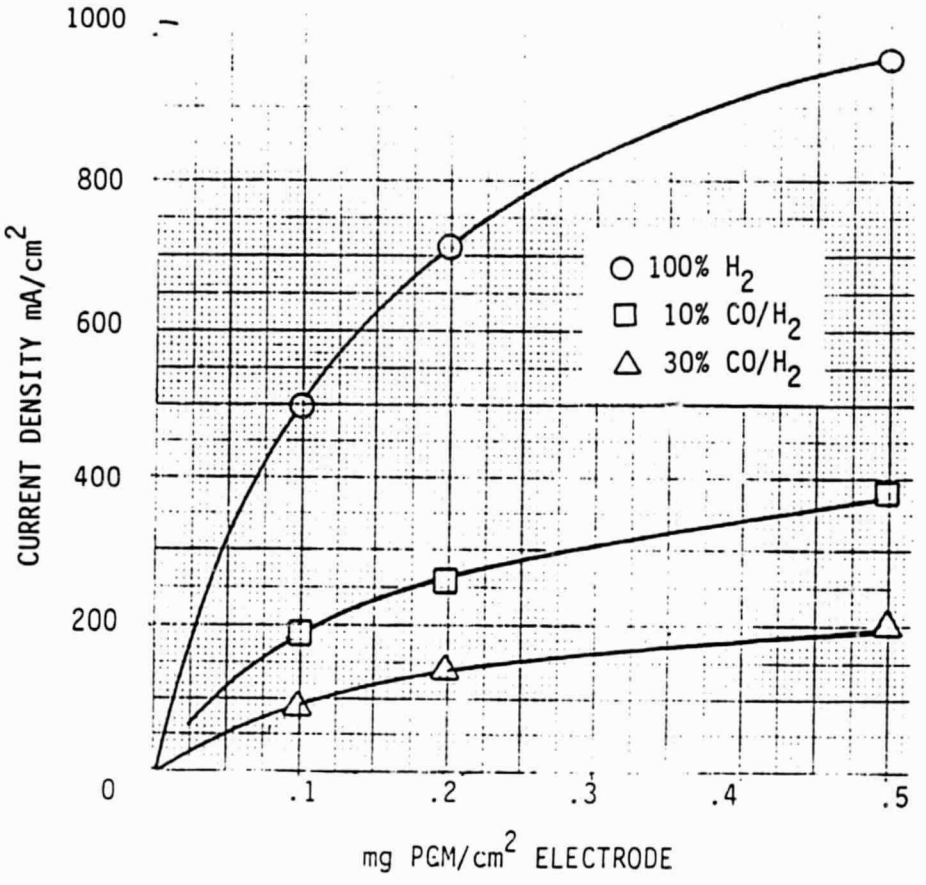

Figure 38. Current density as a function of catalyst loading for constant thickness electrodes at various CO concentrations. Polarization is 25mV from RHE. Electrocatalyst contains 35 atom % Pt.

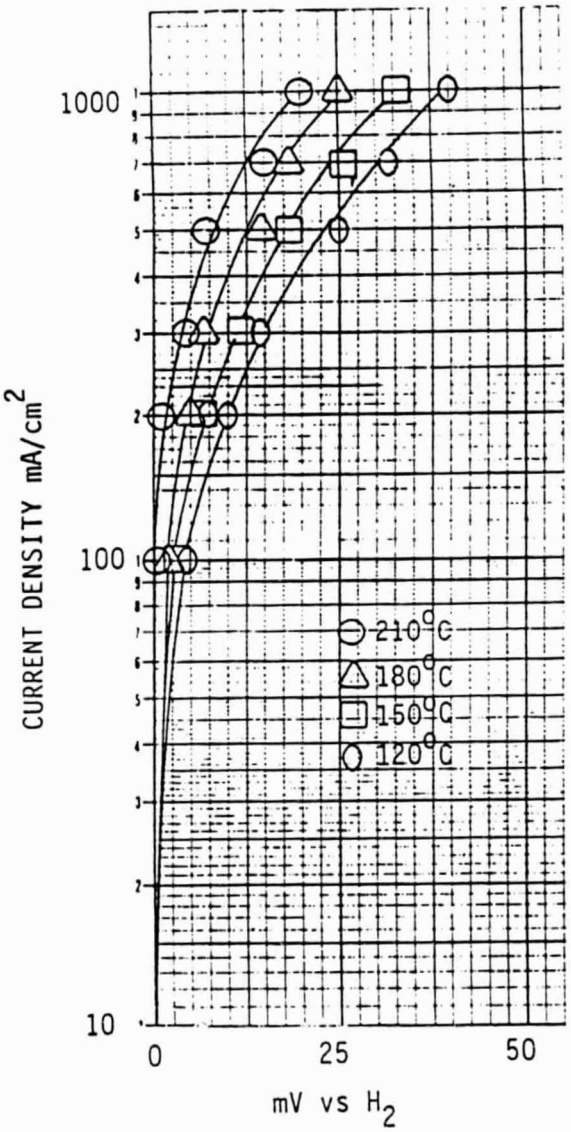

Figure 39. Anode performance for leelctrode P-54, 0.5mg PGM/cm^2. Catalyst is 10% PGM/Consel I. Electrode contains 30% PTFE and was run at various temperatures in 100% H_3PO_4 on 100% H_2.

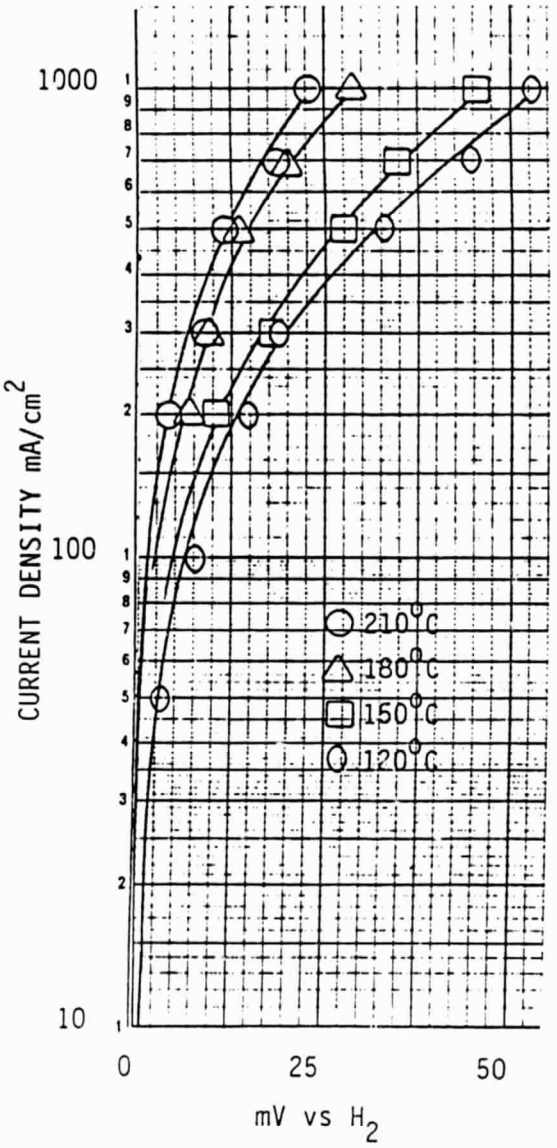

Figure 40. Anode performance for electrode P-55, 0.2 mg PGM/cm^2. Catalyst is 4% PGM/Consel I. Electrode Contains 30% PTFE and was run at various temperatures in 100% H_3PO_4 on 100% H_2.

10% PGM/Consel I catalyst and an apparent activation energy of 5.6 kcal/mole and 4.9 kcal/mole at 10 and 25 mV, respectively, for the 4% PGM/Consel I catalyst. Within the limitations of the experimental error, these values are approximately equal to those found for 10% Pt/Vulcan XC-72R. Such low activation energies usually indicate a diffusion controlled reaction, and we therefore cannot at this time comment upon the mechanism of H_2 oxidation on Pt/Pd alloys versus Pt.

In Figures 41 and 42 the temperature dependent current density at 10 and 25 mV and 10 and 30% carbon monoxide levels is plotted along with the 100% hydrogen data. By plotting the data this way, it is easy to generate the apparent adsorption isotherms for carbon monoxide on the catalyst as a function of temperature and electrode potential.

From the isotherms it is possible to draw a site-availability comparison to Pt. The site-availability comparison must be approached carefully, since the site availability of the PGM catalyst is apparently lower than that for platinum but we cannot be totally certain that structural (diffusion) factors are not rendering such a comparison invalid at this time. Only if both catalysts are under 100% activation control or have the same mix of diffusion and activation control would this comparison be valid. Optimization of electrode structures will change the $1-\theta_{CO}$ ratios.

Even though the relative number of sites for hydrogen oxidation for our catalysts (4% PGM and 10% PGM) is lower than that for 10% platinum on Vulcan XC-72, it may be possible that the total number of <u>active sites</u> is greater and that a greater dispersion has been achieved by adding palladium to the platinum. Due to the lower atomic weight of palladium, higher dispersions can be achieved.

Progress in reducing the cost of the anode is shown in Figure 43. The solid line is the performance versus cost for 10% Pt on Vulcan XC-72R at various electrode loadings and is constructed from data obtained in this laboratory. The performance is based on the polarization at 200 mA/cm^2 for a 10% CO/90% H_2 fuel. The dollar cost is normalized to the cost of a 0.5 mg Pt/cm^2 electrode. As a further point of reference, the commonly accepted performance value for

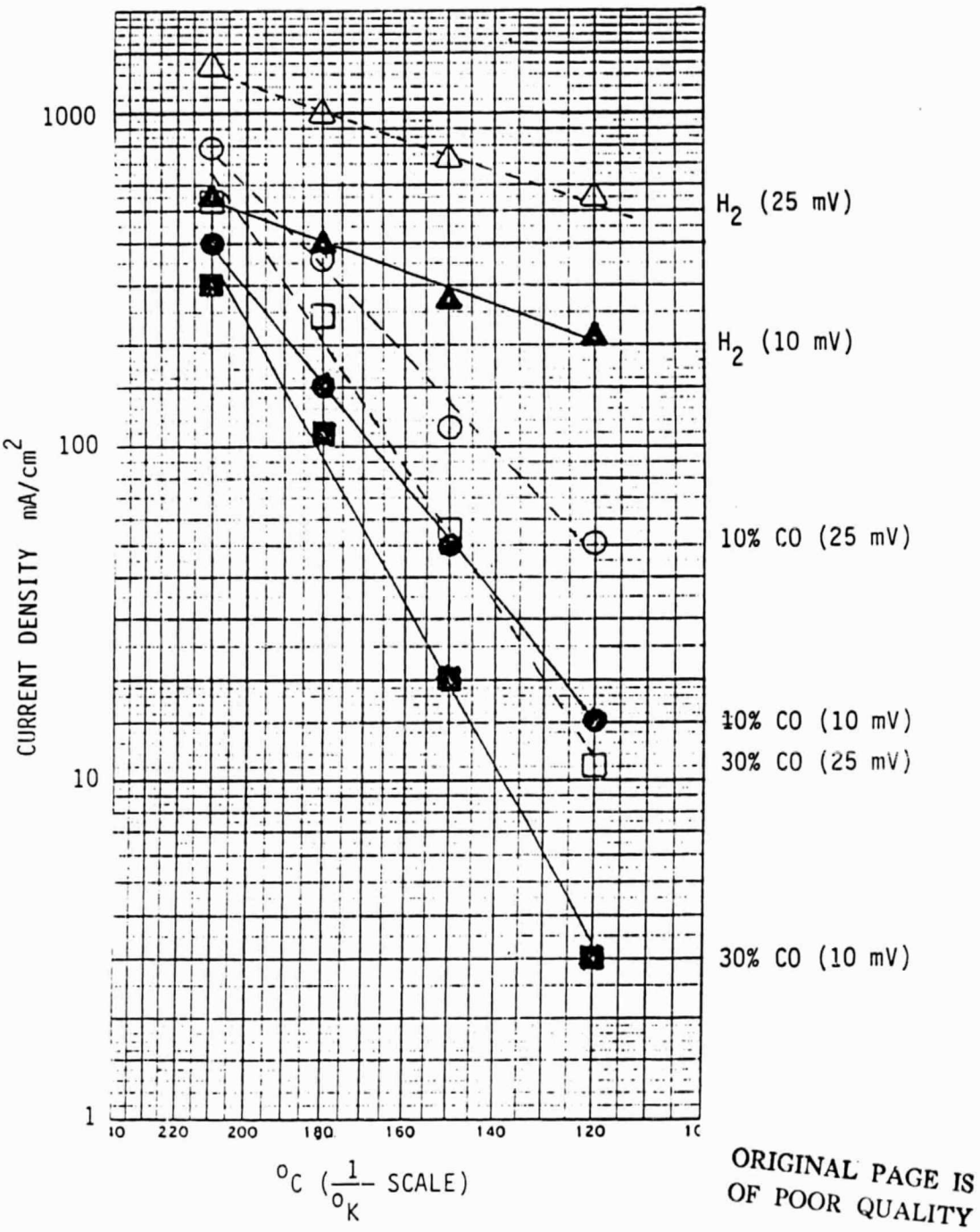

Figure 41. Current density as a function of 1/T for hydrogen oxidation on 100% H_2, and 30%CO/H_2 at 10mV and 25mV polarization, in 100% H_3PO_4. Electrode number P-54, 0.5 mg PGM/cm^2, 30% PTFE. Catalyst is 10% PGM on Consel 1.

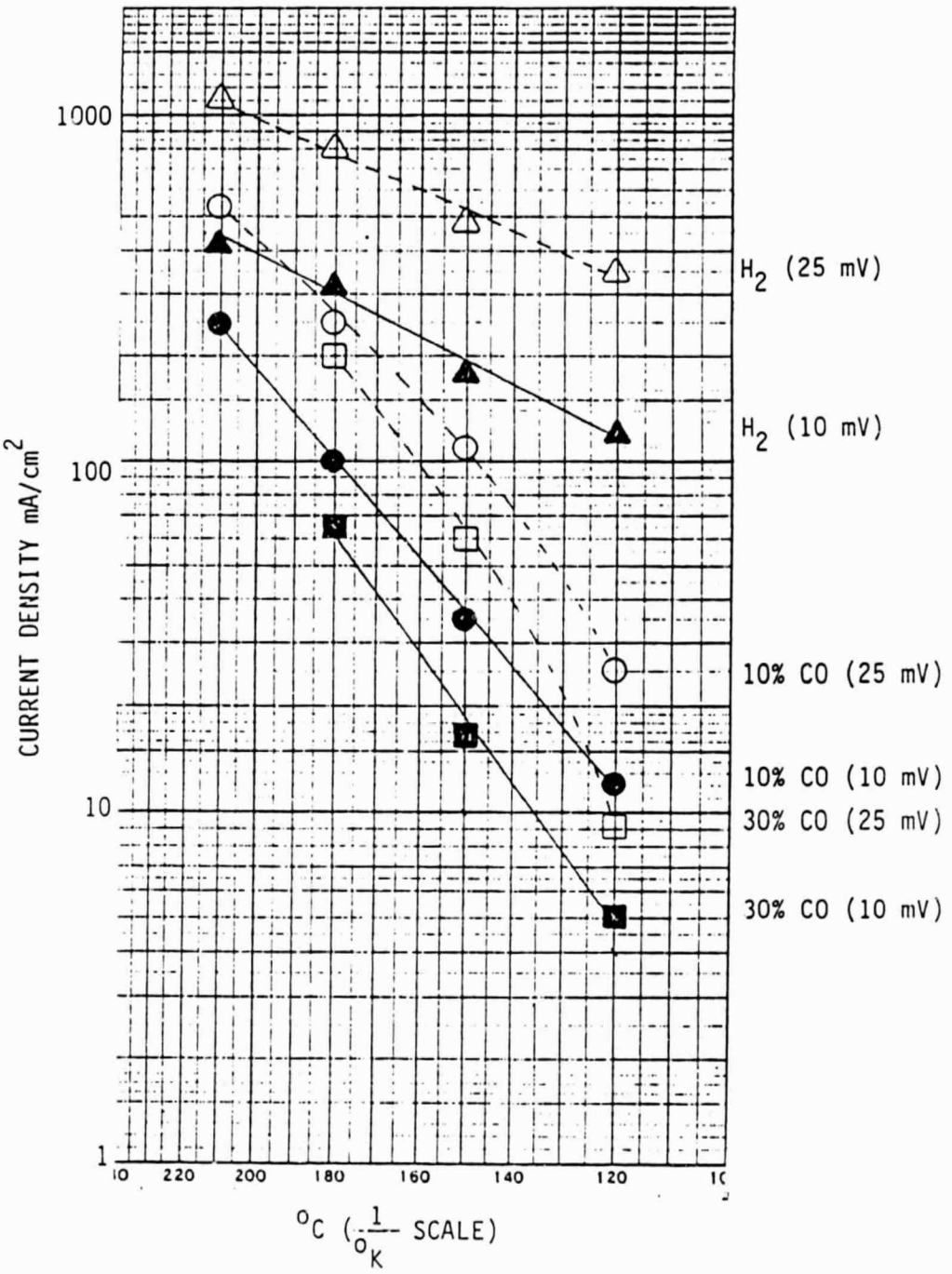

Figure 42. Current density as a function of 1/T for hydrogen oxidation on 100% H_2, 10%CO/H_2, and 30%CO/H_2 at 10mV and 25mV polarization, in 100% H_3PO_4. Electrode number P-55, 0.2mg PGM/cm^2, 30% PTFE. Catalyst is 4% PGM on Consel 1.

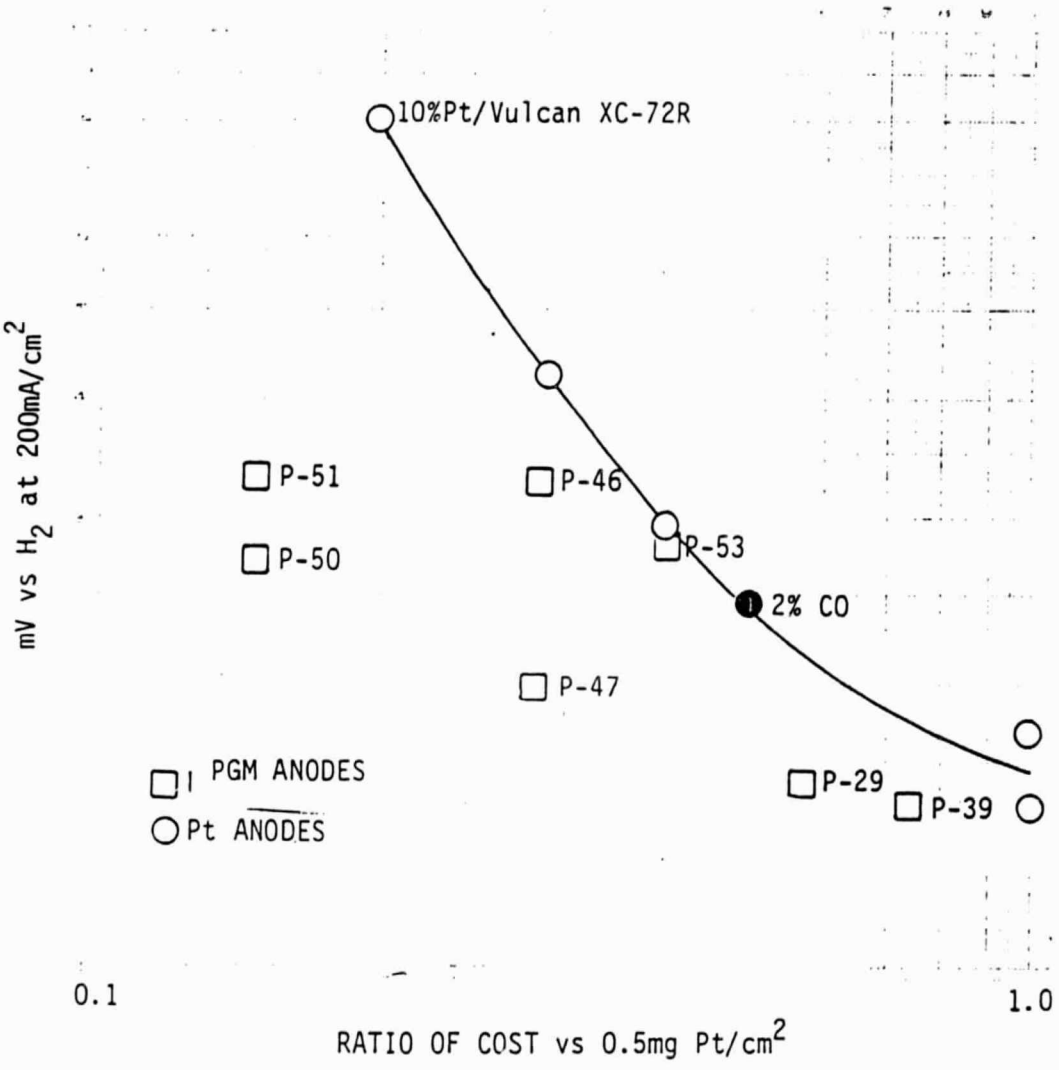

Figure 43. Comparison of anode electrode performances at 180°C in 100% H_3PO_4 on 10% carbon monoxide 90% hydrogen at 200mA/cm^2 as a function of catalyst cost ratioed to the cost of 0.5mg Pt/cm^2 Pt/Vulcan XC-72R.

80% H_2, 2% CO and 18% CO_2 with .25 mg Pt/cm^2 at 180°C is 25 mV polarization at 200 mA/cm^2. This point is shown as the solid circle in Figure 43. It is clear that any electrocatalyst which falls below the line for state-of-the-art 10% Pt on Vulcan XC-72R electrocatalyst will result in lowering the cost of the anode. All of our alloy preparations operate in this region of lower cost, with the P-50 catalyst combination preferred at this time (2 w/o loading of 50/50 w/o Pt/Pd).

The performance comparisons for the platinum/palladium alloy catalysts are presented in Figure 44. When the polarization data at 200 mA are plotted, it can be seen that the polarization of this catalyst shows a minimum at 50% platinum/palladium catalyst. The 100% Pt catalyst (blackened-in symbols in Figure 44), had only been heat treated to 200°C and not 700°C as our alloy catalysts had been. The 700°C heat treatment ensures alloying of the constituents. The heat-treated catalyst performance is lower than the unheat-treated 100% Pt/Consel I catalyst performance, probably due to thermal growth of the metal crystallites.

Using the performance data from this heat treated catalyst as data points in Figure 44 allows us to draw the trend line of polarization as a function of a/o Pt. The maximum performance (minimum polarization) appears at an alloy composition slightly greater than 50 a/o Pt.

iia. Noble Metal - Refractory Metal Mixtures - Anodes

The catalytic activity of rhenium supported on Consel I for hydrogen oxidation is essentially negligible. The polarization of a 100% rhenium/Consel I catalyst was 350 mV at only 10 mA/cm^2 current density for 100% H_2.

Performance curves for a 74 a/o Pt/Re, 49 a/o Pt/Re and 24 a/o Pt/Re alloy catalyst, respectively, were obtained at 180°C in 100% H_3PO_4 on 100% H_2, 10% CO/H_2, and 30% CO/H_2. These catalysts each contained 10% total metal (Pt + Re). The dilution of platinum by rhenium decreases the activity for hydrogen oxidation. No benefit can be seen on the performance under 100% H_2, and no increased tolerance for CO poisoning can be seen.

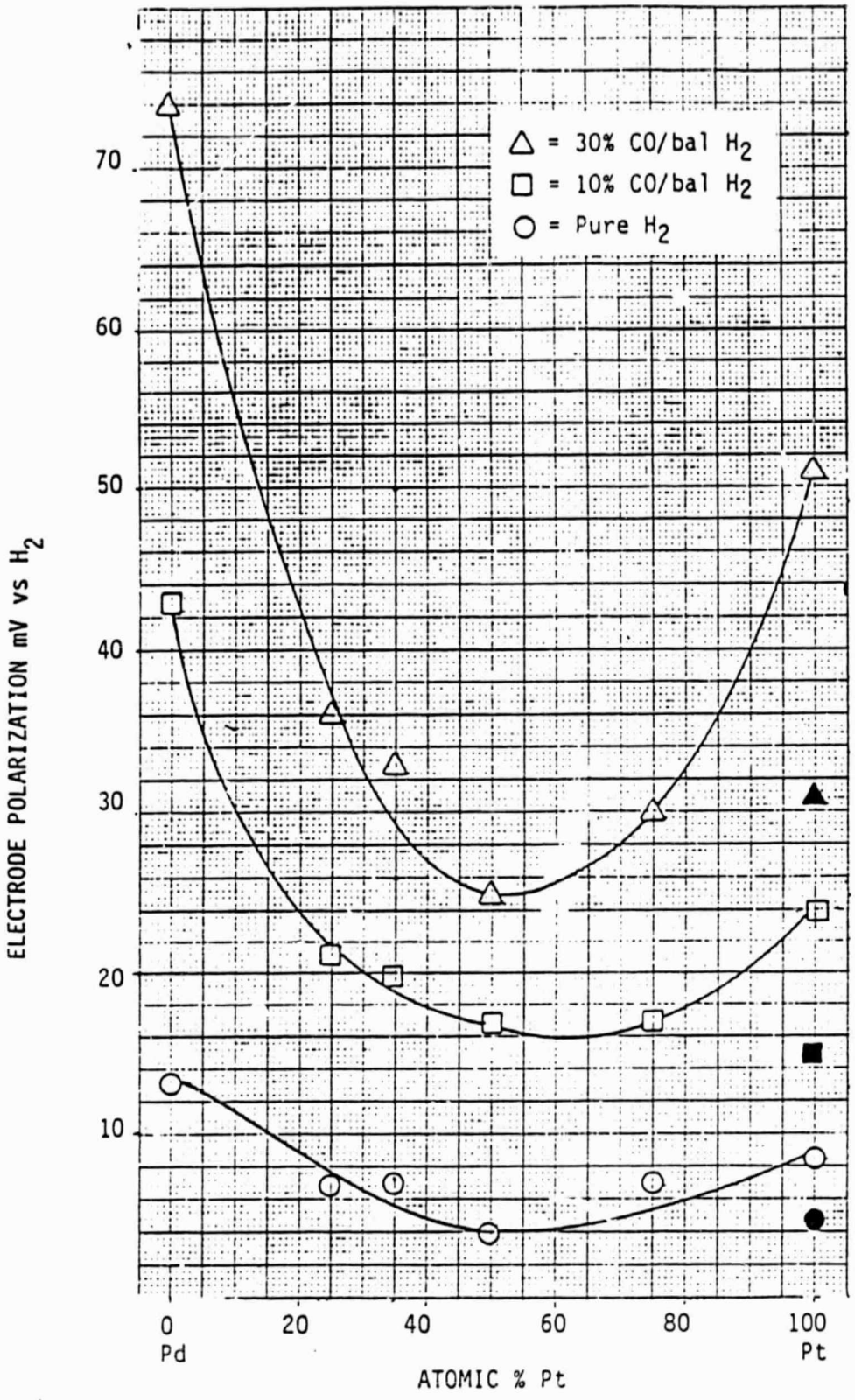

Figure 44. Anode polarization at 200 mA/cm^2 as a function of a/o platinum for various fuel gases. The catalyst is 4% PGM/Consel I and was fabricated into gas diffusion electrodes (30% PTFE) with a loading of 0.2 mg PGM/cm^2. These data were obtained at 180°C in 100% H_3PO_4. Open Symbols for catalysts heat treated to 700°C. Solid symbols for standard 4% Pt/Consel I catalyst.

iib. Noble Metal - Refractory Metal Mixtures - Cathodes

As expected from the low surface areas measured for platinum-tungsten and platinum-molybdenum, the performances of these catalysts are lower than for platinum alone. The relevant performance data are given in Table XVII with a comparison to a typical platinum on Consel I catalyst.

TABLE XVII
Performance Characteristics for Platinum-Refractory Metal Alloys for Oxygen Reduction at 180°C

Catalyst	Tafel Slope	Activity at 900 mV (O_2)	Polarization (Air) at 200 mA/cm^2
Pt + W/Consel I	120 mV/Decade	69 microA/cm^2	555 mV
Pt + Mo/Consel I	120	29	605
Pt + V/Consel I	120	90	700
Pt/Consel I	100	61	712

The data show that these catalysts do not perform as well as the best platinum on Consel I for oxygen reduction. This poorer performance could be due to the low surface area of these catalysts as presently prepared. Until a high surface area preparation of platinum with tungsten or molybdenum is developed, a valid determination of the performance of these catalysts cannot be made.

The performance of a platinum-vanadium intermetallic catalyst was determined and the performance data are summarized in Table XVII.

Even though the post-test surface area is only 44 m^2/gram, the performance of this catalyst is probably better than platinum alone. The activity of Pt-V for oxygen reduction is calculated to be 90 micro A/cm^2, which is at the top of the range for platinum (L. Bregoli, Electrochim. Acta, 23, 489 (1978)). This high an activity for oxygen reduction is only occasionally measured for platinum on carbon catalysts. The polarization at 200 mA on air for Pt-V is 700 mV, which again is as good as for platinum on carbon. These results are very encouraging for Pt-V electrocatalysts.

The companion EPRI 1200-2 program has developed advanced electrocatalyst

supports, some of which have been utilized in this present DEN3-176 program. A new support, which was identified as Consel IV, has been developed in the EPRI 1200-2 program. This support was catalyzed using our process technology with the platinum-vanadium intermetallic. Performance data were obtained on oxygen and air (Electrode #99). Reasonable performance parameters for oxygen reduction on platinum are a Tafel slope of 90 mV at 180°C, 100% phosphoric acid. The performance levels achievable are tabulated in Table XVIII.

TABLE XVIII

Performance Characteristics for Platinum-Vanadium on ConselIV for Oxygen Reduction

Electrode P99 - 0.5 mg Pt/cm^2 Electrode

i	Air at Atmospheric		Pure O_2 at Atmospheric and Air at 5 atm.	
mA/cm^2	Actual	Projected	Actual	Projected
300	686	725 (mV vs H_2)	757	805 (mV vs H_2)
200	714	750	781	820
100	755	775	819	850
10	865	870	939	940

Although some improvement could be made in the preparation technique to produce a higher surface area catalyst, the performance of this catalyst as a cathode is promising, as shown Figure 45.

Preparation of platinum-vanadium on Vulcan XC-72R (EC-215) produced an excellent electrocatalyst. The cathodic performance curve, shown in Figure 46, is as good as the best platinum on Vulcan electrocatalyst.

The addition of tantalum and niobium to palladium did not improve the catalytic activity as either a cathode or an anode. Palladium on Consel I will operate as an anode at 200 mA/cm^2 and give a potential of 11 mV (vs H_2) and will operate at 250 mV (vs H_2) at 200 mA/cm^2 on air.

The addition of niobium decreased the anode performance to 156 mV at 200

C-2

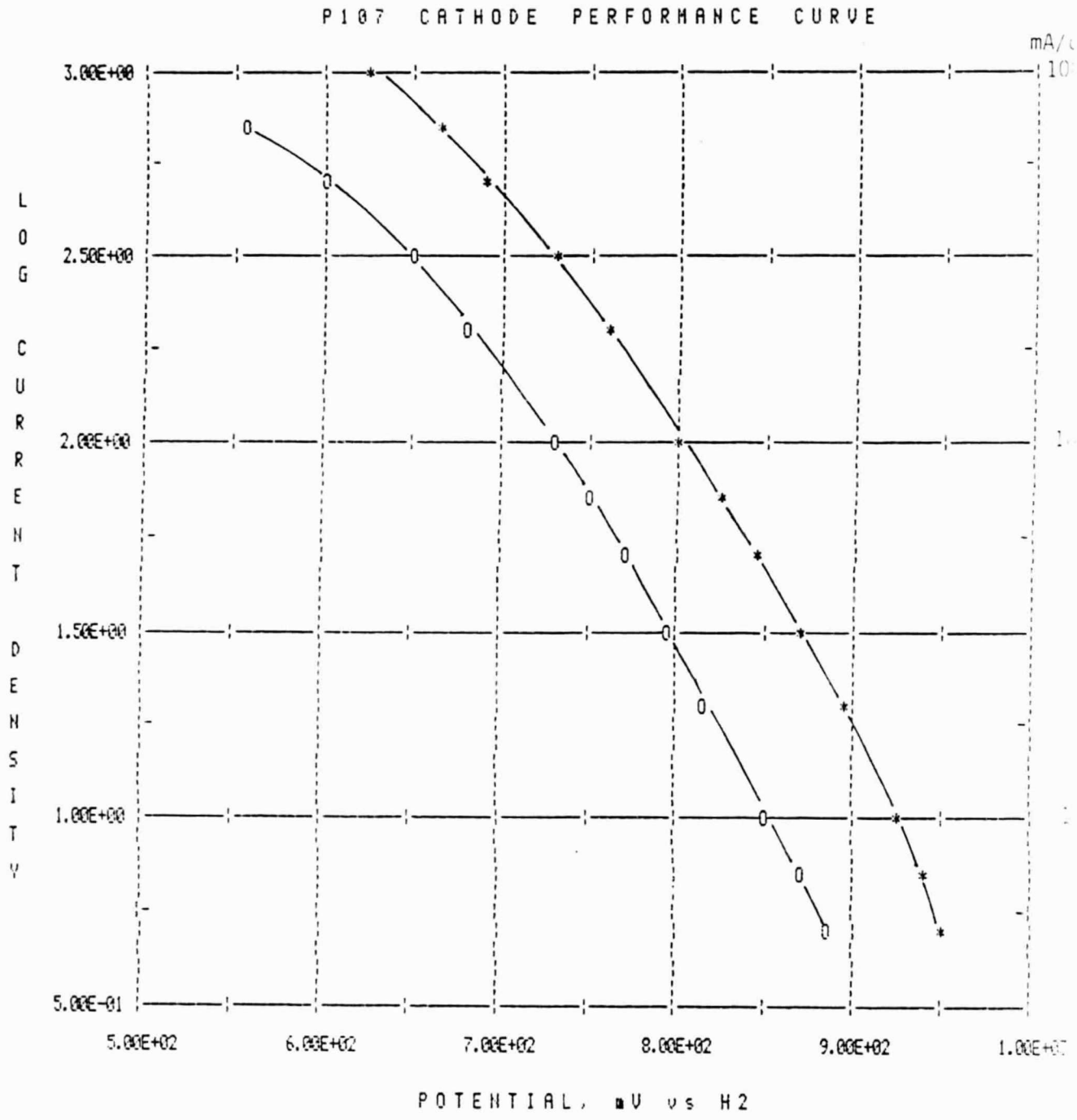

Figure 45. Cathodic performance of electrode P-107 made from a 10% Pt/Consel IV electrocatalyst. The electrode contains 0.5mg Pt/cm^2 and was run in 100% H_3PO_4 at 100°C on air (0) and O_2(*).

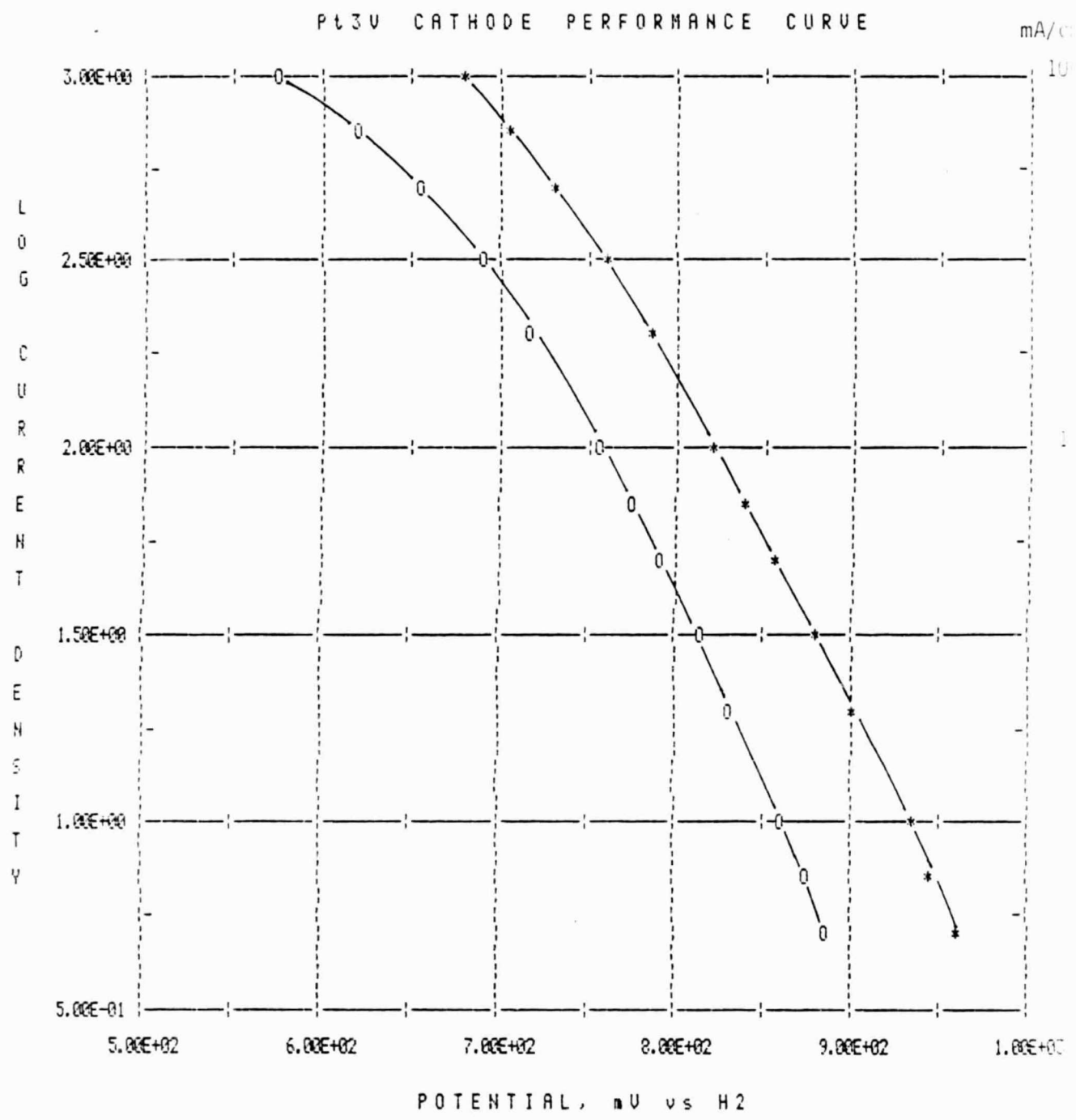

Figure 46. Cathodic performance of electrode P-84 made from a 10.8% Pt-V/Vulcan XC-72R (Pt:V ratio=11:1) electrocatalyst. The electrode contains 0.5mg Pt-V/cm and was run in 100% H_3PO_4 at 180°C on air (0) and O_2(*).

mA/cm^2 and the cathode performance was so poor that it would not operate at 200 mA/cm^2 on air. The addition of tantalum produced similarly poor results. The hope that the addition of tantalum or niobium would produce a more platinum-like performance is obviously not yet realized. It must be remembered that this was an initial attempt to produce palladium intermetallic and improved preparations may be possible.

Catalyst EC-152, a platinum-tantalum intermetallic on Consel I, has performance characteristics which are not as good as platinum on Consel I by itself. At 200 mA/cm^2 a 0.5 mg/cm^2 loaded electrode of EC-152 operates at a potential of 590 mV in 180°C, 100% H_3PO_4 (vs > 700 mV for platinum on Consel I).

A number of noble metal-refractory metal catalyst preparations were formed into gas diffusion electrode structures and run in 100% phosphoric acid at 180°C as oxygen and air electrodes. In particular, the electrocatalyst performance for the platinum-vanadium intermetallic supported on Consel IV were determined. Table XIX shows the catalyst designations, electrode numbers, and the apparent platinum surface area pre-test and post-test.

TABLE XIX
Surface Areas of Platinum-Vanadium Intermetallics on Consel IV

Catalyst #	Electrode #	Composition	Pre-Test	Post-Test
EC-154	P-108	0.54 mg Pt-V/cm^2 electrode 10.8% Pt-V/Consel IV	80 m^2/g	88 m^2/g
EC-155	P-109	0.27 mg Pt-V/cm^2 electrode 10.8% Pt-V/Consel IV	90 m^2/g	77 m^2/g
EC-157	P-112	0.27 mg Pt-V/cm^2 electrode 5.4% Pt-V/Consel IV	105 m^2/g	88 m^2/g

Although reasonable linearity is obtained for the Tafel plots, we are still concerned about the significance of this linearity, since it is not truly diagnostic of the electron transfer reaction. The Tafel slope on oxygen is of the order of 105-110 mV, which we think is high and gains are indicated that

are yet to be made with improvements in the electrode structure. Nevertheless, these electrodes and electrocatalysts show promise since the Consel IV support is a high surface area graphitized carbon that has been doped substitutionally with another element.

iii. Noble Metal Sulphides - Cathodes

The best performance previously obtained on a platinum sulphide catalyst was 7.2 mA/mg PtS_2 versus 24 mA/mg for platinum at 900 mV. This is not surprising since the surface area of the platinum sulphide is probably very low (see Task 6). The Tafel slope for platinum sulphide is 120-130 mV/decade whereas the platinum on Vulcan XC-72R has a Tafel slope of 100 mV/decade. Since the Tafel slopes are similar, granted that perhaps the structure of the platinum sullphide catalyst electrode has not been optimized, it appears that the lower performance of the platinum sulphide catalyst may be due to the very low surface area obtained by present preparation techniques. There are significant gains yet to be made on improving the method of catalyst preparation.

An improved sulphide catalyst gives a Tafel slope for oxygen reduction at 180°C in 100% H_3PO_4 of 115 mV/decade; the activity is 14 mA/mg PtS, and the potential at 200 mA/cm^2 on air is 651 mV (vs H_2). Although this does not yet match the performance of platinum alone, it is much improved over previous preparations of platinum sulphide.

Reformed Methanol Anode

Due to interest in the use of methanol as a fuel cell fuel for transportation (Los Alamos) and for man-pack Army power systems (Fort Belvoir), it is of some considerable importance that the performances of advanced electrocatalysts and electrode structures be evaluated. Methanol has the distinct advantage that it is water soluble and, therefore, the water for the steam reforming may be added to the fuel prior to introduction to the steam reformer itself. This leads to system simplicity. The effluent from a steam reformer with methanol and water as the fuel is 75% H_2, 0.5% CO, and 24.5% CO_2, showing a lower carbon monoxide concentration than steam reformed hydrocarbons.

We have performed tests using a methanol steam reformate gas mixture with the platinum-palladium alloy (50 a/o Pt) supported on Consel I that was previously developed. In order to flex the performance curves and to use the carbon monoxide concentration as a probe for the electrode structure and electrocatalyst performance the electrode performance characteristics on hydrogen containing up to 5% carbon monoxide were obtained. This provided a bracketing for the carbon monoxide poisoning curves that were obtained previously for hydrogen oxidation on platinum electrocatalysts where the carbon monoxide poisoning levels ranged from 1% to 30%. Anode performance curves as a function of carbon monoxide partial pressure and temperature with 75% H_2 are shown in Figures 47 through 50.

In Figures 47 through 50 it should be noted that for 75% H_2 the open circuit potential at 180°C must be 7 mV from the reversible H_2 potential when pH_2 is 1 atm (n=2). At room temperature, of course, the Nernst reversible potential shifts by 4.5 mV for pH_2 = 0.75 atm. An Arrhenius analysis of these curves is shown in Figure 51 using the current densities at 20 mV versus the standard hydrogen potential in the same electrolyte.

Figure 51 shows the effect of temperature on the reaction rate for 75% hydrogen with 0.5% CO. These values are then corrected for the hydrogen partial pressure to show the performance values that would be obtained at 100% hydrogen. The apparent reaction rate values for hydrogen from Figure 51 are also shown at 20 mV in the absence of carbon monoxide. It can be seen that the slopes of the two sets of data (with carbon monoxide and without carbon monoxide) are different with convergence at higher temperatures. From these values it is possible to derive an <u>apparent</u> surface coverage of the metal electrocatalyst by the carbon monoxide poison, by comparison of the reaction rates at constant potential, and constant temperature, in the presence and absence of the carbon monoxide poison.

The purpose for deriving an <u>apparent</u> surface coverage of the metal electrocatalyst by a poison is to provide a determination for changes in catalyst preparation techniques, supports, and electrocatalyst materials influencing the performance criteria. In actual fact, the technically

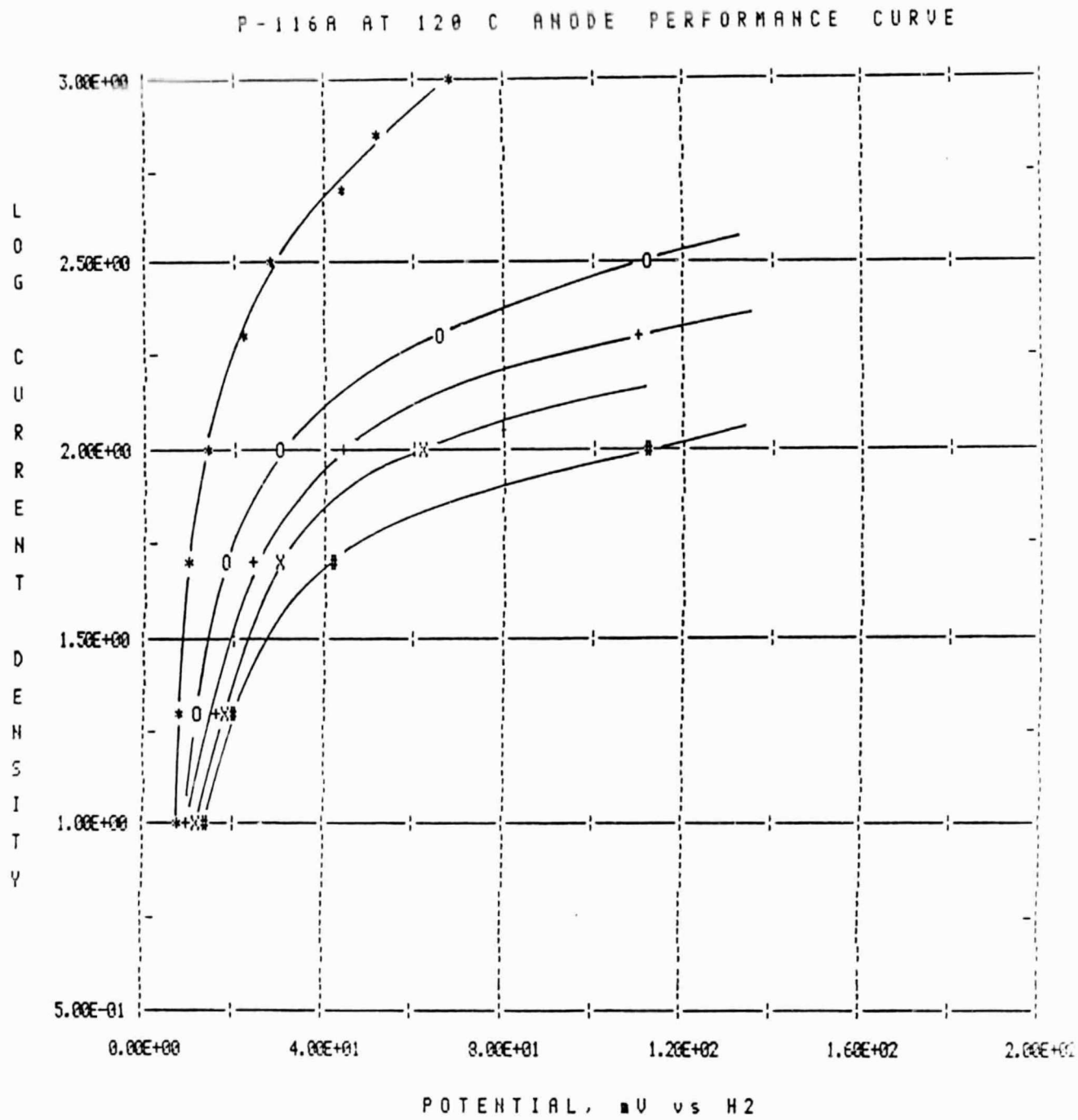

Figure 47. Electrode Catalyst EC 123.
Pt-Pd alloy (50 a/o Pt) 4 w/o PGM on Consel I. 0.2 mg PGM/cm^2 electrode, 30 w/o PTFE. (÷) 75% H_2, 1% CO; (X) 75% H_2, 2% CO; (#) 75% H_2, 5% CO; (*) H_2; (0) 75% H_2, 0.5% CO. Bal N_2.

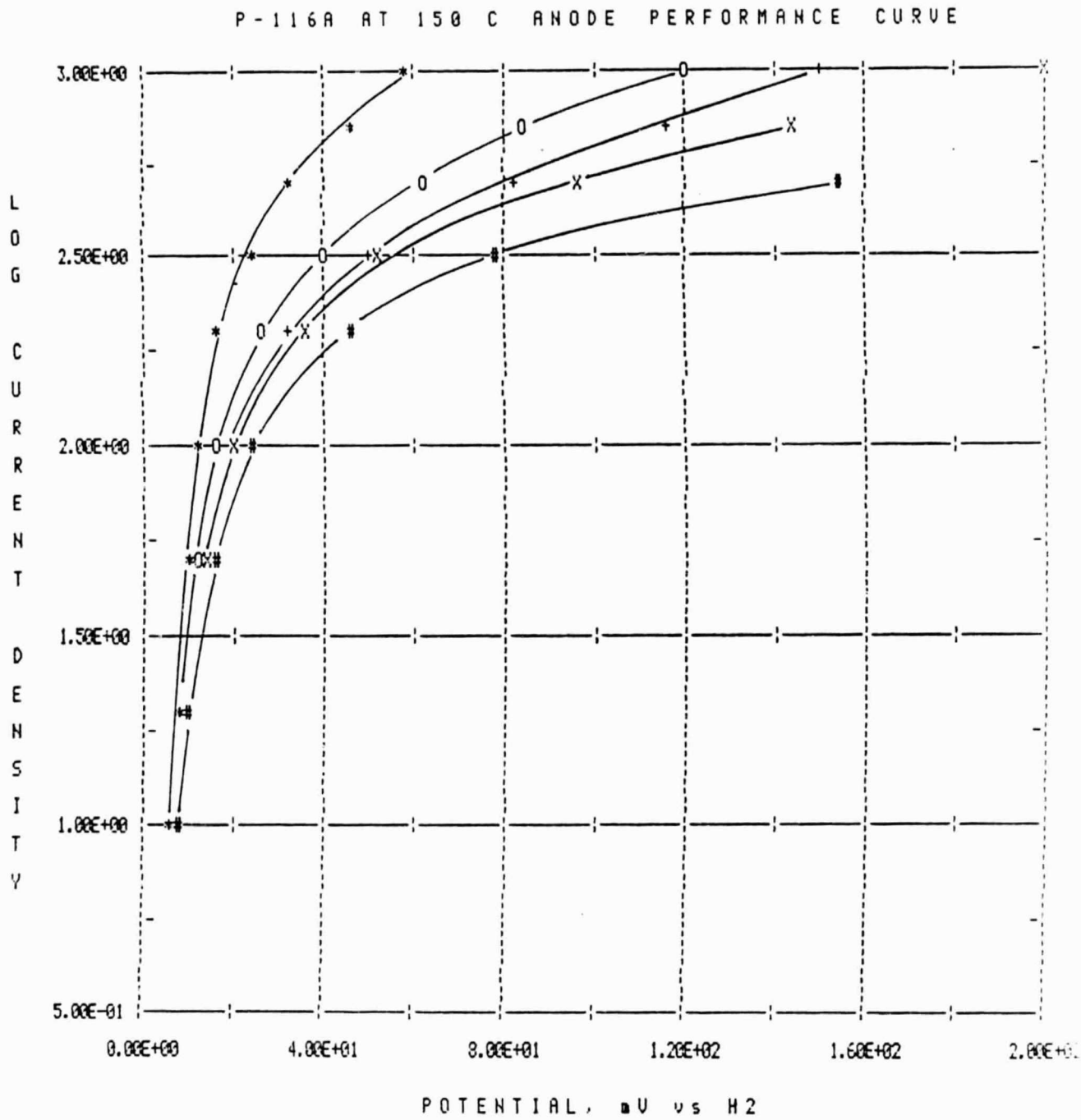

Figure 48. Electrode Catalyst EC 123.
Pt-Pd alloy (50 a/o Pt) 4 w/o PGM on Consel I. 0.2 mg PGM/cm^2 electrode, 30 w/o PTFE. (*) 75% H_2; (0) 75% H_2, 0.5% CO; (+) 75% H_2, 1% CO; (X) 75% H_2, 2% CO;(#) 75% H_2, 5% CO. Bal. N_2.

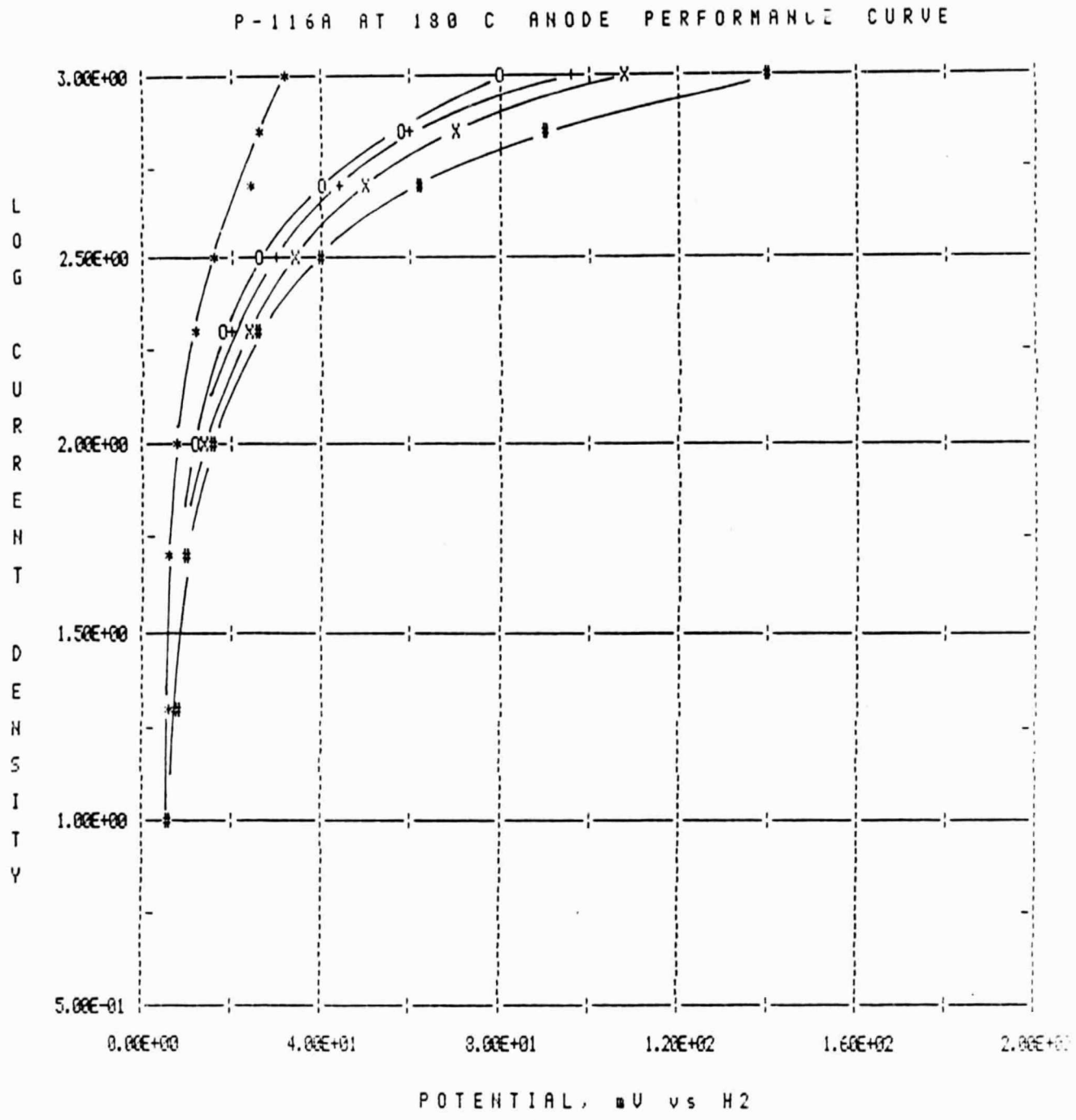

Figure 49. Electrode Catalyst EC 123.
Pt-Pd alloy (50 a/o Pt) 4 w/o PGM on Consel I. 0.2 PGM/cm^2 electrode, 30 w/o PTFE. (*) 75% H_2; (0) 75% H_2, 0.5% CO; (+) 75% H_2, 1% CO; (X) 75% H_2, 2% CO; (#) 75% H_2, 5% Co. Bal. N_2.

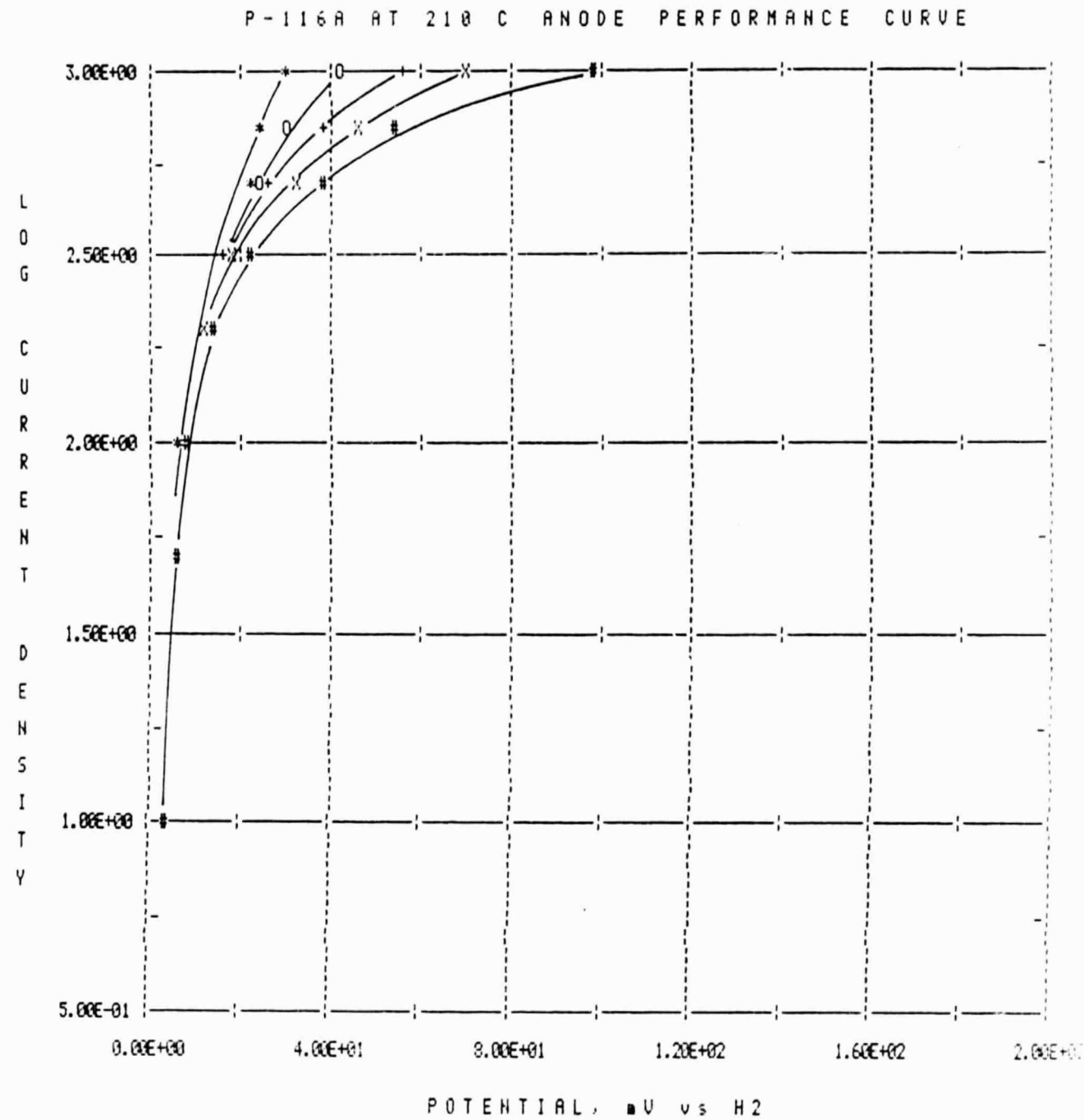

Figure 50. Electrode Catalyst EC 123.
Pt-Pd alloy (50 a/o Pt) 4 w/o PGM on Consel I. 0.2mg PGM/cm^2 electrode, 30 w/o PTFE. (*) 75% H_2; (0) 75% H_2, 0.5% CO; (+) 75% H_2, 1% CO; (X) 75% H_2, 2% CO; (#) 75% H_2, 5% CO. Bal. N_2.

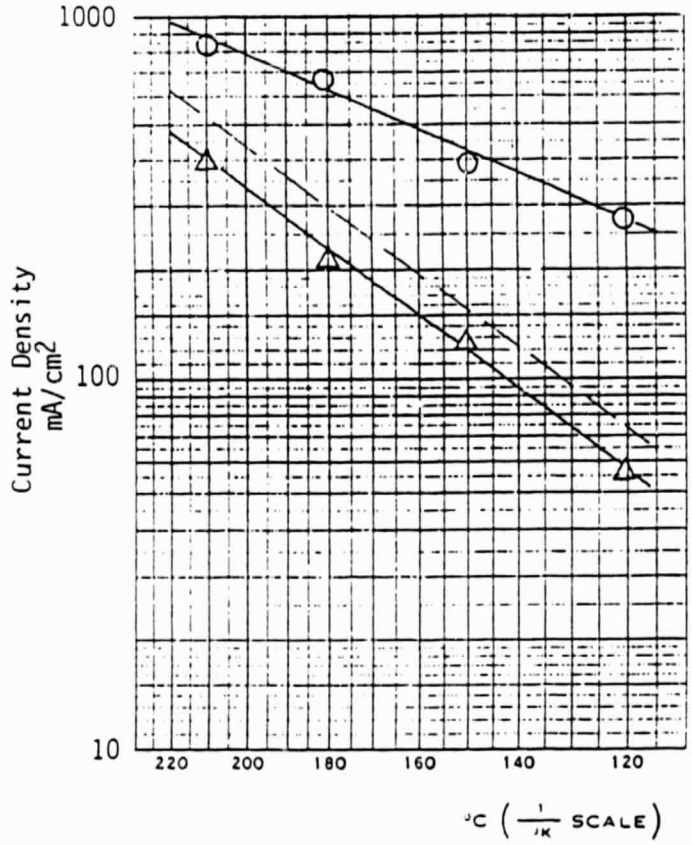

Figure 51. Arrhenius plot of hydrogen molecule oxidation at 20 mV (O). 75% H_2, 0.5% CO, 24.5% CO_2 (Δ). Dashed line correcting for H_2 partial pressure to give values at 100% H_2. Electrode contains 0.2 mg PGM/cm^2; 4 w/o PGM on Consel I; 50 a/o Pt, 50 a/o Pd.

important feature for an anode electrocatalyst is the free surface on the metal particle available for reaction of the hydrogen molecule, $(1-\theta)$, rather than the poison coverage (θ), by the carbon monoxide. The change in available electrocatalyst surface with temperature should have the function similar to the Arrhenius function, due to the similarity of the change in the equilibrium coverage, which is itself dependent upon the change in the kinetics of adsorption and desorption with temperature. The function is plotted in Figure 52. In order to compare the results on the platinum-palladium alloy electrocatalyst with platinum, we have chosen to compare the available electrocatalyst surfaces with 1% carbon monoxide in the gas stream.

Previously, we had shown the effect of carbon monoxide poisoning for platinum supported on the turbostratic Vulcan XC-72R. Analyzing that data in a similar manner to the analysis presented here for the platinum-palladium alloys on Consel provides the change in available surface area on the platinum electrocatalysts with temperature, also shown in Figure 52.

At this point, the data appear to show that in the presence of the same partial pressure of carbon monoxide, the available surface for hydrogen oxidation on platinum is greater than the available surface for hydrogen oxidation on the platinum-palladium alloy at the same temperature. In fact, such a conclusion is too simplistic since the carbon supports are quite different and the electrode structures are probably controlled by the interaction on the carbon support with the PTFE. Previously, we had carried out perturbation experiments for platinum supported on the Consel I. Variations in the Teflon content between 2.5 and 30% showed significant variations in the anode performance levels for this electrocatalyst with hydrogen oxidation in the presence of carbon monoxide. The performance curves correlated with the response of the electrode potential to perturbations.

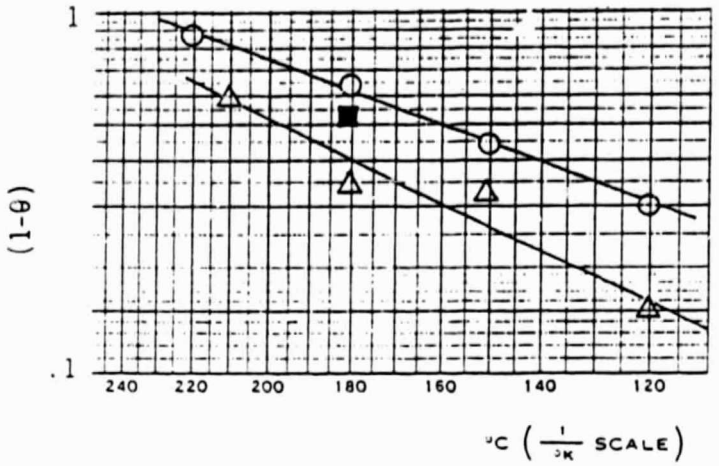

Figure 52. Available surface area on metal electrocatalysts as a function of temperature. (O), 0.5 mg Pt/cm^2 electrode, 10 w/o Pt on Vulcan XC-72R, 25 mV (DEN-3-176, May 31, 1980). (Δ), 0.2 mg PGM/cm^2 electrode, 4 w/o PGM on Consel 1, 50 a/o Pt, 50 a/o Pd, 20 mV polarization. (■), 0.5 mg Pt/cm^2 electrode, 10 w/o Pt on Consel 1. All data obtained for hydrogen oxidation in the presence of 1% CO electrocatalyst poison.

TABLE XX

Apparent Coverages of Platinum Electrocatalyst by Carbon Monoxide with Changes in the PTFE Levels of the Electrode Structure

PTFE w/o	10% H_2 mA at 100 mV	10% H_2 + 1% CO mA at 100 mV	$1-\theta$
2.5	600	60	0.1
10.0	700	52	0.07
20.0	1300	700	0.54
30.0	640	350	0.54

Table XX shows that the apparent surface coverage of carbon monoxide on platinum operating at 180°C with 10% H_2 and 1% CO, depends dramatically on the degree of wet-proofing of the electrocatalyst. Where the electrocatalyst has a thick electrolyte film at low PTFE levels, the available electrocatalyst surface for hydrogen oxidation is small. On the other hand, at high PTFE levels, the available electrocatalyst surface for hydrogen oxidation is high. The reason for this is almost certainly that with a thick electrolyte film, where the electrocatalyst is consuming the hydrogen diffusion to the surface, the localized carbon monoxide level within the electrolyte film adjacent to the metal electrocatalyst particle becomes significantly higher than the carbon monoxide level in the incoming gas stream. The performance of the electrocatalyst then becomes controlled by the ability of the carbon monoxide level within the electrolyte film to relax by diffusion from the electrocatalyst surface to the gas phase. If the electrolyte film is thick, the liquid phase diffusion restricts the ability of the electrocatalyst surface concentration to diminish; hence, the apparent poisoning becomes greater.

The value for the apparent poison coverage at high PTFE levels in Table XX is inserted into Figure 52 and shows good agreement with the sets of data. Again, it should be pointed out that this electrocatalyst contained 10 w/o Pt on the Consel support so that it has the commonality with the metal electrocatalyst for the platinum-palladium on the Consel I support values. It

has long been recognized that electrodes made with turbostratic Vulcan XC-72R produce good electrode structures, probably due to the ability of the carbon to develop thin electrolyte films within the electrode structure when bonded with Teflon. It is concluded from the data that we have presented so far, that the poisoning characteristics and the performances of the electrodes are tremendously influenced by the electrode structure and that this goes hand in hand with the fundamental electrocatalytic activity for the metal electrocatalyst particles. The same conclusion holds for cathodes, since the feature that is important is the mass transport of the reactant molecules to the electrocatlyst surface. At the same molecular reaction rate, the mass transport from the gas phase to the electrocatalyst site will require the same concentation gradient through the electrolyte film, irrespective of the reacting species.

Electrocatalyst Utilization

To provide an understanding for the operation of gas diffusion electrodes, it was reasonable that the influence of temperature over the range 120-210°C be evaluated together with the influence of the carbon monoxide poison as a probe over the range 0% CO to 5% CO. Earlier, such an examination had been carried out on the platinum-palladium low loaded alloy designated EC-123 (P-116).

It should be recognized that although we had indicated that the key carbon monoxide poisoning concentration in the anode gas stream for steam reformed methanol was 0.5% carbon monoxide, it is fortuitous that the latest fuel mixture for steam reforming and shifting of hydrocarbons in United Technologies' pressurized power plant at 120 psia is 70% hydrogen, 1% carbon monoxide and 29% carbon dioxide (Quarterly Report #4, Contract DEN-3-191, February 1, 1981-April 30, 1981). Clearly, the results that we are presenting are exactly targeted on both steam reformed methanol and steam reformed and shifted hydrocarbons for the UTC pressurized fuel cell.

All data were obtained in our test stands, allowing 16 hours after electrode insertion for the electrocatalyst layer to fill. The high performance BC 1200 potentiostats with automatic IR correction and compensation were used. All of the electrodes were of the same thickness and contained the same amount of

Teflon. All electrodes were sintered at the same temperature.

In order to derive the apparent isotherms for carbon monoxide poisoning of the hydrogen reaction on the platinum or PGM electrocatalyst surface, comparisons were made between the rate of the hydrogen oxidation reaction on an unpoisoned surface and that performance attained for the same hydrogen partial pressure in the presence of different partial pressures of carbon monoxide at the same potential (20 mV). A tabulation is given in Table XXI for these apparent isotherms together with tabulations from the electrodes P-116. The apparent available surface area ($1-\theta_{CO}$) as a function of carbon monoxide concentation and temperature are shown in Figure 53.

Not all of the hydrogen entering the fuel cell anode can be oxidized, since the degree of consumption is related to the operating potential. At 180°C with 20 mV polarization (vs RHE) the surface equilibrium partial pressure due to the Nernst relationship is 0.35 at. Since the incoming partial pressure for hydrogen is 0.75 at. (giving an open circuit potential of 5.5 mV at 180°C), then the available hydrogen concentration differential is 0.4 at. which must support the electrocatalytic reaction rate.

In order to ascertain whether or not the adsorption isotherms in Figure 53 are truly representative of the adsorption equlibrium kinetics in the absence of diffusion, one has to perform other analyses of the data. It is well known that at low reaction rates, kinetic parameters are dominant, whereas at high reaction rates, diffusion interferences are obtained so that the reaction rate is no longer directly proportional to the catalyst surface area or even the catalyst loading. This enters into the dimension of catalyst utilization and effectiveness factor. It is not our purpose to enter into detailed discussions of effectiveness factors for electrocatalysts at this time. Suffice to say, for a given catalyst particle size, the reaction rate should double if the catalyst particle density also doubles. If the reaction does not increase by the surface area increase multiple, then diffusion limitations are indicated and the catalyst utilization is low. One approach is to determine specific reaction rates on low loaded electrodes and compare those reaction rates with electrodes at higher loadings. Since we have taken care to catalyze the electrode materials with uniform metal particles by means of a

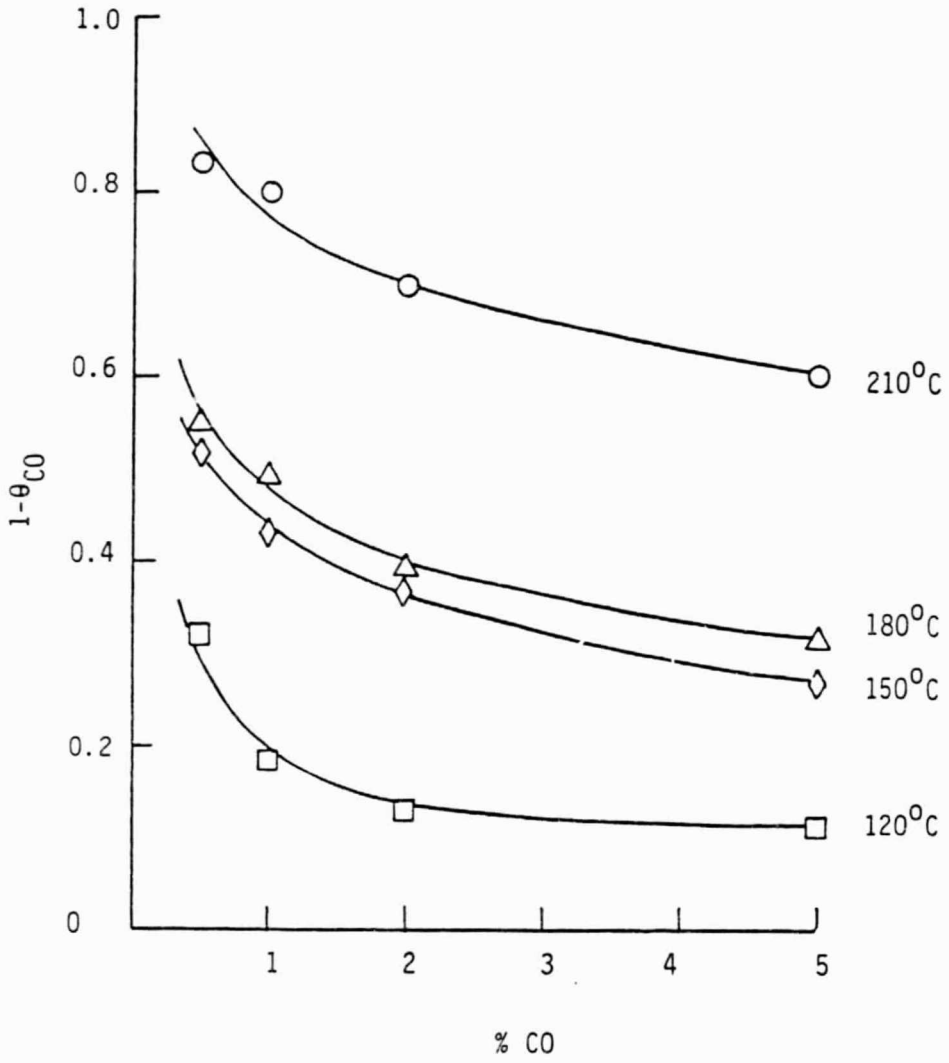

Figure 53. Electrode P-116. Apparent available surface areas on platinum as a function of temperature and carabon monoxide levels.

TABLE XXI

Influence of Temperature and Carbon Monoxide Partial Pressure on Apparent Electrocatalyst Surface Available for Hydrogen Molecule Oxidation

P-116

Gas Mix of 75% H_2 Plus (Balance N_2)	Current Density (mA) at 20 mV Polarization							
	120°C		150°C		180°C		210°C	
		$1-\theta_{CO}$		$1-\theta_{CO}$		$1-\theta_{CO}$		$1-\theta_{CO}$
0% CO	181	1.0	270	1.0	420	1.0	470	1.0
0.5% CO	58	.32	140	.52	230	.55	390	.83
1% CO	33	.18	115	.43	205	.49	375	.80
2% CO	24	.13	100	.37	165	.39	330	.70
5% CO	21	.11	72	.27	135	.32	280	.60

P-117

0% CO	200	1.0	260	1.0	300	1.0	360	1.0
0.5% CO	11	.055	100	.38	145	.48	320	.88
1% CO	7	.035	52	.20	130	.43	290	.80
2% CO	5	.025	35	.135	110	.36	260	.72
5% CO	3.4	.017	22	.085	92	.31	200	.55

P-118

0% CO	235	1.0	300	1.0	315	1.0	350	1.0
0.5% CO	45	.19	160	.53	240	.76	305	.87
1% CO	30	.13	140	.47	225	.71	300	.85
2% CO	20	.085	110	.37	200	.63	295	.48
5% CO	13	.055	76	.25	170	.54	270	.77

P-91

0% CO	240	1.0	320	1.0	420	1.0	500	1.0
0.5% CO	56	.23	200	.63	320	.76	400	.8
1% CO	32	.13	170	.53	300	.71	385	.77
2% CO	26	.11	150	.47	280	.67	365	.73
5% CO	20	.08	120	.38	250	.59	350	.70

TABLE XXI (Continued)

Influence of Temperature and Carbon Monoxide Partial Pressure on Apparent Electrocatalyst Surface Available for Hydrogen Molecule Oxidation

P-119

Gas Mix of 75% H_2 Plus (Balance N_2)	Current Density (mA) at 20 mV Polarization							
	120°C		150°C		180°C		210°C	
		$1-\theta_{CO}$		$1-\theta_{CO}$		$1-\theta_{CO}$		$1-\theta_{CO}$
0% CO	220	1.0	320	1.0	340	1.0	370	1.0
0.5% CO	38	.17	140	.44	270	.79	330	.89
1% CO	27	.12	120	.37	250	.73	320	.86
2% CO	20	.09	110	.34	220	.65	280	.76
5% CO	14	.06	80	.25	200	.59	260	.70

P-119S

0% CO	230	1.0	280	1.0	380	1.0	430	1.0
0.5% CO	39	.17	150	.53	290	.76	370	.86
1% CO	29	.12	135	.48	270	.71	350	.81
2% CO	22	.09	120	.43	240	.63	320	.74
5% CO	16	.07	80	.29	220	.58	280	.65

P-121

0% CO	230	1.0	320	1.0	380	1.0	400	1.0
0.5% CO	58	.25	200	.62	320	.84	380	.95
1% CO	38	.17	160	.50	280	.74	360	.90
2% CO	30	.13	115	.36	260	.68	340	.85
5% CO	10	.04	100	.31	240	.63	320	.80

colloidal deposition process, then the variation in electrocatalyst surface area is reflected in the variation in the number of particles which is controlled by the metal loading. Two sets of data are plotted in Figures 54 and 55. In Figure 54, the current density is shown for hydrogen oxidation at 210°C in the absence of a poison as a function of the catalyst loading. It is clear that the low loaded electrocatalyst (which is 1 w/o Pt on carbon) is nearly as active as the 10 w/o Pt on carbon. Since the current density would be 0 at 0 w/o PGM on carbon, we are allowed to extrapolate through the lowest loading datum to anticipate the current density that would be obtained at higher loadings with efficient utilization of the catalyst. It is clear that even at 4 w/o PGM, the current density that should be observed is at least two or three times greater than is obtained.

This means that at least 70% of the catalyst is not being utilized. From examination of the performance curves, for hydrogen oxidation in the presence of carbon monoxide at the 1% level and at 180°C, we may construct Figure 55. The multiple of the increase in current density between the 1 w/o Pt and 10 w/o Pt does not reflect the increase in surface area on the electrocatalyst or the increase in the loading by the platinum. If we assume (reasonably) that at constant temperature the true CO poisoning isotherm on the metal particle surface does not change, then the current density on the 10 w/o Pt electrocatalyst should be ten times that of the 1 w/o Pt on carbon electrocatalyst (if the catalyst particles have the same size). It may be that there are diffusion effects even at the 1 w/o Pt level but further data must be obtained to support that contention.

Extrapolating from the current density that is obtained on the 1 w/o electrocatalyst to the 4 w/o PGM on carbon electrocatalyst shows that the current densities expected would be at least two to three times greater than have been observed. Significant gains in catalyst utilization are yet to be made.

We can make a rough estimate for the maximum current density that should be derived with 0.4 at. hydrogen partial pressure differential (40% H_2 utilization) at 180°C in 100% H_3PO_4. At 20 mV polarization, the hydrogen evolution reaction (reverse reaction) decreases and the free surface for

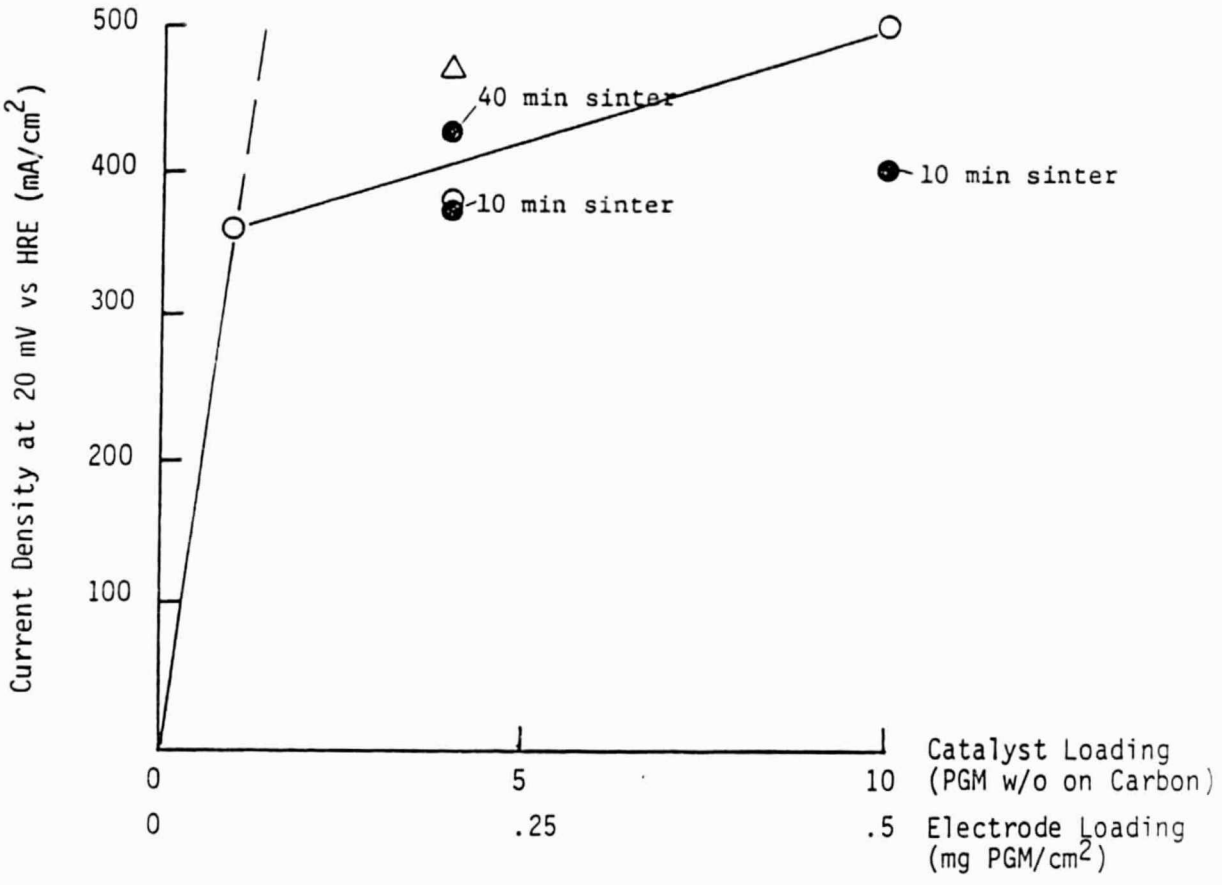

Figure 54. Hydrogen oxidation reaction rates on platinum supported on Vulcan XC-72R (O) and on platinum-palladium supported on Consel I (Δ). Gas mixture 75% hydrogen; balance nitrogen. 210°C, 100% phosphoric acid. Platinum supported on Consel I (●).

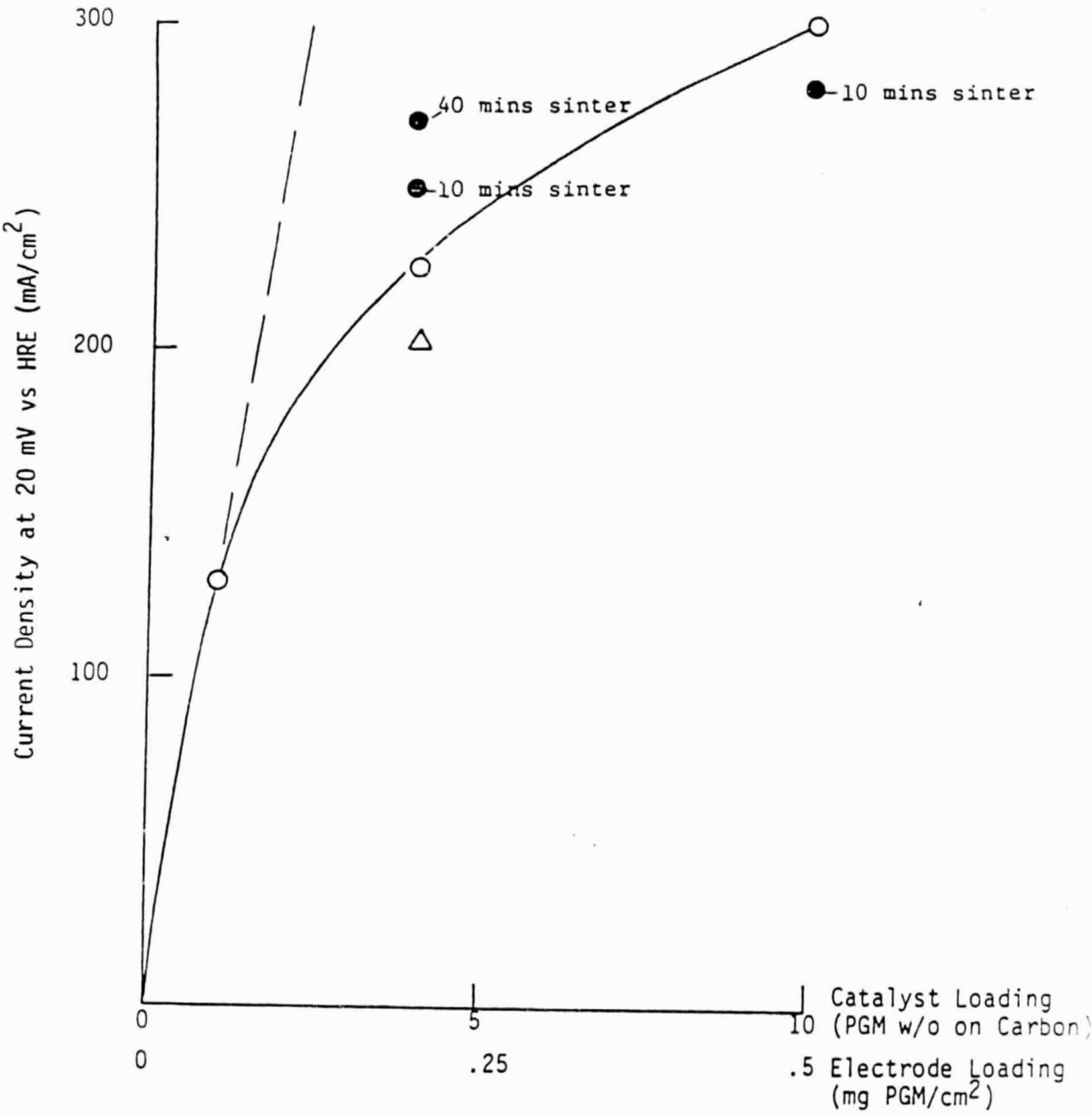

Figure 55. Hydrogen oxidation reaction rates on platinum supported on Vulcan XC-72R (O) and on platinum-palladium supported on Consel I (△). Gas mixture 75% hydrogen; 1% CO; balance nitrogen. 180°C, 100% phosphoric acid. Platinum supported on Consel I (●).

dissociation of the hydrogen molecule (Tafel reaction) increases. A dispersed platinum electrocatalyst of 60 m^2/g Pt (which is not as high as our electrocatalysts studied here) will have a surface of 600 cm^2/mg Pt. Since the exchange current for hydrogen molecule oxidation on platinum in acid is 20 mA/cm^2 (P. Stonehart, J. Electroanal. Chem., 1977, 77, 245-248), then at room temperature in dilute acid, the kinetic limitation (exchange current) becomes at least 12,000 mA/mg Pt.

With increase in temperature, the hydrogen dissociation reaction rate increases by 4 kcal/mole but the gas solubility can be expected to decrease by an equal magnitude.

These estimates show that current densities of 1,200 mA could be expected for hydrogen molecule oxidation on 0.1 mg Pt having only 60 m^2/g surface area, provided that all of the platinum electrocatalyst was utilized. With a hydrogen utilization of 40% (see before) the estimates of kinetically limiting current densities are then 480 mA/0.1 mg Pt. Figure 54 shows a hydrogen oxidation current of 350 mA/0.1 mg Pt at 210°C and 20 mV. This electrocatalyst has a surface area higher than 60 m^2/g but the exact solubility of hydrogen is an unknown. Even though the inexact calculation given here is close to the observed measurement, the platinum utilization is probably still low and the real kinetic limitation for hydrogen molecule oxidation may be twice the value so far observed.

Although the results presented so far have been obtained on hydrogen oxidation, using CO poisoning as the probe, it is important to note that these conclusions are truly applicable to oxygen molecule reduction at the cathode also. Since the same electrode structures (and in some cases actual electrodes) have been used historically to obtain both anode and cathode data, it is important to note that at the current densities and electrocatalyst loadings where diffusional effects are noted for an anode, then at the same current densities approximately the same diffusional interferences will be obtained at cathodes. It is true that at the anode the hydrogen molecule oxidation reaction is a two electron process, whereas at the cathode the oxygen molecule reduction reaction is a four electron process. The flux of the reacting molecules through the liquid electrolyte film is related to the

product of the molecule solubility and diffusivity and since both molecules in the electrolyte are non-polar, the solubility trends of the gas molecules in aqueous electrolytes at the same temperature are expected to be similar. On the other hand, the diffusivity of hydrogen in aqueous solutions is twice that of the oxygen molecule (see "Physicochemical Hydrodynamics" V. G. Levich, Prentice-Hall, N.J., 1962, p. 325, and K. Klinedinst, J. A. S. Bett, J. MacDonald, and P. Stonehart, Journal of Electroanalytical Chemistry, 57 (1974) 281-289). The sum total of this discussion shows that although the overall electron transfer for the hydrogen molecule oxidation reaction is one-half that of the oxygen molecule reduction reaction, the diffusivity is twice as great so that at the same current densities in gas diffusion electrodes when diffusion played a role, the mass transfer characteristics that are seen at the anode will be reflected in an identical way at the cathode. It can be concluded, therefore, that if the catalyst utilization at the anode is less than 30% for a 4 w/o electrocatalyst and is less than 10% for a 10 w/o catalyst, then the same utilizations will be obtained at the cathodes for the same catalyst loadings.

In order to evaluate the operation of gas-diffusion electrode structures, some fundamental information is required regarding the solubility and diffusivity of the reacting gas molecules in the electrolyte environment. When coupled with estimates of the thicknesses of the electrolyte films on the electrocatalysts and an understanding of the electrocatalyst structure, then operation of the electrode may be understood more fully and subjected to further development.

Information on solubility and diffusivity of oxygen in hot concentrated phosphoric acid is given in the Klinedinst paper up to 150°C and 96% H_3PO_4. From Figure 2 of that paper, the solubility-diffusivity product for oxygen in 100% phosphoric acid, together with temperature dependence of the D_OC_O product can be extrapolated. That relationship is shown in Figure 56, which is particularly interesting since the D_OC_O product increases linearly with temperature. There is no other information on the related solubility-diffusivity of hydrogen.

In order to explore the effect of electrode preparation technology on

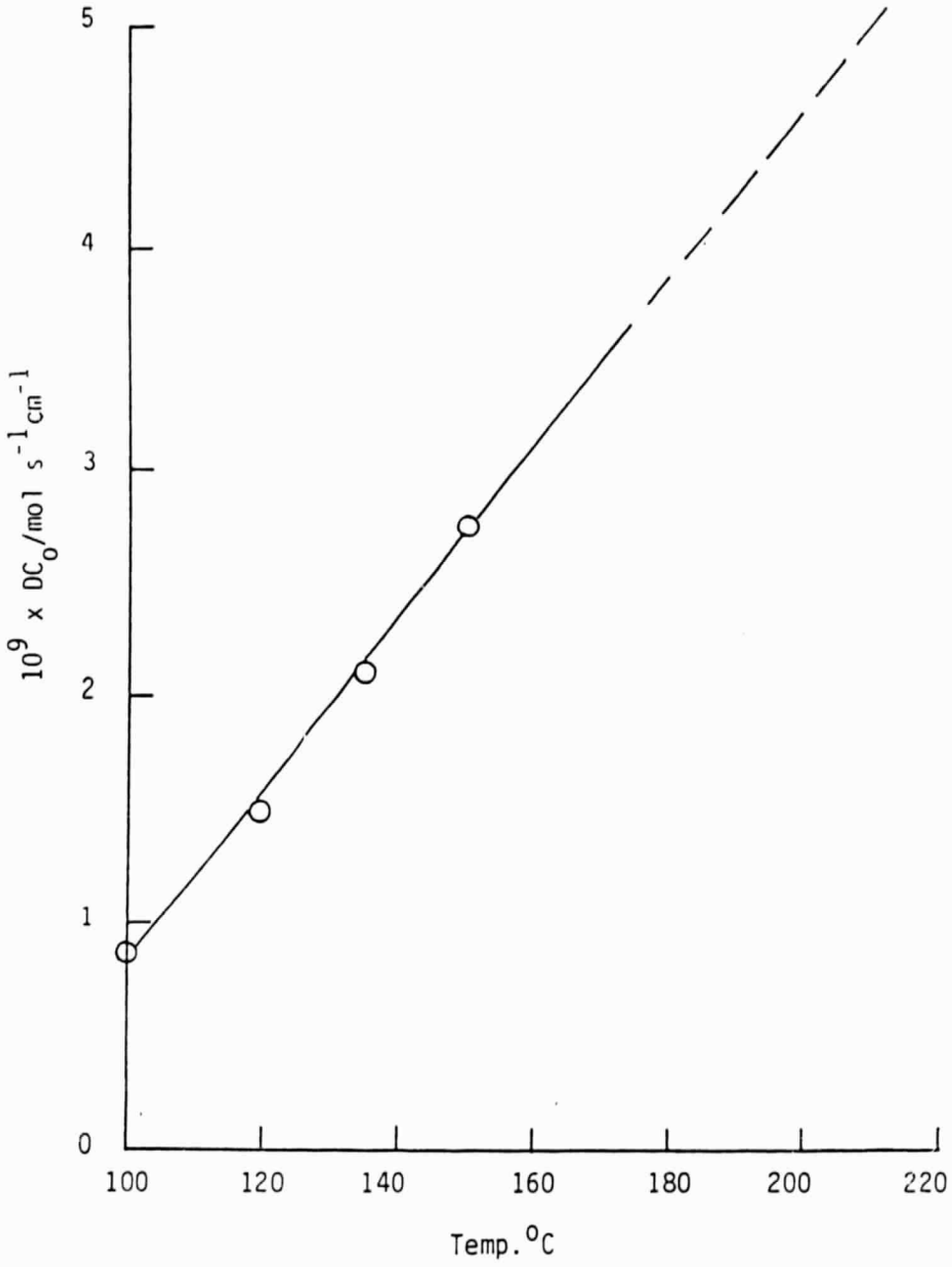

Figure 56. Solubility-Diffusivity product of oxygen in 100% phosphoric acid. Data extrapolated from Figure 2 of K. Klinedinst, J. A. S. Bett, J. MacDonald, and P. Stonehart, Journal of Electroanalytical Chemistry, 57 (1974) p. 285.

electrocatalyst utilization, a series of electrodes were prepared where the sintering time for the Teflon was extended. Since it had been shown previously that the thermal sintering of Teflon in contact with carbon blacks produced degradation and flow of the Teflon polymer (K. A. Klinedinst, W. M. Vogel and P. Stonehart, J. Materials Science, 1976 11, 794-800), it was reasoned that the electrode film thickness could be lowered by thinning the Teflon coating on the carbon. Table XXI Electrode P-119 contains 4 w/o platinum on Consel I (EC-124) with 30% PTFE sintered 10 minutes at 315°C. Electrode P-119S is the same as P-119 except that the sintering time at 315°C was 40 minutes. Electrode P-121 contained 10 w/o platinum on Consel I with 30% PTFE sintered for 10 minutes at 315°C. The influence of temperature and carbon monoxide partial pressure on the apparent electrocatalyst surface available for hydrogen molecule oxidation is included in Table XXI. Analyses of the performance results are included in Figure 54 for hydrogen oxidation at 210°C in the absence of carbon monoxide and in Figure 55 for hydrogen oxidation at 180°C in the presence of 1% carbon monoxide. Preliminary conclusions show that the utilization of the electrocatalyst is low in all instances, but that with extended sintering of the Teflon the utilization increases. We do not have sufficient data with many electrodes to know the degree of performance scatter. Further work in this direction will clearly be fruitful.

Tasks 12 and 13

During the end of this program, the final assembly of the sub-scale single cell test stand drew to a close. We have now demonstrated the operation of the single cell test stand. Our efforts on this contract then focused on developing the capability to operate and monitor this cell for longer time periods. The best way to handle long term monitoring is to computerize the operation of the test stand. At a minimum, the voltage and current density of the cell must be monitored continually. The hardware and software developed to handle the data acquisition of the subscale single cell are described below.

When we had finished the data acquisition system and started running electrodes in the single cell, it soon became apparent that electrolyte management is more difficult than anticipated. As we began operating single

cell tests, we found that the electrode performance declined rather rapidly after the first day of operation. The performance of the cell could be revived by adding fresh electrolyte to the electrolyte reservoir. At first the thought was that by the addition of proper Teflon gasketing, the leaking of the electrolyte from the electrolyte reservoir could be stopped. Several trials at improving the gasketing clearly demonstrated that the present design of the glassy carbon cathode plate (which contains the electrolyte reservoir) is not capable of preventing the electrolyte from slowly leaking out of the reservoir. We have abandoned the present design in favor of a newer one which takes into account the experience gained thus far in managing the electrolyte. Relocation of the gas and electrolyte feed channels will fix this problem.

The data acquisition system centers around the use of two computers. A Heath/Zenith H89 master computer and a Zilog Z8671 slave computer. This configuration allows us to monitor the daily operation of the test stand by the use of a small inexpensive dedicated computer board (the Z8671) and free up the main computers for other work. Although the Z8671 single board computer is a very good control and monitoring device, it is lacking in its capability to manage, store, and display the data. Once the data is received from the Z8671, the H89 can store it on disk, mathematically analyze the data, print it out or display it in graphical form. Our H89 computers are interfaced with a Hewlett-Packard Model 7470A Graphics Plotter, which is programmed to plot out the data in graphic form. The HP 7470A is a high resolution plotter and will be used to generate data plots as an aid to data analysis and for insertion into our progress reports.

We have identified the Zilog Z8671 (Z8) single-chip microcomputer as the best candidate for fulfilling the role of a slave computer. Using only seven IC chips and a minimum of discrete devices, this computer can be assembled on a 4-1/2 inch square circuit board. This computer board has three parallel input/output ports for interfacing to the test stand and a serial port for communication with a terminal or master computer (Zenith H89). The computer has 2 kilobytes of internal ROM which contains the monitor program and a Tiny BASIC interpreter. Having this BASIC interpreter on the Z8 board greatly simplifies software development. As will be seen below, the Tiny BASIC program in the Z8, although small, is the real workhorse of the system.

Although the board presently has three parallel ports, one serial port and 4 kilobytes of RAM, it can easily be expanded and additional ports and memory up to 64 kilobytes of program memory and 62 kilobytes of data memory can be added by connecting I/O, RAM and ROM boards to the Z8 bus.

The system being built around this computer consists of a NLS digital panel meter to provide the digital information for transmittal to the Z8 computer. The input to this meter is controlled by a computer controlled analog multiplex switch. The Z8 can be programmed to control this switch and choose any of several analog voltage sources to monitor. All of the functions and conditions of this test stand can be read by the meter as voltage through application of the appropriate transducer to convert the readings (voltage, current, temperature, pressure, flow rate, etc.) into a voltage. The computer then contains the appropriate transfer curve to translate a voltage back into the proper units. The meter provides on-site visual information to the operator and since its digital information is available in multiplexed BCD (binary coded decimal) form at the edge card connector, it is placed on the Z8 bus for storage and management. The BCD information and data control information from the NLS meter is fed into a buffer and demultiplexer before being placed on the Z8 data bus, in order to tailor this information to conform to the requirements of the Z8 data bus. A Real Time Clock based upon the National Semiconductor MM58267A Microprocessor Real Time Clock chip is connected to the Z8 computer bus to provide necessary timing control and information. Both the meter multiplexer and Real Time Clock are under control of the Z8 computer. The digital panel meter can take one data reading approxmately once every 1/3 of a second, which is fast enough for controlling and monitoring the test stand. If faster data rates are needed, the meter can be replaced with faster A/D converters. The data rate with which the Z8 computer can cope extends down to approximately the one millisecond range, depending upon the application software needed. The present system can store approximately 350 current and voltage data pairs along with the time information in the Z8 data buffer. As mentioned previously, this can be extended by adding additional RAM boards to the Z8 bus.

The final link in the hardware system is the master computer. Since the Z8 has available a serial output port, it can easily be connected to any of our

Zenith H89 computers along a RS-232 port. The data gathered by the Z8 computer will be periodically downloaded to the master computer for permanent storage on magnetic disk. The master computer can then manage the data and prepare it for analysis or display in the preparation of status reports.

The software package to manage this system is divided into three programs. A machine code program residing in the Z8 is used to read data from the NLS meter and the Real Time Clock, pack it into a minimum number of bytes and store it in the memory buffer. We have found that a machine code program was necessary for this function since the Tiny BASIC interpreter was too slow to keep up with the NLS meter. Although the meter makes only three conversions per second, the information is available for only a brief time at the edge card connector. Since it is multiplexed and refreshed continuously, each digit is valid at the edge card connector for only about 6 milliseconds. When the data is first input from the NLS meter, it is placed in a mini-buffer in raw form. This is done to achieve maximum speed. This routine is performed by the Z8 computer in about 125 microseconds. The data is then packed into 5 bytes and stored in the maxi-buffer. The program then reads the Real Time Clock and adds the time information to the maxi-buffer. This program also controls the multiplexing of the input to the NLS meter. At the conclusion of its tasks, the machine code program returns control to the Z8 resident Tiny BASIC program.

The Tiny BASIC program is the real workhorse of the system. The Tiny BASIC program is the communications link with the master computer. On power-up, the Z8 computer does not contain any programming except for the BASIC Interpreter and the monitor ROM. The master computer stores the Z8 BASIC program and the machine code program. The Z8 is programmed through the serial I/O port. On power-up, the Z8 can accept a BASIC program through the serial port. The master computer transmits this program over the RS-232 bus. One task of the BASIC program is to accept the machine code program from the master computer and store it in the appropriate memory locations. Once these two programs have been received by the Z8 and a start command is issued by the master computer, the Z8, after initializing all buffers and memory pointers, enters a routine which continuously transmits status information to any listening master computer. That status information presently consists of whether or not

the Z8 is running, at what time interval the Z8 is programmed to take data, the time since the last datum was taken, and how many data are in the maxi-buffer. While it is doing this, it is also continually monitoring the interrupt line from the Real Time Clock. The Real Time Clock is generating interrupts at a preprogrammed rate. The interrupt rates available are: 10Hz, 1Hz, 1/min, 1/hour, 1/day, 1/month. The BASIC program counts these interrupts and initiates a data gathering routine whenever a preprogrammed number of interrupts has been counted. In this manner, the limited interrupt schedule of the Real Time Clock can be overcome and a widely variable time interval can be generated and utilized to cause branching to other program routines. We presently have the Real Time Clock generating interrupts every minute. Since the Z8 can count up to 65,536, we can use any time interval from 1 minute to 65,536 minutes to initiate a data gathering excursion. That is, we can take data from once per minute to once per 45 days. By reprogramming the Real Time Clock, we can vary that rate from 10Hz to a datum every 5500 yrs. The BASIC program transfers control to the machine code program for data gathering. The Z8 program can be interrupted at any time by the master computer and told to perform other tasks. One of these tasks is to change the data gathering frequency. Another of these tasks is to initiate a cold start. A cold start clears the memory buffers and initialize the program pointers. This is usually done to initializes the Z8 prior to the beginning of a new test or after all the data has been transferred from the Z8 to the master computer. The final task that the Z8 BASIC program must accomplish is to transfer the contents of its data buffer over to the master computer. While it is sending over this data, the Z8 is still counting interrupts and servicing data gathering requests so that no data will be lost. When it has accomplished this task, it returns to interrupt monitoring and status updating. The Z8 does not clear out its data buffer until the operator is satisfied that the data was trasnmitted faithfully. The operator then signals the Z8 to clear its buffer by commanding a cold start.

The master computer program is menu driven and can best be explained by going through the menu items. Before the menu is displayed on the CRT screen, the program sets up communication with the Z8 computer and interrogates the Z8 as to its status. The program then informs the operator as to the state of the Z8. It reports the number of data in the buffer, the time since the last

datum was taken and the frequency at which data are taken. The program also determines if the Z8 is actively acquiring data and reports that information to the operator.

Item 1. REPROGRAM Z8

This routine resets the Z8 computer and programs it. It transmits the Z8 BASIC program and the machine code program which is permanently stored on magnetic disk. It does not start the Z8 program running.

Item 2. DATA TRANSFER

This routine interrupts the Z8 normal routine and initiates the data transfer function in the Z8. As the data is received from the Z8 buffer it is decoded into readable form and displayed on the CRT screen. When the operator has verified that the data is valid, it is either stored on disk as a new file or updates an existing file. The disk data file then becomes independent of the program and can be used by other programs for manipulation, generating status reports, figures, etc.

Item 3. PRINT DATA

This routine is a general utility which reads a data file from disk and displays it on the CRT screen or prints it out to the line printer. This is done independently of the Z8 computer and, therefore, does not affect its operation.

Item 4. START Z8 (CLEAR BUFFER)

This is a cold start routine for the Z8. It clears the Z8 buffer and leaves the Z8 gathering data. Any data in the Z8 buffer are lost unless it was transferred to the H89.

Item 5. CHANGE FREQUENCY

This routine allows the operator to change the frequency at which data are

being accumulated. The routine only changes the frequency, it does not clear the buffer or disturb the Z8 computer in any other way.

Item 6. QUIT

Exits the H89 program and returns to the operating system. The operation of the Z8 is unaffected. This routine will issue a warning if the Z8 is not running.

Item 7. Z8 STATUS

Without disturbing the Z8, this routine will update the Z8 status. It will report to the operator the data frequency, the time since the last datum was taken, and the number of data in the buffer.

CONCLUSIONS

The objective of this electrocatalyst program was to explore the feasibility for lowering electrocatalyst costs while at the same time maintaining or increasing the electrocatalyst activity above that obtained for platinum as a hydrogen electrode or as an oxygen electrode in phosphoric acid fuel cells. It is worthwhile to enumerate the significant advancements that have been achieved and to point the way to beneficial directions for further research. An initial part of the program was to further categorize platinum supported on carbon supports. The carbon supports that were used were Vulcan XC-72R and Consel. The Consel was a proprietary carbon material developed under a companion EPRI program (1200-2) and is described as being a steam-activated acetylene black with a BET surface area of $250 m^2/g$. In this NASA program, adsorption isotherms were obtained for carbon monoxide coverages on the platinum electrocatalyst surfaces as a function of temperature and carbon monoxide partial pressure. These isotherms were derived from polarization data obtained on anode catalyst formulations with hydrogen as a fuel containing small percentages of carbon monoxide. Significant reductions in cost were obtained when platinum was alloyed with palladium in a highly dispersed manner on a steam-activated acetylene black carbon support. Patent disclosures were written for these platinum-palladium alloy combinations as anode electrocatalysts in hot phosphoric acid.

The literature has previously described "crystallite size effects" for platinum supported on carbon as oxygen electrocatalysts. Since the sizes of crystallites that have been examined are large, these results were unexpected. Careful examination of the literature data and by changing the carbon supports experimentally, it was shown that specific activity for oxygen reduction on platinum crystallites was dependent on the inter-crystallite distances and not on the crystallite sizes. This means that one of the controlling features for the operation of efficient electrocatalysts is the structure of the electrocatalyst support and the structure of the electrode itself. The results indicate that kinetic effects are not controlling the electrode performance, but that structural effects of these carbon supported materials are dominant. Very little is known about the influence of carbon supported structures and interactions with the Teflon to produce a convoluted reactive

mass. The electrode structure itself is a dynamic system with the electrolyte continually moving through a three-dimensional structure as a function of temperature, current density and partial pressures of the reactants.

For cathode catalysts, platinum was reacted with refractory metals in order to stabilize the metal crystallite structures. Some improvements were obtained using vanadium that had been reported in the patent literature and developed by Lawrence-Berkeley Laboratories.

The preliminary results on the utilization of the electrocatalyst on porous electrode structures showed only about 20% of the electrocatalyst is available for reaction. This was deduced for anode electrocatalysts and by direct extension to cathode electrocatalysts also. Much more work needs to be done on improving the electrode structures in conjunction with improving electrocatalyst spacial distributions on the carbon supports.

APPENDIX - DERIVATION OF EQUATION 5

Crystallite size determination by voltammetry requires measuring the pseudocapacity associated with the adsorption of hydrogen on the surface of the crystallites. For palladium crystallites there is not only a pseudocapacity associated with hydrogen adsorption on the crystallite surface, but also a pseudocapacity due to the absorption of hydrogen into the interior of a palladium crystallite. The ratio of hydrogen to palladium atoms on the surface can reasonably be assumed to be 1:1. For absorbed hydrogen, the hydrogen to palladium ratio has been reported to be less than 1:1 and depends upon temperature and hydrogen partial pressure (Palcyewska, Advances in Catalysis, 24, 248, 1975).

Using spherical geometry, a relationship between crystallite size and hydrogen adsorption plus absorption pseudocapacitance can be developed using an arbitrary value for R, the ratio of hydrogen to palladium for absorbed hydrogen. The value of R can be determined by correcting potentiodynamic hydrogen pseudocapacity to microscopically determined cyrstallite size.

The total pseudocapacitive charge (Q) on one gram of palladium crystallite is:

$$Q = \#cQ_c \tag{1}$$

where Q_c is the charge per crystallite and #c is the number of crystallites per gram.

$$\#c = V_T/V_c \tag{2}$$

where V_T is the total volume of one gram of palladium and V_c is the volume of an average crystallite.

If I_a equals the number of internal atoms in a crystallite and S_a equals the number of surface atoms in a crystallite:

$$Q_c = I_aRe + S_ae \tag{3}$$

where e is the charge per hydrogen atom ($e = 1.602 \times 10^{-19}$ coul.) and R is the H/Pd ratio for internal Pd atoms.

$$I_a = T_a - S_a \tag{4}$$

(T_a = total atoms in a crystallite)

Therefore:

$$Q_c = (T_a - S_a)\, Re + S_a e \tag{5}$$

or:

$$Q_c = \{T_a R + S_a\,(1-R)\}e \tag{6}$$

The value of T_a can be determined from V_c, the volume of a crystallite, and V_a, the volume of a single atom.

$$T_a = V_c/V_a \tag{7}$$

The value of S_a is determined by:

$$S_a = A_c/A_{ac/s} \tag{8}$$

where A_c is the surface area of a crystallite and $A_{ac/s}$ is the cross sectional area of a single atom.

Therefore:

$$Q_c = \left(\frac{V_c}{V_a} R + \frac{A_c}{A_{a\ c/s}}\ (1 - R) \right) e \tag{9}$$

and since $Q = \#cQ_c$:

$$Q = \frac{V_T}{V_c} \left(\frac{V_c}{V_a} R + \frac{A_c}{A_{a\ c/s}} (1 - R) \right) e \tag{10}$$

or:

$$Q = \left(\frac{V_T}{V_a} R + \frac{V_T}{V_c} : \frac{A_c}{A_{a\ c/s}} (1 - R) \right) e \qquad (11)$$

Using the following relationships. (d_c = crystallite diameter; d_a = atom diameter):

$$V_T = 1/p \qquad A_c = \pi d_c^2 \qquad A_{a\ c/s} = \frac{\pi d_a^2}{4}$$

$$V_a = M/Np \qquad V_c = \frac{\pi d_c^3}{6}$$

where M = molecular weight; N = Avagadro's number; p = density.

Equation (11) becomes:

$$Q = \frac{NRe}{M} + \frac{(1-R)e}{d_c} \left(\frac{24}{\pi p}\right) \left(\frac{\pi NP}{6M}\right)^{2/3} \qquad (12)$$

or setting:

$$A = \frac{Ne}{M} \text{ and } B = \left(\frac{24}{\pi p}\right) \left(\frac{\pi NP}{6M}\right)^{2/3} e \qquad (13)$$

$$Q = AR + \frac{(1-R)}{d_c} B \qquad (14)$$

or

$$d_c = \frac{B(1-R)}{Q-AR} \qquad (15)$$

To obtain d_c in $\mathring{A}$ use:

$$A = 9.07 \times 10^2 \text{ and } B = 1.10 \times 10^4$$